

BIOLOGICAL ACTIVITIES OF LEVAN-BASED POLYMERS:  
IN SILICO APPROACH



by  
Binnaz Coşkun

Submitted to Graduate School of Natural and Applied Sciences  
in Partial Fulfillment of the Requirements  
for the Degree of Doctor of Philosophy in  
Chemical Engineering

Yeditepe University  
2017


BIOLOGICAL ACTIVITIES OF LEVAN-BASED POLYMERS:  
IN SILICO APPROACH

APPROVED BY:

Prof. Dr. Seyda Malta  
(Thesis Supervisor)

  
.....

Assoc. Prof. Dr. Kazım Yalçın Arga

  
.....

Assoc. Prof. Dr. Tuğba Davran Candan

  
.....

Assoc. Prof. Dr. Ali Demir Sezer

  
.....

Assist. Prof. Dr. Levent Organ

  
.....

DATE OF APPROVAL: .... / .... / 2017

## ACKNOWLEDGEMENTS

I would like to express my gratitude to my advisor Prof. Dr. Seyda Malta who gave me the opportunity of complete this dissertation. I appreciate for her patient, endless help and support during my graduate and postgraduate education in Yeditepe University. It was great to be a member of her research group. And Ebru Toksoy Öner is another important member of this thesis. I'm very thankful for her to give me the opportunity of working in this study. This thesis cannot be finished without them. I appreciate to Tunç Morova for docking studies. Also I want to thank Prof. Rahmi Özlük, Dr. Nihat Baysal, Dr. Deniz Rende, the instructors and the assistants of Chemical Engineering Department of Yeditepe University.

I'm very thankful to my dear friends Gülçin Cem Özer, Melek Şekerci Çetin and my roommate Barış Emek for making our days tolerable, enjoyable and special during our education. In addition, I'm thankful to Nermin Şen, İlayda Acaroğlu, Şelale Gülyuva and Avram Aruh for their friendship and support.

I'm deeply thankful to my precious Coskuncan, Kavusturan, Akın and Bayrakdar families for their love and endless support in every part of my life especially to my first nephew Hasan Poyraz Akın who encourages me in everytime I feel hopeless. And also I would to express my special thanks to my husband Efe Kavuşturan for his love, patient, support and insightfulness. I dedicated my dissertation to them.

## ABSTRACT

### **BIOLOGICAL ACTIVITIES OF LEVAN-BASED POLYMERS: *IN SILICO* APPROACH**

Oligo- and polysaccharides play an important role in various biological mechanisms such as immune response, adhesion and signal transduction by covering the surface of most cells. Hence considerable research has been directed on elucidating the biological activity mechanism of these polysaccharides by structure-function analysis. Use of different *in vivo* and *in vitro* bioactivity assays in such studies prevents to make generalizations in relating the chemical structure and conformation to the observed biological activity. Moreover, diversity of their conformations and their structural heterogeneity make polysaccharides the most challenging type of biopolymer for experimental and theoretical characterization studies. Levan is a naturally occurring polymer which is composed of  $\beta$ -D-fructofuranose with  $\beta$  (2 $\rightarrow$ 6) linkages between fructose rings. It is a homopolysaccharide that has great potential to be used as a functional biopolymer in foods, feeds, cosmetics, and pharmaceutical and chemical industries. Limited success of current technologies in analyzing the 3D structure of polysaccharides promoted the use of computational methods in structure-function studies. The main objective of this work is to study the conformations of levan-based polymers in different media, conditions and potential drug delivery systems by using molecular dynamics (MD) simulations. The conformation of levan chains were analyzed in terms of radius of gyration ( $R_g$ ), end-to-end distance ( $R$ ), bond length, bond angle, chord length, torsion angle, radial distribution function and mean square displacement. The conformational difference was obtained between single levan chain, multiple levan chain and sulphated levan in different media and temperatures which may affect the biological activity of biopolymers.

## ÖZET

### LEVAN BAZLI BİYOPOLİMERLERİN BİYOLOJİK AKTİVİTELERİ: *IN SILICO* YAKLAŞIMI

Oligo ve polisakkaritler bağışıklık sistemi, dokuların yapışması ve hücrel sinyal iletimi gibi biyolojik mekanizmalarda önemli rol oynarlar. Bu sebeple oldukça önemli çalışmalar, yapı-fonksiyon analizleri ile bu polisakkaritlerin biyolojik aktivite mekanizmalarını aydınlatmaya yönelmiştir. Bu çalışmalarda değişik hücre içi ve hücre dışı biyoaktivite deneylerinin kullanımı, kimyasal yapı ile gözlemlenen biyolojik aktivitede konformasyonun ilişkilendirilmesini önlemektedir. Buna ek olarak, polisakkaritlerin konformasyonlarındaki çeşitlilik ve yapısal çokyapımlılık, polisakkaritleri deneysel ve teorik karakterizasyon çalışmaları için en ilgi duyulan biyopolimer tipi haline getirmiştir. Levan, fruktoz halkalarında  $\beta$  (2 $\rightarrow$ 6) bağları bulunan ve doğal ortamda oluşan  $\beta$ -D-fructofuranoz tipi polimerdir. Gıdada, beslenmede, kozmetikte, ilaç ve kimya endüstrisinde fonksiyonel biyopolimer olarak kullanımı yüksek potansiyele sahip bir homosakkarittir. Polisakkaritlerin 3D yapısal analizindeki günümüz teknolojisinin sınırlı gelişmiş olması yapısal-fonksiyon çalışmalarında bilgisayar metotlarının kullanımını desteklemektedir. Bu çalışmanın amacı, levan bazlı polimerlerin moleküler dinamik simülasyonlarını kullanarak değişik ortamlarda, kondisyonlarda ve potansiyel ilaç taşınım sistemlerinde konformasyonlarını çalışmaktır. Levan zincirinin konformasyonları, dönme yarıçapı ( $R_G$ ) iki uç arasındaki uzaklık ( $R$ ), bağ uzunluğu, bağ açısı, kiriş uzaklığı, torsiyon açısı, radyal dağılım fonksiyonu ve ortalama mesafe değeri hesaplanarak analiz edilmiştir. Biyopolimerlerin biyolojik aktivitesine etkisi olduğu düşünülerek tek levan zincirinin, çoklu levan zincirinin ve sulfatlanmış levan zincirinin değişik ortam ve sıcaklıklardaki konformasyonları elde edilmiştir.

## TABLE OF CONTENTS

ACKNOWLEDGEMENTS .....	iii
ABSTRACT .....	iv
ÖZET .....	v
LIST OF FIGURES .....	xi
LIST OF TABLES .....	xvii
LIST OF SYMBOLS/ABBREVIATIONS .....	xxii
1. INTRODUCTION .....	1
2. THEORETICAL BACKGROUND .....	3
2.1. FRUCTANS .....	3
2.2. LEVAN .....	5
2.3. MOLECULAR DYNAMICS STUDIES OF POLYSACCHARIDES .....	6
2.4. PRODUCTION OF LEVAN .....	13
2.5. LEVAN IN FOOD APPLICATIONS .....	16
2.6. LEVAN IN COSMETIC APPLICATIONS .....	17
2.7. DRUG DELIVERY .....	17
2.7.1. Targeted Drug Delivery .....	18
2.7.2. Controlled Drug Delivery .....	19
2.7.2.1. Diffusion Controlled Release .....	20
2.7.2.2. Erosion-Chemically Controlled Release .....	21
2.7.2.3. Swelling Controlled Release .....	21
2.7.2.4. Osmotic Controlled Release .....	22
2.7.3. Studies Involving Polysaccharides in Drug Delivery .....	23
2.8. LEVAN IN DRUG DELIVERY AND BIOMEDICAL APPLICATIONS .....	25
2.9. APPLICATIONS OF LEVAN DERIVATIVES .....	27
3. METHODOLOGY .....	30

3.1. CONFORMATIONAL ANALYSIS .....	30
3.1.1. Molecular Dynamics .....	31
3.1.1.1. Force Fields .....	32
3.1.1.2. Verlet Algorithm .....	33
3.1.1.3. Ensembles .....	34
3.1.1.4. Periodic Boundary Conditions .....	35
3.1.2. Explicit & Implicit Systems .....	35
3.1.3. Berendsen Thermostat & Barostat .....	36
3.1.4. Chain Characteristics .....	37
3.1.4.1. End-to-end Distance and Radius of Gyration .....	37
3.1.4.2. Bond Torsion .....	39
3.1.4.3. Bond Length .....	40
3.1.4.4. Chord Length .....	40
3.1.4.5. Mean Square Monomer Displacement (MSMD) .....	40
3.1.6. Radial Pair Distribution Function (RDF) .....	42
3.1.7. Student T-Test .....	43
3.1.8. Docking .....	44
3.2. COMPUTATIONAL WORK .....	45
3.2.1. Xenoview .....	45
3.2.2. LAMMPS .....	46
3.2.3. Visual Molecular Dynamics (VMD) .....	46
3.2.4. Python .....	47
3.2.5. SwissDock .....	48
3.2.6. UCSF Chimera .....	48
4. RESULTS AND DISCUSSION .....	49

4.1. SIMULATIONS WITH SINGLE LEVAN CHAIN WITH DIFFERENT LENGTHS IN VACUUM AT 298 K .....	49
4.1.1. End-to-end Distance In Vacuum At 298 K .....	50
4.1.2. Radius of Gyration in Vacuum at 298 K .....	51
4.2. SIMULATIONS WITH SINGLE LEVAN CHAIN STRUCTURE IN DIFFERENT MEDIA AT 298 K AND 310 K .....	52
4.2.1. End-to-end Distance of Single Chain in Different Media at 298 K and at 310 K .....	54
4.2.2. Radius of Gyration of a Single Chain in Different Media at 298 K and at 310 K .....	56
4.2.3. Chain Characteristics of a Single Chain for Different Media at 298 K and at 310 K .....	59
4.2.4. Radial Distribution Function Analysis (RDF) of a Single Chain in Different Media at 298 K and 310 K .....	72
4.3. SIMULATIONS WITH 9 ORIGINAL LEVAN STRUCTURE IN DIFFERENT MEDIA AT 298 K AND 310 K .....	76
4.3.1. End-to-end Distance for 9 Levan Chains in Different Media at 298 K and at 310 K .....	77
4.3.2. Radius of Gyration of 9 Levan Chains in Different Media at 298 K and at 310 K .....	79
4.3.3. Chain Characteristics for 9 Levan Chains in Different Media at 298 K and at 310 K .....	84
4.3.4. Radial Distribution Function Analysis (RDF) for Levan Chains at 298 K and at 310 K .....	93
4.3.5. Diffusivity Coefficients for 9 Levan Chains in Different Media at 298 K and 310 K .....	99



4.4. SIMULATIONS WITH 9 SULFATED LEVAN STRUCTURE IN DIFFERENT MEDIA AT 310 K .....	103
4.4.1. End-to-end Distance for 9 Sulfated Levan Chains in Different Media at 310 K .....	104
4.4.2. Radius of Gyration of 9 Sulfated Levan Chains in Different Media at 310 K .....	106
4.4.3. Chain Characteristics for 9 Sulfated Levan Chains in Different Media at 310 K .....	109
4.4.4. Radial Distribution Function Analysis (RDF) for 9 Sulfated Levan Chains in Different Media at 310 K .....	119
4.4.5. Diffusivity Coefficients for 9 Levan Chains in Different Media at 298 K and 310 K .....	125
4.5. DOCKING STUDIES .....	130
4.5.1. Coagulation .....	130
4.5.2. Thrombin .....	131
4.5.3. Heparin Glycosaminoglycan .....	132
4.5.4. Docking Studies .....	132
4.5.5. Docking Results .....	135
5. CONCLUSION AND FUTURE WORK .....	139
REFERENCES .....	142
APPENDIX A .....	166

## LIST OF FIGURES

Figure 2.1. Structure of levan and inulin .....	4
Figure 2.2. Molecular Dynamics Flow Chart .....	5
Figure 2.3. Coarsed grained model representation .....	9
Figure 2.4. Schematic representation of reservoir device in diffusion controlled release .....	20
Figure 2.5. Schematic representation of monolithic device in diffusion controlled release .....	20
Figure 2.6. Schematic representation of erosion controlled release .....	21
Figure 2.7. Schematic representation of swelling controlled release .....	22
Figure 2.8. Schematic representation of osmotic controlled release .....	22
Figure 3.1. Molecular Dynamics Flow Chart .....	31
Figure 3.2. An example of an equation used to calculate the atomic interactions .....	32
Figure 3.3. Energy equation used in PCFF .....	33
Figure 3.4. Periodic Boundary Condition .....	35
Figure 3.5. Schematic representation of explicit and implicit systems .....	36
Figure 3.6. Random coils in different solvents .....	38

Figure 3.7. Representation of end-to-end distance ( $R$ ) and radius of gyration ( $R_G$ ) .....	38
Figure 3.8. $\phi$ (phi), $\psi$ (psi), $\omega$ (omega) bonds for levan structure .....	39
Figure 3.9. Schematic representation of chord length .....	40
Figure 3.10. The representation of radial distribution function .....	43
Figure 3.11. Levan Structure in Xenoview .....	46
Figure 4.1. Snapshots for 9, 12, 18 fructose rings of levan over 1 ns.....	50
Figure 4.2. End-to-end distance of levan chains with different number of fructose rings in vacuum with respect to time .....	51
Figure 4.3. Radius of gyration of chains with different number of rings in vacuum with respect to time .....	52
Figure 4.4. End-to-end Distances Comparison for one levan chain of 12 fructose rings in different media over time at .....	54
Figure 4.5. Radius of Gyration Comparison for one levan chain of 12 fructose rings in different media over time .....	57
Figure 4.6. End-to-end Distance over Radius of Gyration Values for one levan chain of 12 fructose rings in different media over time .....	59
Figure 4.7. Bond length for one levan chain of 12 fructose rings in different media over time .....	60
Figure 4.8. Bond angle of 12 fructose single chain in different media with respect to time .....	61

Figure 4.9. Chord length of 12 fructose single chain in different media with respect to time .....	63
Figure 4.10. Schematic representation of monomer beads at 298 K and 310 K .....	64
Figure 4.11. Representation of freely joint chain model .....	65
Figure 4.12. Representation of the modified freely joint model .....	66
Figure 4.13. Histogram of the distribution of the dihedral angle between monomer bead 12 fructose single chain in vacuum and water systems over 5 ns .....	70
Figure 4.14. Histogram of the distribution of the dihedral angle between monomer beads of 12 fructose single chain in water and saline systems over 5 ns .....	71
Figure 4.15. Representation of Radial Distribution Function .....	72
Figure 4.16. RDF for 12 fructose single chain in vacuum with 1 ns intervals .....	73
Figure 4.17. RDF for 12 fructose single chain in all media 4 ns-5 ns intervals .....	73
Figure 4.18. End-to-end distance of 9 levan chains with 12 fructose units in different media with respect to time .....	78
Figure 4.19. Radius of Gyration of 9 levan chains in different media with respect to time .....	80
Figure 4.20. $\langle R^2 \rangle / \langle R_G^2 \rangle$ for 9 levan chains in water and saline solution systems .....	81
Figure 4.21. Bond Length values of 9 levan chains in different media with respect to time .....	83

Figure 4.22. Bond Angle Values of 9 levan chains in different media with respect to time .....	86
Figure 4.23. Chord Length values of 9 levan chains in different media with respect to time .....	88
Figure 4.24. Schematic representation of monomer beads in multiple chain systems .....	89
Figure 4.25. Torsion Angle of 9 levan chains in different media with respect to time ....	90
Figure 4.26. RDF of all monomer beads with each other in vacuum .....	94
Figure 4.27. RDF of all monomer beads for all systems between 24 ns and 25 ns .....	94
Figure 4.28. Intra-RDF of vacuum system with 1 ns intervals .....	96
Figure 4.29. Intra-RDF of all systems between 24 ns and 25 ns .....	96
Figure 4.30. Inter-RDF of vacuum system with 1 ns intervals .....	97
Figure 4.31. Inter-RDF of all systems between 24 ns and 25 ns .....	98
Figure 4.32. MSD graphs for 9 levan chains in water with respect to time .....	99
Figure 4.33. $g_3(t)$ graphs for 9 levan chains in water and saline systems with respect to time .....	99
Figure 4.34. Hydrodynamic radius of a polymer .....	101
Figure 4.35. Sulfated Levan Structure .....	104
Figure 4.36. End-to-end distance of 9 sulfated levan chains with 12 fructose units in different media at 310 K with respect to time .....	105

Figure 4.37. Radius of Gyration values of 9 Sulfated Levan Chains in Different Media at 310 K with respect to time .....	107
Figure 4.38. $\langle R^2 \rangle / \langle R_g^2 \rangle$ values of 9 sulfated levan chains at 310 K with respect to time .....	109
Figure 4.39. Bond Length values for 9 Sulfated Levan Chain Systems at 310 K during 25 ns .....	110
Figure 4.40. Bond angle values for 9 Sulfated Levan Chain Systems at 310 K during 25 ns .....	111
Figure 4.41. Chord Length values for 9 Sulfated Levan Chain Systems at 310 K during 25 ns .....	112
Figure 4.42. Histogram of Torsion Angle values for 9 Sulfated Levan Chain Systems at 310 K during 25 ns .....	113
Figure 4.43. RDF of all monomer beads in sulfated levan chains with each other in vacuum at 310 K .....	120
Figure 4.44. RDF of all monomer beads of 9 sulfated levan chains for all systems between 24 ns and 25 ns at 310 K .....	120
Figure 4.45. Intra-RDF of 9 sulfated levan chains in vacuum system at 310 K .....	122
Figure 4.46. Intra-RDF of 9 sulfated levan chains in different media between 24 ns and 25 ns at 310 K .....	122
Figure 4.47. Inter-RDF of 9 sulfated levan chains in vacuum system at 310 K .....	124
Figure 4.48. Inter-RDF of 9 sulfated levan chains in different media between 24 ns and 25 ns at 310 K .....	124

Figure 4.49. MSD of 9 sulfated levan chains in water at 310 K with respect to time .....	126
Figure 4.50. MSD $g_3(t)$ of 9 sulfated levan chains in different media at 310 K with respect to time .....	126
Figure 4.51. Structure of Thrombin .....	131
Figure 4.52. Chemical structure of the disaccharide repeating unit of heparin .....	132
Figure 4.53. Levan structures obtained from MD simulations .....	136
Figure 4.54. The structures of Thrombin (Purple region: Exosite II; green region: Active site) with Heparin (red structure) and SHL-9 (red structure) with lowest $\Delta G$ .....	137
Figure 4.55. The structures of inhibited Thrombin (Yellow region: Exosite II; purple region: Active site closed with rhodniin) with Heparin (red structure) and SHL-9 (red structure) with lowest $\Delta G$ .....	138

## LIST OF TABLES

Table 2.1. Microorganisms produce Levan .....	15
Table 3.1. Ensemble Types .....	34
Table 4.1. Simulated systems with one levan chain of various number of fructose units in vacuum at 298 K .....	49
Table 4.2. Simulations of one levan chain in different media at 298 K and 310 K .....	53
Table 4.3. Average End-to-end Distance values between 2 ns and 5 ns for all systems at 298 K and 310 K .....	55
Table 4.4. Average Radius of Gyration values between 2 ns and 5 ns for all systems at 298 K and 310 K .....	57
Table 4.5. Average End-to-end Distance over Radius of Gyration values between 2 ns and 5 ns for all systems at 298 K and 310 K .....	59
Table 4.6. Average Bond Length values between 2 ns and 5 ns for all systems at 298 K and 310 K .....	61
Table 4.7. Average Bond Angle values between 2 ns and 5 ns for all systems at 298 K and 310 K .....	62
Table 4.8. Average Chord Length values between 2 ns and 5 ns for all systems at 298 K and 310 K.....	64
Table 4.9. Theoretical End-to-End Distance Calculated From Bond Lengths $\langle R^2 \rangle_f$ .....	65



Table 4.10. Theoretical End-to-End Distance Calculated From Bond Lengths and Bond Angles $\langle R^2 \rangle_t$ .....	67
Table 4.11. Characteristic Ratio of Levan Chain in Different Media at 298 K and 310 K	68
Table 4.12. Expansion Factor for Single Levan Chain in Different Media at 298 K and 310 K .....	69
Table 4.13. Free Energy values for water and saline systems at 298 K and 310 K .....	71
Table 4.14. RDF values of the all systems at their peak point at 298 K and at 310 K .....	74
Table 4.15. Summary of all results of single levan chain simulations .....	75
Table 4.16. Simulation parameters for 9 chains systems at 298 K and 310 K .....	77
Table 4.17. The Average end-to-end distance values of 9 levan chains at 5 ns - 25 ns at 298 K and 310 K .....	79
Table 4.18. Average Radius of Gyration values of 9 Levan Chains in Different Media at 298 K and 310 K between 5 ns - 25 ns .....	81
Table 4.19 End-to-end Distance and Radius of Gyration Comparison of Single and Multiple Chain Systems at 298 K and 310 K .....	82
Table 4.20. Average End-to-end Distance over Radius of Gyration values between 2 ns and 5 ns for all systems at 298 K and 310 K .....	84
Table 4.21. Average Bond Length Values of 9 levan chains between 5 ns – 25 ns For All Systems at 298 K and 310 K .....	85

Table 4.22. Average Bond Angle Values of 9 levan chains between 5 ns -25 ns at 298 K and 310 K .....	87
Table 4.23. Average Chord Length values of 9 levan chains between 5 ns-25 ns at 298 K and 310 K .....	88
Table 4.24. Theoretical End-to-End Distance Calculated From Bond Lengths at 298 K and 310 K .....	89
Table 4.25. Theoretical End-to-End Distance Calculated From Bond Lengths and Bond Angles .....	90
Table 4.26. Characteristic Ratio of Levan Chain in Different Media at 298 K and 310 K .....	91
Table 4.27. Expansion Factor for Multiple Levan Chains in Different Media at 298 K and 310 K .....	91
Table 4.28. Free Energy values for water and saline systems at 298 K and 310 K .....	93
Table 4.29. RDF values of the all systems at their peak point at 298 K and at 310 K .....	95
Table 4.30. RDF-Intra values of the all systems at their peak point at 298 K and at 310 K .....	97
Table 4.31. RDF-Inter values of the all systems at their peak point at 298 K and at 310 K .....	98
Table 4.32. Diffusion Coefficients for 9 Levan Chains in Water and Saline Systems at 298 K and 310 K .....	100
Table 4.33. Agglomeration values for multiple chain systems at 298 K and 310 K .....	102


Table 4.34. Simulation Parameters of Sulfated Levan Structure Systems .....	104
Table 4.35. The Average end-to-end distance values of 9 sulfated levan chains at 5 ns – 25 ns at 310 K .....	106
Table 4.36. Average Radius of Gyration values of 9 Sulfated Levan Chains in Different Media at 310 K between 5 ns - 25 ns .....	108
Table 4.37. Average $\langle R^2 \rangle / \langle R_g^2 \rangle$ values of 9 original and sulfated levan chains at 310 K .....	109
Table 4.38. Average Bond Length Values of 9 sulfated levan chains Between 5 ns – 25 ns For All Systems at 310 K .....	111
Table 4.39. Average Bond Angle Values of 9 sulfated levan chains between 5 ns -25 ns at 310 K .....	112
Table 4.40. Average Chord Length values of 9 sulfated levan chains between 5 ns-25 ns at 310 K .....	114
Table 4.41. Theoretical End-to-End Distance Calculated From Bond Lengths at 310 K .....	114
Table 4.42. Theoretical End-to-End Distance Calculated From Bond Lengths and Bond Angles .....	115
Table 4.43. Characteristic Ratio of Levan Chain in Different Media at 310 K .....	116
Table 4.44. Expansion Factor for Sulfated Levan Chains in Different Media at 310 K .	117
Table 4.45. Free Energy values for water and saline systems at 310 K for 9 Sulfated Levan chains .....	118

Table 4.46. RDF values of the all sulfated levan systems at their peak point at 310 K ..	121
Table 4.47. Intra-RDF values of the all sulfated levan systems at their peak point at 310 K .....	123
Table 4.48. Inter-RDF values of the all sulfated levan systems at their peak point at 310 K .....	125
Table 4.49. Diffusion Coefficients for 9 Sulfated Levan Chains in Water and Saline Systems at 310 K .....	128
Table 4.50. Agglomeration values for sulfated multiple chain systems at 298 K and 310 K .....	128
Table 4.51. Summarized results for all systems with 9 levan chains .....	129

**LIST OF SYMBOLS/ABBREVIATIONS**

$a$	Acceleration
C	Characteristic Ratio
D	Diffusion Coefficient
F	Force
$g_{ij}(r)$	Density distribution
$g$	Mean Square Displacement
$k$	Boltzmann Constant
$l$	Bond Length
m	Mass
M	Molarity
MW	Molecular Weight
$n$	Number of Segments
p	Probability
$r$	Position
R	End-to-end Distance
$R_g$	Radius of Gyration
T	Temperature
$t$	Time
$v$	Velocity
$\alpha$	Expansion Factor
$\Delta G$	Free Energy
$\epsilon$	Dielectric Constant
$\phi$	Torsional angle
FTIR	Fourier Transform Infrared Spectroscopy
HPLC	High-Performance Liquid Chromatography
kDa	Kilo Dalton
LAMMPS	Large-scale Atomic/Molecular Massively Parallel Simulator
LJ	Lennard Jones

MD	Molecular Dynamics
$\mu$ VT	Grand Canonical Ensemble
NMR	Nuclear Magnetic Resonance
NPT	Isobaric-Isothermal Ensemble
NVE	Micro Canonical Ensemble
NVT	Canonical Ensemble
PCFF	Polymer Consistent Force Field
RDF	Radial Distribution Function
SHL	Sulfated Halomonas Levan
TGA	Thermogravimetric Analysis



## 1. INTRODUCTION

In recent years, the biological activities of glucan, fucoidan, homo- and heteropolysaccharides have received considerable attention. Majority of these studies are about the protection of biological systems under stress conditions. Plants in cold and dry climate contain fructan at high levels and these environmental conditions trigger fructan biosynthesis. Hence, these biopolymers have an important role in the protection of these plants and the studies related to transgenic plant resistant to environmental conditions focuses on fructan biosynthesis mechanisms [1, 2].

Polysaccharides and carbohydrates/protein complexes have become increasingly important in the development of drugs. The characterization of three dimensional structure of these complexes is difficult with the methods of today's technology. Polysaccharides have plenty of conformational variations due to the properties like variety of monomers, ability to form branches and unstable chirality [3]. In the last years, Molecular Dynamics (MD) simulations are used to retrieve comprehensive information to understand the conformations of glucans and their dynamic properties [4].

Levan is a polymer of  $\beta$ -D-fructofuranose with  $\beta$  (2 $\rightarrow$ 6) linkages between fructose rings. It is distinguished from other polysaccharides by its properties like low viscosity, high solubility in oil, stability to heat, acid and alkali media and good biocompatibility. Levan is also used in food, cosmetics, chemical or pharmaceutical industries as emulsifier, encapsulating agent, stabilizer and thickener. Because of these exceptional properties, levan became a focus of interest especially in the last decade [5, 6].

In this study, molecular dynamics simulations are used to investigate the conformations of fructan polymers of levan type in different media and conditions. These conformations are investigated in terms of radius of gyration ( $R_g$ ), end-to-end distance ( $R$ ), bond length, bond angle, chord length, torsion angle, radial distribution function and mean square displacement. Computer simulations were carried out to understand the properties of molecules in terms of their structure and microscopic interactions between the molecules. Inter and intra radial distribution functions are used for this purpose. These simulations are complementary to the experiments and they enable the researchers to gain information

about the molecular level of structure and biological activities that can hardly be accessible with experimental studies.

Out of the levan structures investigated, one type of levan structure is chosen and is derivitized by sulfation at different number of rings and positions. Initially, levans of various lengths and simulated. Then, one levan with a particular length is chosen and 9 of the same are simulated together. These simulations were carried out both at 298 K and 310 K and at varying saline concentrations and in vacuum. Then the 9 levans are derivitized by sulfation at all fructose rings and simulations are carried out at 310 K. After investigation of structural and interactive properties of sulfate derivitized levans, they are then used in docking studies with thrombin and antithrombin to investigate the effect of sulfation on the anticoagulant efficiency of levan sulfate.



## 2. THEORETICAL BACKGORUND

### 2.1. FRUCTANS

In recent years, several studies have been published about the biological activities of glucan, fucoidan, homo- and heteropolysaccharides. But the knowledge about fructans which are homopolymers of fructose stays at a limited level and is confined to specific issues. Most of these studies are about the protection of biological systems under stress conditions. The plants in cold and dry climate contain fructan at high levels and these environmental conditions trigger fructan biosynthesis [1]. Fructans are synthesized from sucrose by fructosyltransferases enzyme to protect the plants from stress environments. They are protective agents of plants from abiotic stresses. *In vitro* studies show that fructans can stabilize the cell membrane by H-bonding to membrane lipids. By this method, they reduce the water outflow from dry membrane [7]. These biopolymers have an important role in protection of these plants and studies related to transgenic plants resistant to environmental conditions mainly focus on fructan biosynthesis mechanisms [1]. Fructans interact with the cell membrane directly to protect the membrane from drought. Mono and bilayer systems were studied and a layer of fructan was observed in both mono and bilayer systems. This layer prevents the interaction of surface active proteins with lipids. And also because of their hydrophobic properties, fructans showed stronger effect than other polysaccharides on other lipid systems. For example, liquid-crystalline lamellar phase has a role in drought protection of plants and fructans stabilize this phase [8]. Another research topic of fructan is their nutraceutical properties. Fructan and fructooligosaccharides are also characterized as functional food because of their prebiotic properties. In particular, inulin which is a type of fructan has the largest market for food industry in the world as a prebiotic [9.10].

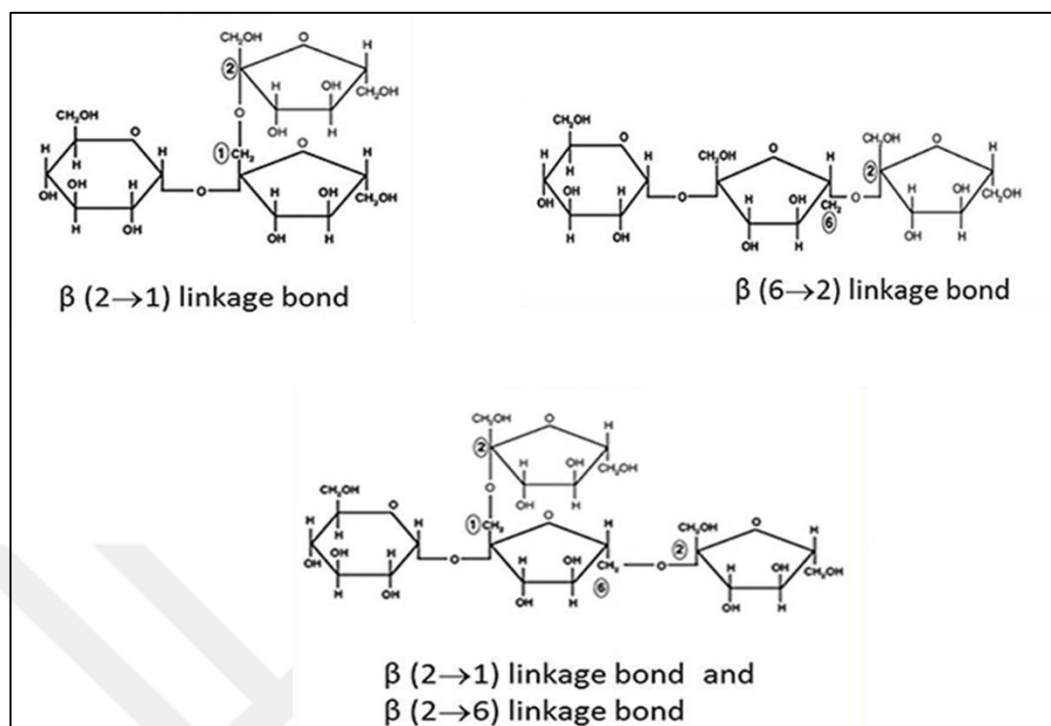


Figure 2.1. Glycosidic Linkages of Inulin, Levan and Graminans [11]

Fructans are polysaccharides consisting of one glucose unit and two or more fructose units. They are divided into different classes depending on the glycosidic linkage between the fructose units. A glycosidic linkage is formed when hydrolysis reaction takes place between the hemiacetal of a sugar with the alcohol of another molecule (may or may not be sugar)  $\alpha$  and  $\beta$  refer to the relative stereochemistry of the reactive centers. For example inulins contain  $\beta$  (2 $\rightarrow$ 1) linkages, levans contain mainly  $\beta$  (2 $\rightarrow$ 6) linkages and graminans contain both of these types of linkages (Figure 2.1).

Inulin type of fructans are present in several fruits and vegetables as a storage carbohydrate. Inulin is the mixture of linear fructose polymers and oligomers which fructose units are linked by  $\beta$  (2 $\rightarrow$ 1) bonds. At the end of each fructose unit, a glucose unit is linked by  $\alpha$  (1 $\rightarrow$ 2) bonds. The length of inulin chains range from 2 to 60 units with degree of polymerization 10 on average [2,12,13].

## 2.2. LEVAN

Levan is a polymer chain that consists of fructose rings with  $\beta$  (2 $\rightarrow$ 6) linkages (Figure 2.2). The properties as low viscosity, stability to heat, acid and alkali media and good biocompatibility differentiate levan from other types of polysaccharides. This polymer type is used in food, cosmetics, chemical or pharmaceutical industries as emulsifier, encapsulating agent, stabilizer and thickener. Therefore, levan becomes the focus of interest in the last decade [5,6].

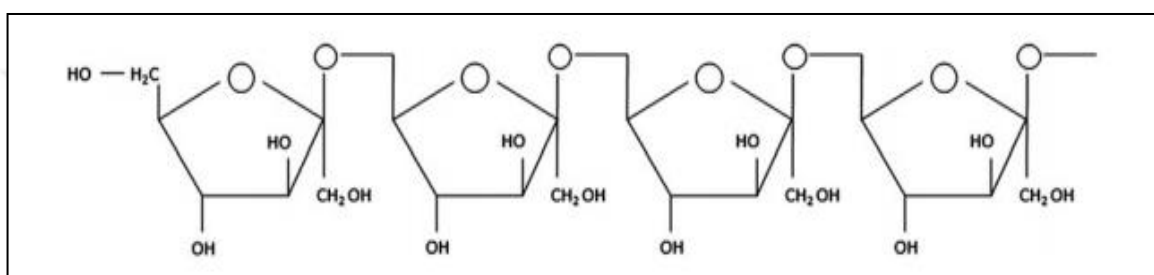


Figure 2.2. Structure of levan [14]

Levans are produced from plant and different organisms. The structure of the biomolecule differs according to the source of the production. Bacterial levans have higher molecular weight than those produced by plant and they have also differ in the degree of branching. Molecular weight of levan produced from plants is generally between 2-33 kDa while bacterial levan's is between 2-10 million Da with possible branching structure [15]. Levan is produced by different microorganisms and the newly isolated halophilic bacterial strain *Halomonas sp. AAD6* was found as the first levan producing microorganism to produce high amounts of levan [16]. Concentration of nutrients in the medium and environmental conditions affect the production of bacterial levan. The structure of these kinds of biopolymers defines their roles in biological activities. For example the varying chemical structure and molecular weight of levan from different bacteria sources were investigated against their antitumor activity. Among the levan produced from *Gluconoacetobacter xylinus*, *Microbacterium laevaniformans*, *Rahnella aquatilis*, and *Zymomonas mobilis* levan produced from *Gluconoacetobacter xylinus* showed lower antitumor activity than others and this was attributed to the low molecular weight of levan produced [17].

### 2.3. MOLECULAR DYNAMICS STUDIES OF POLYSACCHARIDES

Structure function analysis for polysaccharides is a challenging field in biotechnology because of multiple possible conformations of the structures. Polysaccharides are composed of monomer units with glycosidic linkages therefore these linkages make them flexible [18]. Molecular dynamics (MD) is an analyzing technique for conformation with solving equation of motion of atoms. This technique has a wide range of applications such as phase transitions, dynamics properties and thermodynamic analysis of the systems [19].

Polysaccharide scleroglucan was studied with explicit molecular dynamics method at two different temperatures. The experimental data of the simulations with two representative disaccharide units were compared with literature to ensure the use of correct MD parameters. A united force field and GROMACS parameters were used because of the complexity of the system. Temperature did not affect the interaction of water molecules with the core of scleroglucan however side chain of the structure have been affected with changing temperature. Increase in the interaction of water molecules with the side chain caused the conformational transition of the structure at low temperature [20].

Eight reducing glucose disaccharides were simulated for 50 ns at 300 K with explicit solvent to investigate their conformations and torsional dynamics and the results are validated with experimental data. Additionally, their intramolecular hydrogen bonding patterns and configurational entropies were analyzed. Kojibiose, sophorose, nigerose, laminarabiose, maltose, cellobiose, isomaltose, and gentiobiose were used in this study and the study showed that (1→6)-linked disaccharides are more flexible, have higher entropy and non- intramolecular hydrogen bonding, whereas cellobiose have higher intermolecular hydrogen bonding and lower configurational entropy with respect to others. All disaccharides have persistent hydrogen bonds except (1→6)-linked disaccharides and they include hydrogen donor in their reducing radical and acceptor in non-reducing radical. Their torsional distribution is unimodal and full rotation occurs after 50 ns [21].

Molecular dynamics simulations were used for conformational analysis of maltose. An adiabatic potential energy surface was calculated by conformational energy minimizations. Molecular flexibility lowers the conformational transition barriers significantly. On the adiabatic surface, several low energy wells were observed. This situation indicates the

possibility of non-negligible equilibrium population distribution. NMR measurements show the real conformation of the structure if this distribution exists in physical system. The molecule was simulated in vacuum and these simulations indicate that the rate of relaxation to the adiabatic surface is slower than typical timescale conformation. This is caused by occurrence of unphysical persistence of hydrogen bonds in vacuum which do not occur in aqueous solution [22].

Almond et. al. studied to predict the molecular shape of cellulose, chitin, mannan, xylan, and hyaluronan in the presence of explicit water solvent. Their aim was to investigate the effect of water on the dynamic structure of polysaccharides with using  $\beta(1\rightarrow4)$ -linkage polysaccharides. These polysaccharides have similar chemical structures except hyaluronan therefore their intramolecular hydrogen bond dynamics and their water interactions should be determined to differentiate them from each other. Cellulose, mannan and chitin prefer stable intramolecular hydrogen bond dynamics. Xylan favors dynamic water bridges whereas hyaluronan has multiple conformations in water. The different dynamic predictions indicate this linkage could not be stabilized with intramolecular hydrogen bonding. However they proposed that the conformations are consistent with the observed X-ray diffraction [23].

Elasticity of polysaccharide molecules is regulated by conformational transition of pyranose ring in the structure as suggested by atomic force microscopy (AFM) stretching measurements. However, the mechanism under this process is not investigated. Lee and his colleagues analyzed the stretching process with molecular dynamics. They used dextran that has  $(1\rightarrow6)$ -linkage because this kind of polysaccharides also have branches form  $\alpha(1\rightarrow3)$  linkages. Pustulan is used for  $\beta$  linked polysaccharide and forced rotation was applied to both polysaccharides to produce elasticity however the conformation of pyranose rings was not affected for  $\beta$  (pustulan) whereas for  $\alpha$  (dextran) the elasticity was affected due to the fact that the rotation occurs in  $\alpha$  linkage and this rotation increases the mechanical complexity of the polymer [24].

Decasaccharide fragment of heparin is simulated with molecular dynamics in aqueous solution to show conformation under physiological conditions. GROMACS force field is used and the charges of heparin are obtained from quantum mechanical calculations. The results are consistent with experimental data therefore this approach is suggested to study heparin interactions with target proteins to develop new antithrombic agents [25].

Becker et. al. studied to calculate the atomic charges of heparin and its conformation with molecular dynamics simulations. They used different atomic charge sets and obtained the best result from Löwdin charge set. NMR conformation of IdoA residue was observed and it was found that small conformational change induced a change in the energy of the interactions of heparin with its environment. This data can be used to design heparin-derived antithrombic compounds [26].

L-iduronic acid in heparin derivatives were used to analyze conformations in terms of intra-ring proton-proton vicinal coupling constants. The mathematical results fit experimental and theoretical results. However this approach causes some errors on J-coupling measurements, force fields and least square fits. The study of Munoz-Garcia and his colleagues tried to reduce these errors with time averaged distance restrained molecular dynamics. The results showed that sulfation at the reducing end facilitates the transition of iduronate ring by the flexibility of C2-C3 torsion [27].

Intermolecular forces binding polysaccharides can be analyzed with molecular dynamics simulations. These forces are crucial to design hydrolysis biomass methods. Cellulose is one of the polysaccharides that is analyzed with molecular dynamics. Integrating molecular models for the systems is important because characteristic time, length scales and chemical pretreatment span orders of magnitude, which affect the degradation of cellulose by enzymatic hydrolysis. The system can be defined as quantum, atomistic and coarse grained to determine the best model. For this aim, four multiscale coarse grained models were considered and the most effective model was investigated with force matching method (Figure 2.3). Intra-chain radial distribution function of each model were compared to obtain this aim. One site and double site coarse grained models were not sufficient to obtain double peak in radial distribution however three and four site models were. Double peak occurs from the distinct conformations of primary alcohol groups in glucose residues. This study is the first coarse grained approach to reproduce molecular features of a polysaccharide. Four site coarse grained model was found as the best approach to reproduce glucose-glucose conformations. This shows the importance of decoupling the pyranose ring from oxygen atom in the glycosidic bond while applying coarse grained model for polysaccharides [28].

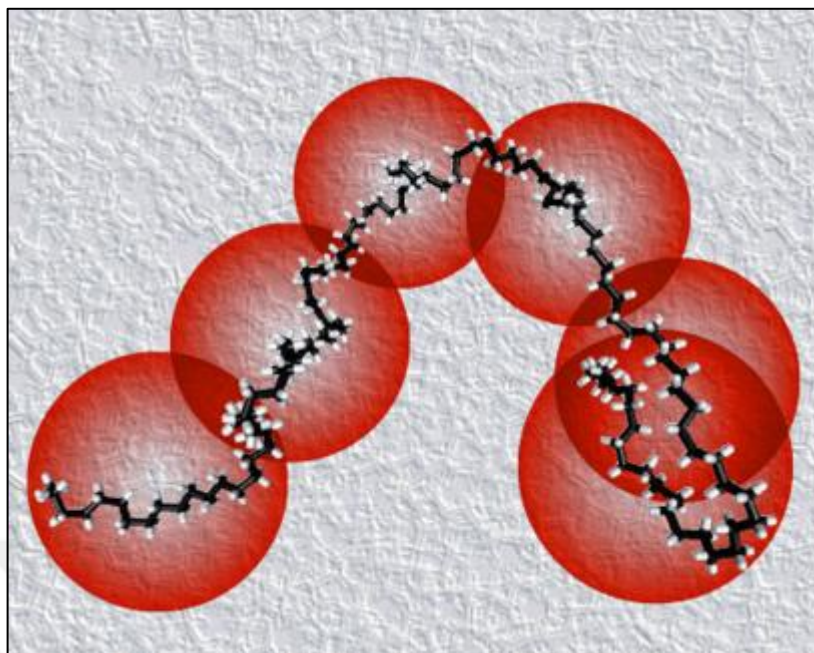


Figure 2.3. Coarse grained model representation [29]

The insolubility of cellulose in aqueous media is a challenging research area. However, cellulose being soluble in supercritical water has been reported. Tolonen and et.al. investigated the determination of the solubility of cellulose in supercritical water with molecular dynamics simulation. The Gibbs energy was analyzed for different densities of supercritical water between nanocrystal and fully dissociated state by using two-phase thermodynamics model. The study suggested that cellulose is soluble in supercritical water in all different densities. The dissociation of cellulose occurred by the entropy gain on chain dissociation and loss of solvent entropy simultaneously. Density increment around cellulose chains also occurred around cellulose chains because of chain dissociation. This circumstance improves the water-water bonding in low density supercritical water [30].

Large amount of cellulose can be soluble in some ionic liquids. Regeneration process is the recovery of solubilized cellulose with an anti-solvent such as water. Regeneration process of solubilized cellulose from ionic solvents is an important process in subsequent enzymatic saccharification reactions and recovery of ionic liquids. The intermolecular interactions were studied to understand the mechanism of dissolution and recovery process with the complex of cellulose, ionic liquid and water with molecular dynamics. Ionic liquid [C2mim][OAc] (1-Ethyl-3-methyl-imidazolium acetate) is used for binary and ternary

mixture of water and cellulose. The interactions between cellulose and ionic liquid lead to the dissolution of cellulose. The interactions of cellulose precipitation in water were also followed during the process to have a better understanding of the molecular forces in the ternary mixture. [31].

The reactivity of glucose with various chemical media is an anticipated research area for conversion of renewable fuels and chemicals. Inorganic salts naturally occur in biomass and affect the product distribution. The interaction of alkali metals with glucose at molecular level is unknown. Therefore Mayes and his colleagues applied Quantum Mechanics to understand this relation from structural and thermodynamic view. From Quantum Mechanics, the effect of sodium ion on  $\beta$ -glucose is found to be subtle. The sodium ion affects the bond length and atomic partial charges less than hydroxymethyl group. However the effect of sodium ion on atomic charges is distinct for  $\alpha$ -glucose anomeric and ring oxygens. To invest the dynamic behavior for the system molecular dynamics was used with explicit water solvent. Both quantum mechanics and molecular dynamics results showed that sodium ions have equal tendency of binding at different positions in glucose that means  $\text{Na}^+$  ion interacts with both  $\alpha$  and  $\beta$ -glucose in a similar fashion [32].

Water affects the dielectric relaxation spectra of polysaccharides. At low temperature, the wet and dry samples of cellulose, starch and dextran show different behavior in terms of dielectric relaxation spectra. Local chain mobility shifted for wet and dry polysaccharides. The studies suggest that drying decreases the relaxation strength which can be explained by their glycosidic linked backbones and their supramolecular structures. Molecular dynamics results were in accordance with the physical parameters [33].

Explicit solvent molecular dynamics is used to determine the conformation of shizophyllan in water. Shizophyllan has  $\beta$  (1 $\rightarrow$ 3) linked glucan with  $\beta$  (1 $\rightarrow$ 6) linked glucose branches which are subjected to conformational change around 7°C in water as a result of an order-disorder transition in the lateral residues. To support this knowledge, hydrogen bonding networks, interactions with water molecules, orientational freedom of residues and orientational correlations were analyzed with molecular dynamics at three different temperatures with two different boundaries. The polysaccharide has a triple helix conformation in water. The limited conformational formation, dense hydrogen bonding network formation at the center of the structure, interchain hydrogen bonding formation



are the driving forces of the stability of the triple helix. By increasing the temperature, moderate and various conformations were observed rather than a sharp transition [34].

To increase the tools for structure function analysis of glycans, hydroxyl groups of glycans are introduced as NMR handles and structural probes. Hydrogen bonds and molecular structure were determined with NMR for a wide range of sample concentrations and temperatures. Molecular dynamics was used to combine the results with NMR. Three detected hydrogen bonds occur from intermolecular interactions. This result may be used for the recognition of glycans by proteins and glycan-glycan interactions [35].

Molecular dynamics is used for polymeric systems to understand the structure of polymers. Polymeric brushes in solvents are studied with molecular dynamics method. The equilibrium structures were compared with the predictions from self-consistent field analysis which determines the energy of the system to predict the conformation. The lower temperature results a phase separation between monomer rich and monomer poor phases. While grafting density and chain length increases, the phase separation disappears. The results are consistent with predictions of density profile, free ends of monomers and the structure factor under good solvents [36].

Self assembled amphiphilic block copolymers are called polymersomes that are developed by many groups to collect information about the nature of self-assembled states. The stability of these structures is studied with respect to both copolymer type and molecular weight. The assemble is analyzed with molecular dynamics simulations and in vivo. Polymersome loading, stealthiness, degradation based disassembly for release control and tumor shrinkage are compared with viral capsids to show the aspects of current and emerging designs [37].

Kremer et. al. presented a bead spring model for a melt of a linear polymer simulated with Monte Carlo simulations. The number of monomers used in this study was between 5-400. The linear polymers were formed as entangled and non entangled with respect to the number of monomers. The dynamics of polymers were defined as Rouse model and reptation model. For single chains, the short length polymers can be defined with Rouse model and while the longer ones with reptation model (thermal motion of very long polymer chains). The simulations results showed that they can estimate the confinement of a polymer and regards the controversy about the interpretation of neutron spin-echo data.

The motion of chains was analyzed and it was possible to visualize the confinement of polymers with different chain lengths [38].

Coarse-grained molecular dynamics simulation is performed for linear polyethylene melts with the length in range of 80-1000 monomers. The dynamics and rheological properties with zero shear rate were investigated and the results were compared with experimental results. The new length scale was proposed which is called slowing down length which is a shorter length from entanglement length. The effective segmental friction increases around slowing down length that leads to increase in diffusivity and viscosity scale. Chain stiffness and interchain interactions caused strong local kinetic constraints as a result of these effects [39].

The polymer and nanoparticle interactions, surface to volume ratio and boundary conditions were explored with coarse grained molecular dynamics simulation to understand the dynamics and structure of the polymer melt. The system consists of bead-spring polymer melt surrounded with nanoscopic particles. The study showed that the chains elongated and flattened near the nanoparticle and this effect does not depends on the interactions studied in the study. The nanoparticles affect the glass transition temperature of a polymer as lower or higher. The increase in surface of the monomer exaggerated the magnitude of the shift in glass transition. The results showed that the surface interactions are dominant in all systems such as ultrathin polymer films or nanofilled polymer melts [40].

Grest and his colleagues proposed an efficient and general algorithm for simulations of polymers which can be used for single, large chains or many chains. The algorithm distinguishes the solvent effects and interchain effects on the dynamics of polymers. The difference in Rouse behavior of ideal chain and real chain was demonstrated for the first time [41].

The diffusion of penetrant molecules through an amorphous polymer was simulated which are methane and polyethylene respectively. The simulation showed that the penetrant molecules stayed in the voids of polymer matrix for a time and jumped to the near void fast. The potential acting between penetrant molecules and polymer was reduced however the motion did not change. Diffusion coefficients were calculated for lower potential systems that exhibits Arrhenius-like scaling behavior. Diffusion coefficients for higher

potentials could be estimated by using scaling behavior. The calculated diffusion coefficients were compared to the values studied before with different model potentials. There are some deviations between the values that might have occurred due to the fact that polyethylene is partially in crystalline state is ignored in the model [42].

In another study, the equilibrium configurational properties of freely moving polymer chains were studied with molecular dynamics simulations. Polymer chains were constructed from linked elastic spheres. The end-to-end distance and radius of gyration values were calculated and the values showed that they vary exponentially with the length of the chain. The results are consistent with Monte Carlo and self-avoiding walk studies. The study suggested that molecular dynamics gives the same quality results as Monte Carlo while preventing the sampling problem [43].

#### **2.4. PRODUCTION OF LEVAN**

Levan can be produced from different bacterial sources by fermentation process. One of these bacteria is *Zymomonas mobilis* used in batch and continuous systems. The effects of parameters on levan production were investigated and optimum values of initial substrate concentration (299.1 g/L), incubation time (42.3 h) and pH (6.0) was found for maximum productivity of levan. Beside of these parameters, lowest dilution rate (flow rate of the medium / bed volume of the bioreactor) results in higher concentration of levan [44]. Sugar cane juice and sucrose was used as substrates in both batch and fed batch processes. *Zymomonas mobilis* was cultivated with different concentrations of these substrates in both processes. The production of levan was improved in batch process and sugar cane juice did not affect the formation of levan. It only increases biomass, sorbitol and ethanol production [45]. Flocculent strain of *Zymomonas mobilis* produces levan at optimum values of sucrose concentration, temperature and pH. Polymer hydrolyses by bacterium at higher pH and high concentrations of levan. Levan is also an important fructose source. Therefore, as the amount of produced levan increases, the fructose amount also increases which induces further production of levan [46].

*Bacillus sp.* has the ability to produce extracellular levansucrase that can be isolated from thermophilic bacterial strain. High molecular weight levan was produced with high concentration from this type of bacteria at 50°C and at the optimum pH value of 6.5.

Sucrose was suggested as a good source for the growth medium [47]. Esawy and her colleagues optimized the levan production from *Bacillus sp.* and analyzed the biological activities of the structure. At pH 8 and in the presence of glucose and yeast, the highest productivity was achieved. The obtained levan showed antitumor activity on different animal and human cancer cells as well as fibrinolytic activity [48].

Levan synthesis is a high cost process therefore the studies attempt to find new resources for production. *Halomonas sp. AAD6* was found to be the only extremophilic bacterium that produces high concentration of levan with sucrose [49]. Additionally, sugar beet molasses and starch molasses were found as fermentation substrate to produce levan instead of sucrose. Produced levan from these sources show characteristic rheological properties at different conditions such as low viscosity and pseudoplastic behaviors. The products were confirmed with molecular characterization and monosaccharide composition as a levan type fructan [50]. Different stimulating factors are analyzed to obtain levan from *Halomonas smyrnensis AAD6T* with high purity to use in industrial applications. Salinity, nitrogen, pH, initial source concentrations, and different production media are found to be effective in levan production. Boric acid increases the sucrose usage and becomes the most effective stimulator in levan production. Conditions of the process in bioreactors are optimized while the chemical structure of levan remains same. Also the biocompatibility of the structures was determined between high range of concentrations. Therefore, *Halomonas smyrnensis AAD6T* is one of the most important microorganism to produce high quality levan [51]. Table 2.1. summarizes the production of levan from different bacterial sources.

Table 2.1. Microorganisms produce Levan [52]

<b>Microorganisms</b>	<b>Source</b>
<i>Aerobacter species</i>	Sucrose
<i>Acetobacter xylinum</i>	Sucrose
<i>Arthrobacter ureafaciens</i>	Sucrose
<i>Bacillus subtilis</i>	Sucrose
<i>Bacillus subtilis (natto)</i>	Sucrose
<i>Bacillus licheniformis</i>	Sucrose
<i>Bacillus methylotrophicus</i>	Sucrose
<i>Erwinia herbicola</i>	Sucrose
<i>Geobacillus stearothermophilus</i>	Sucrose, fructose, glucose, raphinose, glycerol
<i>Gluconacetobacter diazotrophicus</i>	Sucrose
<i>Halomonas smyrnensis</i>	Sucrose, sugar beet molasses, starch molasses
<i>Lactobacillus reuteri</i>	Sucrose
<i>Lactobacillus sanfranciscensis</i>	Sucrose
<i>Leuconostoc mesenteroides</i>	Sucrose
<i>Microbacterium laevaniformans</i>	Sucrose, pulm syrup
<i>Paenibacillus polymyxa</i>	Sucrose
<i>Pseudomonas fluorescens</i>	Sucrose
<i>Saccharomyces cerevisiae</i>	Sucrose
<i>Serratia levanicum</i>	Sucrose
<i>Streptococcus salivarius</i>	Sucrose
<i>Streptococcus mutans</i>	Sucrose
<i>Xanthophyllomyces dendrorhous</i>	Sucrose
<i>Zymomonas mobilis</i>	Sucrose, sugar beet molasses, sugar cane molasses

Another way to lower the cost of production is to find new carbohydrate sources. Commercial sucrose, molasses and sugar cane syrups were compared in production of levan from *Zymomonas mobilis* microorganism. In fermentation media with sugar cane syrup and commercial sucrose, levan production is higher than the medium with molasses.

Sugar cane syrup produced less levan from commercial sucrose however biomass production was higher [53].

## 2.5. LEVAN IN FOOD APPLICATIONS

Antibacterial activities of levan with high molecular weight and also low molecular weight were investigated. Levan structures cause antibacterial activity by themselves. Levan with low molecular weight shows the most antibacterial activity on foodborne pathogenic bacteria. Therefore, levan was added to bread making process. Pathogenic bacteria are also added into bread samples. The viability of these bacteria decreases in bread samples with low molecular weight levan. Levan compounds are proposed as potential sweeteners for reduction in pathogenic contamination [54].

Water-insoluble levan was produced from *Bacillus licheniformis* to be used as selective plugging agent in microbial enhanced oil recovery. Despite *Bacillus licheniformis* can grow on sugar such as glucose, fructose and sucrose, levan was produced only on sucrose. Plugging application can be controlled to produce levan under the conditions. Suitable parameters were optimized for oil reservoirs such that temperature should be less than 55°C, pH between 6 and 9, pressure less than 500 atm and 4% or less salt concentration [55].

Levan has antihyperlipidemic and antiobesity effect as a food additive. It blocks the increase of lipid level in blood and also blocks the increase of body fat. Levan and its partial hydrolysate type were used and they can be prepared as tablets, powders, capsules, etc.[56].

Levan can also be used as a probiotic in food industry. Levan type fructans are produced from *Lactobacillus sanfranciscensis*. It is nontoxic and dissolves in both hot and cold water. Levan type structures changed the composition of gut bacteria during fermentation process. Levan is shown to improve gut function as a probiotic [57].

## 2.6. LEVAN IN COSMETIC APPLICATIONS

In cosmetics, levan produced from *Zymomonas mobilis* shows great effects in skin moisturizing, cell proliferating and skin inflammation. Levan increases the cell viability in bioartificial skin according to cell proliferation test results. Levan shows moisturizing effect almost the same as hyaluronic acid and as well as a similar cell proliferation effect in human fibroblast and keratinocyte cell lines [58].

Levan is used as a whitening ingredient in cosmetics. It has a melanin production inhibitory effect, tyrosinase activity inhibitory effect and pigmentation inhibitory effect [59]. Levan and its complex with drugs can be used to prevent or improve skin disorders such as spots and sunburns. An oral dose of approximately 120-600 mg levan provides allergy inhibitory effects [60].

## 2.7. DRUG DELIVERY

Nanotechnology is expected to enhance all industries including biotechnology. One of the most promising area of nanotechnology is the nanomedicine. Nanomedicine has benefits to human life such as targeted drug delivery, rational drug design and personalized health care [61]. Drug delivery systems are the formulations or tools to deliver the therapeutic substance into the body with higher efficiency by controlling the rate, time and targeted place. The process starts with the administration of the substance, continues with the release of this substance and ends with transport of active agent through the biological membrane. Drugs can be introduced to the body in different ways such as oral, inhalation, transdermal, rectal, parental. The introduced way depends on the disease, the desired effect, and the product. Drugs can be introduced to the unhealthy organ directly or they can be given into that organ systematically [62]. Drug delivery systems are studied to minimize the degradation and loss, to prevent the body from side effects and to increase the bioavailability and accumulation of drug in the required zone [63]. The strategies for formulation of drug delivery systems are designed with different chemical compounds in recent years. The extensive range of bioactive substances emerges as potential drug candidates. The mutual and important aim of formulation is to optimize the systems for providing desired dosage at a chosen rate, at a selected time and to the targeted biological

site [64]. Nanocarriers are for delivery of small molecule drugs and also nucleic acids and proteins. The drug delivery systems will reduce the side effects and increase the efficiency of the use of drugs [65]. Most of the research studies are focused on the carrier systems such as biodegradable polymers, polylactides and composite materials, cells, microcapsules, lipoproteins, polysaccharides [64, 66]. Each of these types has their own advantages and disadvantages therefore it should be chosen according to the whole relevant considerations. These carriers degrade slowly, be stimuli reactive such as temperature or pH and conjugated with the specific antibodies [66]. In drug delivery systems, natural polysaccharides are glaring because of their important properties. Covalent crosslinking, ionic crosslinking, polyelectrolyte complex and self-assembly of hydrophobically modified polysaccharides are four methods to prepare nanoparticles [67]. Delivering the active drug to the targeted site is an important problem in treatment of diseases. The ordinary application of drugs shows less effectiveness, poor biodistribution and lack of selectivity. Therefore, most of the research studies are focused on the control and target of drug delivery methods.

### **2.7.1. Targeted Drug Delivery**

Targeted drug delivery (site-specific) is a method which is studied to deliver the drug to the targeted site effectively and release the drug when it is required. Site targeted drug delivery is divided into three groups; such as first order, second order and third order targeting. First order targeting is the restricted distribution of drug to the organ or tissue. Second order targeting is the delivery of drug complex to specific cell types such as tumor cells and normal cells. The third one is the release of drug with a carrier at preselected intracellular sites [68].

Targeted drug delivery systems is essential to provide high and exclusive accumulation at the targeted site while avoiding the health organs from site effects. The system should be specific so that accumulation can occur only at targeted site. Another important point is retention of active drug at the desired site of the body so that the drug can be more effective [69].

The targeted systems can also be classified as physical targeting, chemical targeting and biological targeting. Physical targeting is delivery of agents to targeted sites because of its



physical properties such as size and composition. This type of targeting can be applied by external factors. Heat, light, ultrasound or magnetic field can be externally applied to the drug to be released. These factors enhance the accumulation in target sites. Chemical targeting uses site specific prodrugs to localize the agents in target sites. The agents can be directed to the target sites by enzymatic or chemical reactions. Biological targeting localizes the agents to target site by using antibodies, peptides, proteins or other molecules. These biological molecules have affinity to receptor sites, organs or other biological sites [69].

This type of drug delivery has an important usage in treatment of cancer. Tumor specific targeting focuses on the remains of drug conjugates inactive until it reaches to the tumor cells. The system based on the interactions of unhealthy cells. Limitation of this system is the lower potential of some drugs after being linked to the targeted cells when the targeted site is not cleaved correctly. Adriamycin conjugates with ethylene glycol are used in cancer treatment. It shows great selectivity to cleavage in tumor cells [70].

### **2.7.2. Controlled Drug Delivery**

The limitations of immediate release dosage of drugs are the unavoidable fluctuations in the drug concentration which may lead to precipitation. Also drugs when administrated frequently increase the risk of missing a dosage. Controlled release drug delivery systems may decrease these limitations. Controlled release drug delivery attempts to control degradation of the drug in the target site. This system delivers and releases the drug continuously for a certain amount of time at a dosage that the body can eliminate. It provides the needed dosage for body without re-administration [71].

The release of drug may be constant for at a period of time, may be cyclic for a long time or it can be initiated by the external forces in controlled drug delivery. The aim of these systems is to increase the efficiency of the drugs by eliminating under or overdosing. Polymers can be used as coatings, to enhance the stability of the drug and to modify release characteristics. Natural or synthetic polymers surround the drug in such a way that the drug releases from the polymer. These systems can be designed as diffusion, erosion, swelling or osmotically controlled release. Polymers are the most important vehicles in drug delivery [72].

### 2.7.2.1. Diffusion Controlled Release

In controlled release, polymers need to be biodegradable. The properties of the polymer such as permeability, biodegradability, biocompatibility and its mechanical properties should be controlled. Polymers can be in glassy state or rubbery state in body temperature. If the polymer is in glassy state which glass transition temperature is above the body temperature, it will be inflexible. Therefore the drug should be released by diffusing through the polymer (Figure 2.4.) [73].

There are two major types of devices to control the release of the drug by diffusion. First one is reservoir and other one is monolithic devices. The simplest form of these devices is polymer based tube filled with the drug and both ends are closed. Rubber silicone, ethylene vinyl acetate copolymers, polyurethane and polyethylene are used for the tubes. Liposomes are produced for this type of drug delivery and these systems are prepared by microencapsulation, spray encapsulation and nanoencapsulation [74].

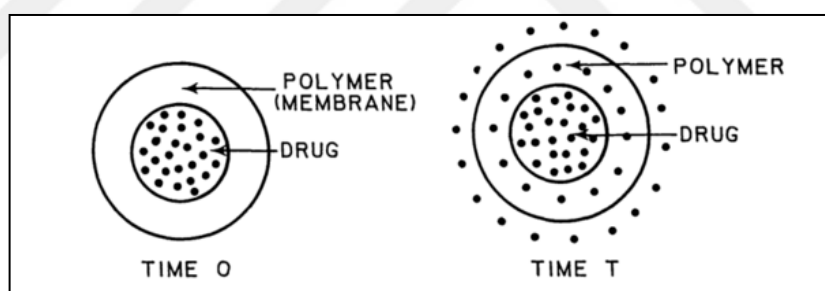


Figure 2.4. Schematic representation of reservoir device in diffusion controlled release [74]

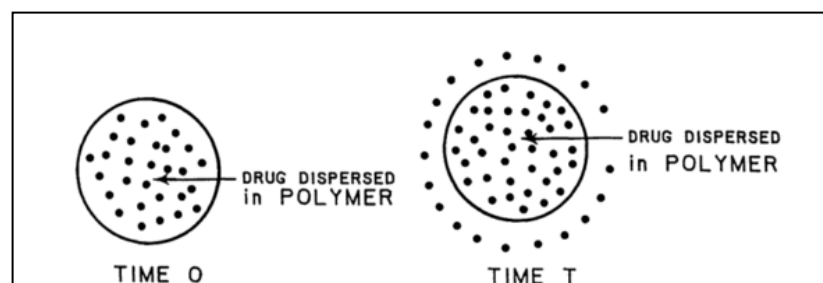


Figure 2.5. Schematic representation of monolithic device in diffusion controlled release

[74]

The other type of device is monolithic device which the drug is distributed through the polymer as in Figure 2.5. The drug can be a separate phase or dissolved in polymer. The same polymers are used with the reservoir devices.

### ***2.7.2.2. Erosion-Chemically Controlled Release***

In erosion controlled release, polymer is also an active participant in the process. The surface of the polymer starts to undergo erosion and drug releases at the same rate with polymer erosion. Figure 2.6 shows the erosion controlled release and these devices can be made by both reservoir or monolithic device. Various polymers are used in these systems such as polyanhydrides, esterified copolymers of methyl vinyl ether and copolymers of lactic and glycolic acids which have bioerodible properties. In chemical reaction controlled release, the drug bonds to the polymer chemically and drug releases by the cleavage of these bonds enzymatically or hydrolytically [74].

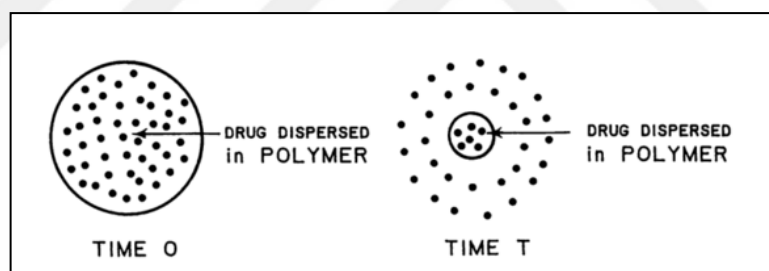


Figure 2.6. Schematic representation of erosion controlled release [74]

### ***2.7.2.3. Swelling Controlled Release***

In swelling controlled release, the size of the polymer membrane is not constant (Figure 2.7.). Therefore the dosage of the drug changes during release process due to the swelling of the polymer. Physically and chemically cross linked polymer gels are used in the design of these systems. By choosing the proper polymer for these systems, it is possible to control the swelling with external parameters such as pH and temperature [75,76].

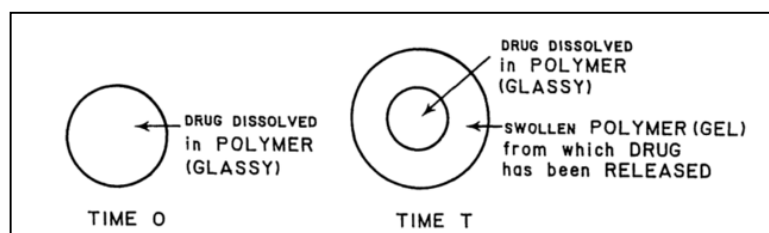


Figure 2.7. Schematic representation of swelling controlled release [74]

#### 2.7.2.4. Osmotic Controlled Release

Osmosis is an important phenomenon which occurs when the membrane is permeable to water, and not to particular solutes. Water flows through the membrane to equalize the concentrations at both sides of the membrane. In osmotic controlled release, drug is covered with semipermeable polymer and exposed to the gastric fluid.

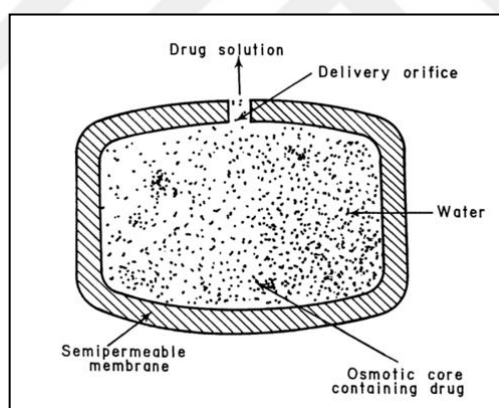


Figure 2.8. Schematic representation of osmotic controlled release [74]

Water flows through the polymer and dissolves the drug in the polymer. The solute concentration changes and drives more water through the polymer. While water flows in, the polymer expands and ruptures because of the osmotic driving force. Drug releases through the delivery orifice as seen in Figure 2.8. The time of release can be designed according to the thickness of the polymer membrane [75].

For drug delivery, the types and release systems are explained at the above sections. These systems are developed to increase the efficiency of the drugs, to decrease the number of

dosage per day and to protect the body from side effects. However these systems have also some limitations and the studies are continued to extinguish them. One of the limitations is while decreasing dosage form, the size of the capsule becomes larger and hard to swallow for oral administrations [77]. Another limitation is that the physical barrier for diffusion process may retain the drugs in the barrier [78]. The degradation of the barrier may be toxic. It will not be a crucial limitation if the purification methods are applied carefully [77]. The research studies on drug delivery systems with polysaccharides are explained in the next section.

### **2.7.3. Studies involving Polysaccharides in Drug Delivery**

In drug delivery systems, natural polysaccharides are the most promising material to use as a nanocarrier. Covalent crosslinking, ionic crosslinking, polyelectrolyte complex and self-assembly of hydrophobically modified polysaccharides are four methods to prepare nanoparticles [79].

Microencapsulation is a simple and cost effective way to capsule bioactive materials with semi permeable polymeric membrane. The purpose of this process is to protect the bioactive material until it is released at the target place. Natural polysaccharides are used as capsules in drug delivery [80].

In drug delivery systems, amphiphilic polysaccharides are more advantageous position because they do not use solvents or surfactants to self assemble. They have intermolecular and intramolecular interactions with water. Hydrophobic segments promote these interactions and provide the formation of these polysaccharides as micelles, nanoparticles, liposomes and hydrogels. Amphiphilic chitosan is one of the most interesting polysaccharides because of its properties such as good biocompatibility, non-toxicity, antimicrobial and bioadhesive properties [81]. Another important polysaccharide used as a carrier is dextran because of its physico-chemical properties and physiological acceptance. Crosslinking or covalent modification are the methods for combination of dextran and drugs [81, 82].

Due to the fact that, polysaccharides are well characterized and produced from natural sources, they are the most promising material in stimuli-responsive drug delivery systems.

Ionic polysaccharides can be crosslinked to obtain hydrogel networks that can be used for switching drug release on-off through diverse mechanisms. Polysaccharide based systems can respond to the hybrids, composites and grafted polymers so they increase the responsiveness and widen the range of stimuli. The effect of pH, ion nature and concentration, temperature, redox potential and magnetic & electric field intensity were studied and it was found that these parameters can regulate the drug release from polysaccharides. Crosslinked ionic polysaccharide networks can be built for delivery of activated drugs and feedback modulated drug delivery systems [83].

Drug delivery systems have great interest for tissue engineering. Biopolymers are essential material to use as nanoparticles because of their properties such as biocompatibility, biodegradability and low immunogenicity. Biopolymers are obtained from polysaccharides, proteins and nucleic acids. Particle size, charge, morphology of surface and release rate of the loaded drugs should be controlled to use these particles in drug delivery systems [84].

Naturally occurring polysaccharides are used for delivery of drugs to human colon. The specialty of colon targeted drugs is the presence of polysaccharides in human colon which is inhabited by the large number of different bacteria. The approaches for colon targeted drugs are fermentable coatings, embedding of the drug in biodegradable mixture and formulation of prodrugs. Different types of polysaccharides such as chitosan, pectin, cyclodextrin, dextran and inulin are studied for these systems [85].

Chitosan is known as one of the most interesting polysaccharide in drug delivery systems because of its properties. Wang and his colleagues synthesized and characterized paclitaxel-loaded nanoparticles based on salicylic acid-grafted chitosan oligosaccharide (COS/SA). The study also includes the molecular dynamics simulations to understand the mechanism of encapsulation of paclitaxel (PTX) by COS/SA process. For drug encapsulation, van der Waals and hydrophobic interactions are major driving forces and also electrostatic and hydrogen-bonding interactions are helpful for COS/SA aggregation. COS/SA nanoparticles are indicated as highly hydrosoluble with respect to the radial distribution and solvent accessible surface area analysis. The nanoparticles can increase the aqueous solubility of hydrophobic drugs. In that work, drug loading systems were studied

and the best theoretical value was found as 10% (w/w). The work provided a new perspective for drug delivery systems for polysaccharides [86].

## 2.8. LEVAN IN DRUG DELIVERY AND BIOMEDICAL APPLICATIONS

Levan produced from *Halomonas smyrnensis AAD6T* is used for encapsulating vancomycin to be potential carrier for antibiotic drugs. To optimize the encapsulation process, three parameters are changed such as drug concentration, polymer concentration and rotating speed. The highest encapsulation capacity was found to depend on polymer concentration. After analysis, vancomycin encapsulated with levan was found to be non toxic at concentrations between 100  $\mu\text{g/mL}$  and 1000  $\mu\text{g/mL}$  [14].

Physicochemical properties of levan structures can be characterized with different instrumental methods after synthesis. Levan structures were produced from *Campanumoea javanica* and *Curcuma kwangsiensis* with molecular weight of 2900 Da and 5300 Da respectively. Their structures were characterized with instrumental methods before biological activity tests. Based on the levan products ability to stimulate macrophage proliferation and enhance phagocytosis it was concluded that levan showed immunostimulating activity and it was proposed as a potential natural immunomodulator [25]. Srikanth and his colleagues characterized their products isolated from *A. xylinum* with FTIR, NMR, TGA and HPLC as levan. In vitro studies showed that levan has potential to be an anti-oxidant and anti-inflammatory agent [87].

The pH and hydrolysis time affect the physicochemical properties of the structure by changing the structural configuration of levan. Runyon et. al., tried to determine the stability of levan by analyzing its properties such as molar mass, root mean square radius, hydrodynamic radius, structure factor and aggregation state in solutions at different pH. Commercial levan produced from *Z. Mobilis* was used. The structure was characterized with asymmetric flow field flow fractionation (AF4) online multiangle light scattering (MALS) and differential refractive index (dRI) detection methods. The results showed that levan structures formed two different populations in the solution. One of them was formed by high molar mass structures and the other one was formed with low molar mass. Random coil configuration was indicated for low molar mass population. High molar mass population had more homogeneous spherical structures due to asymmetric flow field flow

fractionation (AF4) results. Fructose formation was observed to determine the stability of levan under different pH conditions. Acid hydrolysis was observed at lower pH condition however at pH 5.5 and higher, no hydrolysis was observed [88].

Vina et. al. analyzed some rheological properties and stability of viscosity of levan solutions obtained from *Zymomonas mobilis* strain 113 "S". Viscosity of solutions can be affected by temperature, pH and salt concentration. The viscosity of levan solutions decreases 1-3% in very acidic media however, returns to normal level at room temperature at pH range between 4 and 11. Salt concentration slightly affects the viscosity of levan solutions. At high temperature, the viscosity is also stable however it is not reversible. Irreversible degradation of levan is obtained at temperatures higher than 70°C and pH value less than 3.5 [89].

Levan can be used as a coating material for microelement nanoparticles to obtain complex that has biological functions. Levan is synthesized from *Pseudomonas syringae* and selenium, iron and cobalt nanoparticles are coated with levan. Dispersion of nanoparticles is achieved upon stabilization by levan and the toxicity of these nanoparticles decreases upon coating. Cobalt nanoparticles coated with levan increases the solubility of the colon bacterium. Nanoparticles coated with levan can be used as food supplements. As a food supplement, levan delivers the nanoparticles safely and efficiently in human body [90].

Levan is a natural polymer which is important for bacterial biofilms. Benigar and his colleagues reported the structural and rheological properties of levan solutions produced from *Zymomonas mobilis*, *Erwinia herbicola* and *Bacillus subtilis*. Viscoelastic properties were obtained from low polymer concentrations and they were checked by X-ray scattering data. At molecular level, the structural differences were analyzed and structural information about polymer systems was obtained. At low concentrations, levan solutions showed Newtonian-like behavior however it showed strong elasticity properties due to strong intramolecular forces. Branching or hydration did not affect the properties of levan obtained from different sources. Levan forms large particles in aqueous solutions therefore they showed low intrinsic viscosity values [91].

Lewis lung carcinoma cells were treated with levan to decrease the oncogenicity of these cells. Direct antitumor effect of polysaccharide levan was studied in mice with different concentration and temperature of incubation. The increase in dose of levan decreases the



extent of tumor. The different temperature and speed of incubation did not affect the reduction in oncogenicity. Levan degraded the tumor cells physically, it did not change the chemical structure of the tumor cells [92]. Leibovici and his coworkers also studied the antitumor mechanism of levan on Lewis lung carcinoma cells. They showed the reduction in tumor incident with levan preincubation which is independent of tumor size [93]. Another study is about the viability of cells during incubation of the tumor cells with levan. DNA, RNA and proteins were not affected however thymidine, uridine and leucine transports were affected. These results show the direct antitumor effect of levan on Lewis lung carcinoma cells [94].

Another curative study about levan shows antioxidant effect and protection effect from cardiovascular disease such as atherosclerosis caused from oxidative stress. The antioxidant effect of levan was shown on high cholesterol mice group by the increase of superoxide dismutase and catalase. Lipid profiles are also positively changed in mice groups with levan. This study shows that levan may have antioxidant effect and protection against atherosclerosis [95].

The product consists of levan and poly- $\gamma$ -glutamic acid of soybeans fermented with *Bacillus subtilis* shows anti-tumor and immunomodularity effects however the structures were not chemically pure. Therefore, the mechanisms of these effects are not well-understood. After the products were purified, they were tested in vitro and in vivo in mice. The study showed that levan has immunomodularity effect on Toll-like receptor 4 signaling and it can be used for protection from allergic disorders [96].

## **2.9. APPLICATIONS OF LEVAN DERIVATIVES**

Derivatives of levan are polymers made by adding cationic or noncationic substituents with chemical reactions. Levan derivatives can be produced as sulfated, phosphated or acetylated that was asserted as anti-AIDS agent and is useful in personal care industry. These derivatives are produced in amounts of 0.2 to 3 sulphates, phosphates and acetates per each fructose ring. They may be used as inhibitors in cell proliferation, excipients in tablet making and they are also used as agents to transform water into gel form [97].

*Bacillus subtilis* NRC1aza produces two types of levan with different molecular weights. Fattaha et. al. studied antitumor and antioxidant activities of these structures and their sulfated derivatives. The structures were confirmed with paper chromatography and HPLC. The levan and its derivatives show high antioxidant activity on 2,2-diphenyl-1-picrylhydrazyl-hydrate (DPPH). Levan derivatives have anti-tumor effect on liver cancer cells. Fattaha et. al. proposed levan and its derivatives as possible antioxidant and anti-tumor agents [98].

Nanostructured thin films to be used as coating material were produced from original levan structure and its oxidized form. Oxidized form shows higher hydrophobic behavior than pure levan structure because of its aldehyde groups. Oxidized levan has a high potential for cell proliferation for all coatings [5].

Levan is also derivatized as acetylated levan, phosphorylated levan and benzylated levan from endophytic bacterium *Paenibacillus polymyxa* EJS-3. The antitumor and antioxidant properties were compared with original levan structure. The derivative forms of levan increases the antitumor and antioxidation effect because of acetyl, benzyl, and phosphoryl groups in the structure. These groups increase electron donating ability and affinity with the receptors in immune cells [99].

Phosphonated levan and chitosan were fabricated using layer by layer assembly to achieve long term adhesiveness. The charges of chitosan and phosphonated levan were measured and the feasibility of construction of layers was monitored. Phosphonated levan films had smooth and homogeneous surfaces. Alginate and chitosan layers were used as a control and phosphonated levan showed more adhesive properties than the control layers [100].

The potential anti-cancer activity of levan and oxidized levan produced from *Halomonas smyrnensis* AADT6 was investigated in vitro. By periodate oxidation method, the aldehyde groups are formed in the structure. Depending on cell type, degree of oxidation is found to increase the anti-cancer activity of levan. Levan-based polymers can be used as potential anti-cancer agents [101]. Levan produced from *B. licheniformis* also shows hypoglycemic activity, antitumor and anti-cytotoxic effect [102].

Natural or modified polysaccharides are important biopolymers which are used as a clot inhibitor. Heparin is the most important anticoagulant. Levan obtained from *Halomonas smyrnensis* AADT6 was modified to integrate sulfate groups in the structure. The

anticoagulant tests were applied to understand the activity of sulfated levan. The results showed that levan has an anticoagulant activity similar to heparin [103].

Limited success of current technologies in analyzing the 3D structure of polysaccharides promoted the use of computational methods in structure-function studies. The main objective of the work is to study the conformations of levan-based polymers in different media, and different conditions by using molecular dynamics (MD) simulations. It is aimed to integrate various levels of information about these biopolymers to be used in potential drug delivery systems with the structure-function analysis based on molecular dynamics simulations.



### 3. METHODOLOGY

#### 3.1. CONFORMATIONAL ANALYSIS

Conformational analysis is the study of structure of a molecule and their effects on its physical, chemical and biological properties. The conformations of the molecules determine their dynamic behavior. This requires to locate the atoms at the minimum point of energy surface, so energy minimization has a crucial role in these analysis. Once the energy minimization of the atoms is complete, this structure can be taken as the starting structure for the dynamic simulations [104].

Disaccharides and polysaccharides are the most abundant biomolecules in life so that their structural analysis is important to determine their structure-function relationship. There are several studies about polymer properties, biological functions in water and other solvents with molecular dynamics. Pereira and co-workers studied eight different disaccharides to determine their conformational dynamics and compare their dynamic properties with molecular dynamics. They also validated their simulation parameters with experimental data [21, 23].

Combination of experimental and theoretical data is the most capable approach to study the conformational analysis of polysaccharides. The accessible conformations of levan and inulin were studied by Alfred French with a computer program called NHMAP. This study determined the conformations by rating a model that can meet glycosidic bond-angle and hard-sphere, interatomic-distance criteria. The rotations about three single bonds of each polymer allow different molecular shapes. Inulin and levan models chirality was determined as right-handed and left-handed, respectively [105].

In this study, conformational analysis was applied to levan and sulfated levan in vacuum and media with different salinity and temperature to understand the relation between their biological activity and structure with molecular dynamics simulations.

### 3.1.1. Molecular Dynamics

Polysaccharides and carbohydrates/protein complexes have become increasingly important in the development of drugs. Characterization of three dimensional structures of these complexes is difficult with the methods of today's technology. Polysaccharides have several conformational variations due to structural properties [106]. X-ray crystallography and NMR spectroscopy lead to different results in the analysis of polysaccharides, oligosaccharides and their conjugates. For this reason, the relation between the structure of glucans and their biological functions cannot be precisely determined. In the last years, Molecular Dynamics (MD) simulations are used to retrieve comprehensive information to understand the conformations of glucans and their dynamic properties [107,108].

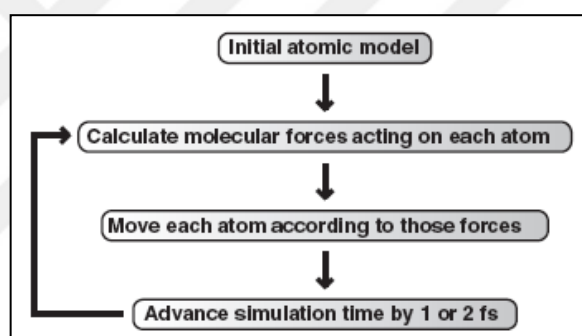


Figure 3.1. Molecular Dynamics Flow Chart [110]

To solve scientific problems, computer simulations are useful and predictive tools utilized in recent years. These simulations are performed with the aim of reproducing experiments to express microscopic details, to explain experiments and also to interpret the structures from X-ray crystallography and NMR experiments. Monte Carlo, Brownian dynamics and molecular dynamics are the most widely used methods. Molecular dynamics method has become a feasible and useful method to understand the time dependent behavior of chemical and biological systems. These simulations are performed together with experiments because of the spatial and temporal resolutions in wide range. Molecular dynamics calculates the dynamics of the systems in real. From calculated forces on each atom, the acceleration is determined with Newton's law of motion. Integration of these

equations yields a trajectory that shows how the position, velocity and acceleration changes with time [109].

### 3.1.1.1. Force Fields

Molecular forces calculated in the second step of Figure 3.2. are based on classical mechanical equations of force. Force field is the parameter set to describe the potential energy of the system. General class of force fields which is applied to the carbohydrates is the potential energy of the system that is expressed as a total energy of bond stretching, angle bending, torsional and non-bonded interactions.

Force fields include both bonded and non-bonded interactions as seen in Figure 3.2. The atomic forces can be classified as bonded and non-bonded interactions. Bonded interactions are the forces between chemically bonded atoms. These are bond stretching, angle bending and torsion. Non-bonded interactions are not related to the bonding interactions of atoms. The non-bonded interactions consist of electrostatic interactions and van der Waals forces. Generally, Coulomb potential is used for electrostatic interactions and Lennard-Jones is used for van der Waals interactions [110].

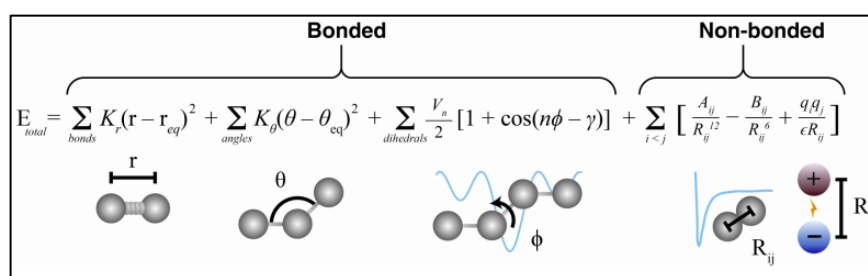


Figure 3.2. An example of an equation used to calculate the atomic interactions [110]

CHARMM [111], AMBER [112], GROMOS [113] and Polymer Consistent Force Field (PCFF) [114] are commonly used force fields for biomolecular systems [115,116]. The main difference between these force fields is the non-bonded interactions term. PCFF has 9-6 Lennard Jones potential which is parametrized for alkyl chains, organic residues and polymers and others force fields have 12-6 Lennard Jones potential as non-bonded

interaction term which is for biological and organic molecules [117]. PCFF with 9-6 Lennard Jones was used in this study because it is the most appropriate force field for polymer systems.

$$\begin{aligned}
 E_{\text{pot}} = & \sum_{ij\text{bonded}} \frac{1}{2} K_{r,ij} (r_{ij} - r_{0,ij})^2 + \\
 & \sum_{ijk\text{bonded}} \frac{1}{2} K_{\theta,ijk} (\theta_{ijk} - \theta_{0,ijk})^2 + \frac{1}{4\pi\epsilon_0\epsilon_r} \sum_{\substack{ij\text{nonbonded} \\ (1,3\text{excl})}} \frac{q_i q_j}{r_{ij}} + \\
 & \sum_{\substack{ij\text{nonbonded} \\ (1,3\text{excl})}} E_{0,ij} \left[ 2 \left( \frac{r_{0,ij}}{r_{ij}} \right)^{19} - 3 \left( \frac{r_{0,ij}}{r_{ij}} \right)^6 \right]
 \end{aligned}$$

Figure 3.3. Energy equation used in PCFF [118]

### 3.1.1.2. Verlet Algorithm

Molecular dynamics simulations are widely used to understand the dynamic behavior of the systems. The efficiency of this method depends on the numerical integration algorithm. There are several algorithms that have been proposed that split into two groups, explicit and implicit algorithms. Runge-Kutta method is one of the most used in implicit algorithms. It is hard to implement however it is more stable than explicit algorithms. Explicit algorithms are easy to use but they become unstable when integration time step is increased. For larger systems, larger time step size is needed so explicit algorithms are useful for large molecular systems. The most used explicit algorithm is Verlet algorithm [119, 120]. It is chosen because of its compatibility for simulating large systems with molecular dynamics simulator.

In traditional molecular dynamics simulations, algorithms are used in order to integrate the equations of motion. Verlet algorithm is a direct integration of the second order equations of motion with using current positions, accelerations and previous positions. At first, the new position is calculated from equations of motion, then new acceleration is calculated for new position using equation 2.1 to 2.3. The new velocity is computed from the average of the two accelerations [119].

$$r(t+\Delta t)=r(t)+\Delta t v(t)+\frac{\Delta t^2 a(t)}{2} \quad (2.1)$$

$$a(t+\Delta t)=\frac{F(t+\Delta t)}{m} \quad (2.2)$$

$$v(t+\Delta t)=v(t)+\frac{1}{2}\Delta t(a(t)+a(t+\Delta t)) \quad (2.3)$$

### 3.1.1.3. Ensembles

In these computational studies, ensemble describes all possible systems with different microscopic states but have the same macroscopic and thermodynamic states. There are different ensembles used in molecular dynamics simulations [121]. NVT ensemble was used to simulate the systems in this study to obtain constant density and kinetic energy that may affect the equilibrium of the systems.

Table 3.1. Ensemble Types [121]

	<b>Micro Canonical Ensemble (NVE)</b>	<b>Canonical Ensemble (NVT)</b>	<b>Isobaric- Isothermal Ensemble (NPT)</b>	<b>Grand Canonical Ensemble (<math>\mu</math>VT)</b>
<b>Number of Atoms (N)</b>	✓	✓	✓	
<b>Volume (V)</b>	✓	✓		✓
<b>Temperature (T)</b>		✓	✓	✓
<b>Pressure (P)</b>			✓	
<b>Energy (E)</b>	✓			
<b>Chemical Potential (<math>\mu</math>)</b>				✓



#### 3.1.1.4. Periodic Boundary Conditions

Molecular dynamics simulations give information about biological systems in macroscopic view. Periodic boundary conditions are applied in simulations to minimize the surface effect in a finite system. As seen in figure below, there is a central unit contained with the systems atoms. In three dimensions this central unit is replicated. When an atom leaves the unit from any edge of the unit, it is considered to enter from the opposite edge of the neighbor unit with the same velocity. This condition enables the atoms move freely in the system and keeps the number of atoms constant during the simulation [119, 120, 121].

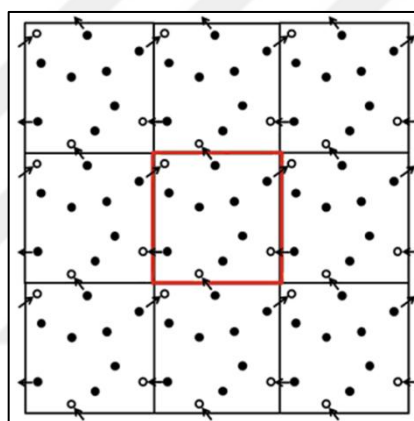


Figure 3.4. Periodic Boundary Condition [121]

#### 3.1.2. Explicit & Implicit Systems

The systems prepared for computer simulations may have different complexity levels. It can be a simple lattice model or large molecules with explicit solvent. Explicit solvent simulations typically require enormous CPU time because the solvent molecules are defined with atoms and bonds in the simulation boundaries which make the systems bigger. To reduce the systems size, many recent studies have been carried out with implicit solvent models. Implicit systems apply the method of representing medium as a dielectric constant calculated from electrostatic interactions instead of using individual molecules. Total number of atoms in the system decreases in implicit systems so that it saves time and computer power. However, implicit systems ignore specific short range effect. It is less

accurate than explicit systems. It is still a question whether implicit models can predict the system's thermodynamics or kinetic parameters as predicted in explicit models. Therefore, each system should be tested for implicit model compatibility [123,124].

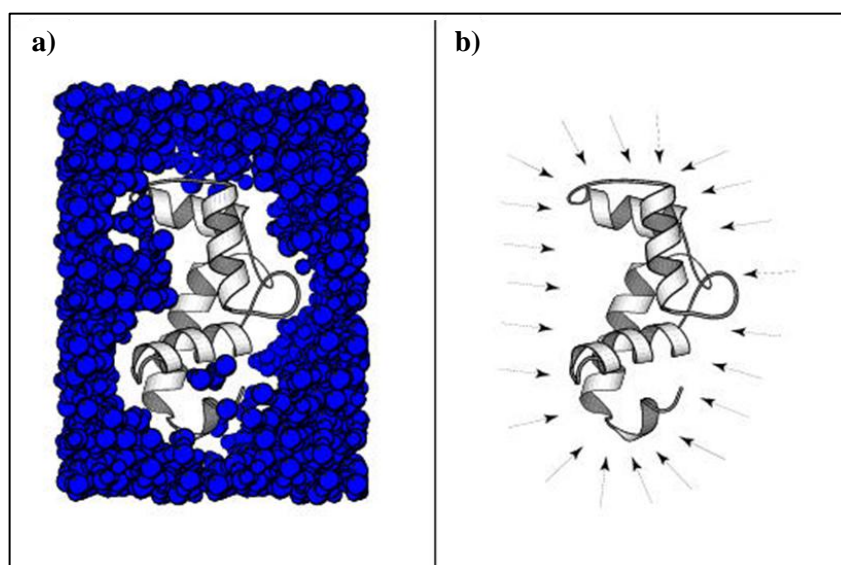


Figure 3.5. Schematic representation of a) explicit and b) implicit systems [125]

### 3.1.3. Berendsen Thermostat & Barostat

In molecular dynamics simulations, the systems temperature and pressure is kept constant with different thermostat and barostat algorithms to generate statistical ensembles. Stochastic Langevin, Andersen, Berendsen and Nose Hoover thermostats are the other examples that used in molecular dynamics. Nose Hoover, Parrinello-Rahman and Berendsen barostat are the most common barostat types [126]. The aim to use constant temperature is to mimic similar experimental conditions, to simulate temperature dependent systems, to discharge the heat for non-equilibrium systems and to increase the efficiency of conformational research. [127]. Thermostats can be local or global. Local thermostat disperses the energy on spatially scale, on the other hand global thermostat disperses energy uniformly. The advantage of global thermostat is that it does not disturb the dynamics of the system [128]. Berendsen thermostat is time irreversible, smooth (continuous velocity trajectory) and deterministic (predictable). This thermostat is suitable for canonical ensemble systems. Thermostat and barostat have large range of usage instead

of calculating with respect to volume and energy so algorithms are formed for keeping both variables constant. Berendsen et. al. presented reliable algorithms for temperature and pressure which are easy to implement[129]. Therefore in this study, Berendsen thermostat and barostat were chosen. Berendsen Thermostat rescales the velocities and barostat rescales the dimension decrease the fluctuations in temperature and pressure [126].

### 3.1.4. Chain Characteristics

#### 3.1.4.1. End-to-end Distance and Radius of Gyration

Polymers are made of atoms connected with covalent bonds which have ability to rotate resulting in a number of different conformations. Therefore it is hard to define the shape of the polymers. To analyze these conformations on a microscopic scale, it is important to understand the properties of the polymer. Some concepts are defined to analyze the structure of these polymers. Random chains are defined with two different measurements. End-to-end distance and radius of gyration is the common measurements of random polymer chains [130]. The end-to-end distance is used to calculate the distance between terminal atoms. The end-to-end distance of a polymer would be small if the chain becomes a tight ball shape. But if the chain is in a good solvent, polymer expands and terminal groups are separated so that the end-to-end distance would be greater [131]. Solvent quality describes the interactions of polymer chains and solvent molecules. It affects the dynamics of the polymer system and depends on salt concentration, temperature, charge and length of the polymer [132]. The size of the polymer depends on solvent quality. Good solvent expands the polymer, poor solvent tightens the polymer. Theta solvent is between these two solvents and all polymers dissolve in theta solvent. Linear random coil expansion factor,  $\alpha$ , defines the quality of solvent and it is equal to 1 for theta solvent [130]. The expansion factor can be expressed as below:

$$\langle r^2 \rangle = \alpha \langle r^2 \rangle_0 \quad (3.1)$$

If the polymer expands in a solvent, the end-to-end distance of the polymer increases, therefore  $\alpha$  should be higher than 1. If the polymer is in a poor solvent, it shrinks and the

end-to-end distance of the polymer decreases which results an  $\alpha$  value lower than 1 (Figure 3.6) [128].

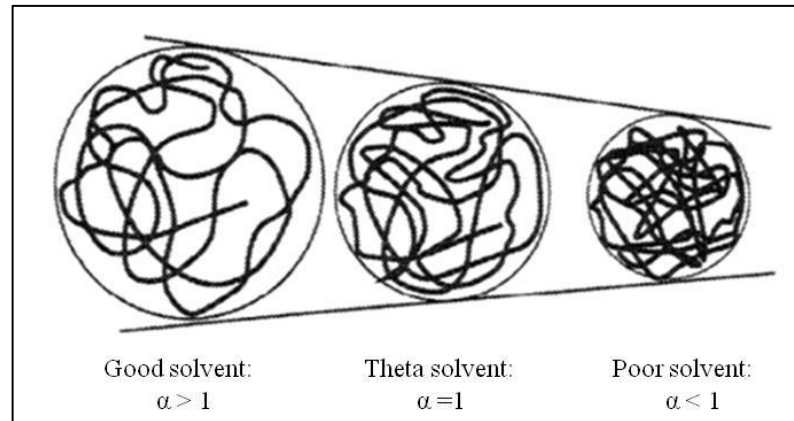


Figure 3.6. Random coils in different solvents [130]

One of the other important concepts is radius of gyration about the center of mass that describes the dimensions of a polymer chain. It is an alternative to measure the size of a polymer which can be experimentally determined with light scattering. A macromolecule is defined to have  $i$  number of atoms of mass  $m_i$ , located at a distance  $s_i$  to the center of mass (Figure 3.7). The square of radius of gyration is defined as the square distance between the atoms and the center of mass [133,134].

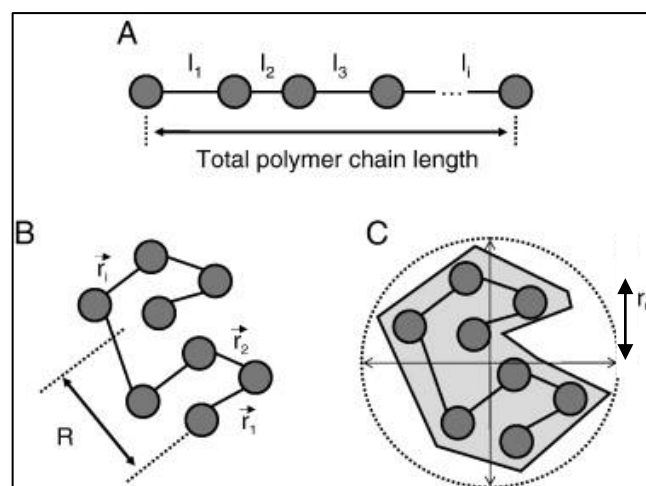


Figure 3.7. Representation of end-to-end distance ( $R$ ) and radius of gyration ( $R_G$ ) [135]

These concepts were used to investigate the conformational properties of long linear polymers in different solvents. Long chain polymers were simulated and the effect of solvents on these concepts was understood [136,137].

### 3.2.4.2. Bond Torsion

Polysaccharides are joined monosaccharides more than one unit together with glycosidic bonds. Glycosidic bonds are a part of the backbone of the structure and they can be easily described with symbols and locants. For levan structure it is described as  $\beta$  (2 $\rightarrow$ 6). The conformations of the polysaccharides differentiate by the location of the glycosidic bonds. Therefore glycosidic bonds are the most flexible bonds in polysaccharide structures [21]. Torsion angle is the angle between two planes. In biomolecules, these planes are formed by choosing four atoms to be consecutively bonded with glycosidic bonds. There are three rotatable bonds in the structure of levan. These bonds are called  $\phi$  (phi),  $\psi$  (psi),  $\omega$  (omega) (Figure 3.8).  $\phi$  and  $\psi$  are required to describe the glycosidic bond from  $i$ th unit to a carbon atom located in the ring of the  $(i-1)$ th unit.  $\psi$  uses the ring oxygen as a reference atom to be specified about the bond from anomeric carbon to the oxygen that joins two units.  $\omega$  is also important when the glycosidic bond forms with a side chain, rather than a ring carbon. (In levan, these angles are O5-C2-O6-C6, C2-O6-C6-C5 and O6-C6-C5-C4 respectively [2]).

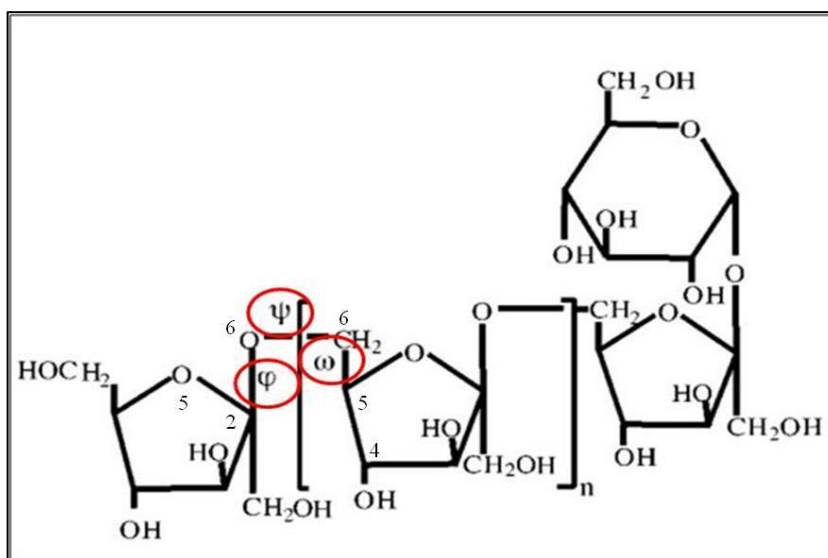


Figure 3.8.  $\phi$  (phi),  $\psi$  (psi),  $\omega$  (omega) bonds for levan structure[2]

### 3.1.4.3. Bond Length

Theoretical and experimental studies determine the nature of polymers, influence of chain structure and composition of polymers in terms of local interactions. These are based on bond length, bond angle and torsion angle distribution. These characteristics of polymers are associated with functional properties. Average end-to-end distance can be calculated from simple bond lengths of a polymer coil. A simple bond length cannot be assumed for more complicated backbone structures like polysaccharides, therefore average end-to-end distance cannot be calculated from bond length directly [138].

### 3.1.4.4. Chord Length

Chord length is an important description for the molecules free path motion. Chord means the length between two faces of the structure. Schematic representation of the chord length is showed in Figure 3.9. It is related to the transport properties of structures in porous media. It helps to define the topology and geometry of polymer chains [139].

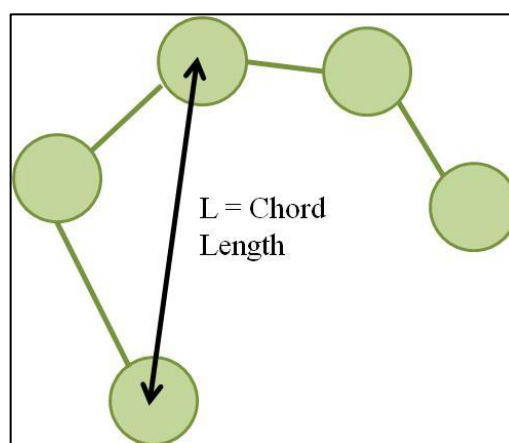


Figure 3.9. Schematic representation of chord length [139]

### 3.1.4.5. Mean Square Monomer Displacement (MSMD)

Mean square displacement is another important quantity measured in molecular dynamics. In this quantity, the plot of the mean square displacement with respect to time shows power law depending on the regime of the polymer chain. Mean square displacement was

calculated as time dependent on center of mass of every single levan chain. The displacement chain's center of mass was shown as  $g_3(t)$ .

$$g_3(t) = \langle [r_{\text{com}}(t) - r_{\text{com}}(0)]^2 \rangle \quad (3.2)$$

The mean square displacement of middle monomers of the chains are  $g_1(t)$ ,

$$g_1(t) = \langle [r_1(t) - r_1(0)]^2 \rangle \quad (3.3)$$

and middle monomer of every single chain with respect to the center of mass of the chain is  $g_2(t)$ ,

$$g_2(t) = \langle [r_1(t) - r_{\text{com}}(t) - r_1(0) - r_{\text{com}}(0)]^2 \rangle \quad (3.4)$$

This quantity was also calculated for two end monomers of the chain  $g_4(t)$ ,

$$g_4(t) = \langle [r_{\text{end}}(t) - r_{\text{end}}(0)]^2 \rangle \quad (3.5)$$

And the displacement of these monomers with respect to the center of mass of the chain is shown below.

$$g_5(t) = \langle [r_{\text{end}}(t) - r_{\text{com}}(t) - r_{\text{end}}(0) - r_{\text{com}}(0)]^2 \rangle \quad (3.6)$$

By using equation derived by Einstein, translational diffusion coefficient was evaluated which is the purpose of the simulations. Translational diffusion coefficient (Eq. 3.7) of the center of mass is an important property to understand the flexibility of polymer chains in solvents in polymer dynamics.

$$D = \frac{1}{6} \lim_{t \rightarrow \infty} \frac{\langle [r_{\text{com}}(t) - r_{\text{com}}(0)]^2 \rangle}{t} \quad (3.7)$$

[140, 131]

### 3.1.6. Radial Pair Distribution Function (RDF)

Radial distribution function is useful to determine the structure of a system. The pair distribution function,  $g(r)$ , gives the probability of finding an atom at a distance of  $r$  from another atom, in a shell  $dr$  compared to the ideal gas distribution. The volume of the shell is:

$$V = \frac{3}{4}\pi(r + \delta r)^3 - \frac{3}{4}\pi r^3 \quad (3.8)$$

$$= 4\pi r^2 \delta r + 4\pi r \delta r^2 + \frac{4}{3}\pi \delta r^3 \approx 4\pi r^2 \delta r \quad (3.9)$$

The number of atoms in the volume element varies as  $r^2$  if the number of particles per unit volume is  $\rho$ . The radial distribution function of a liquid is intermediate between the solid and the gas, with a small number of peaks at short distances, superimposed on a steady decay to a constant value at longer distances. Higher radial distribution functions are rarely calculated. In molecular dynamics simulation, the radial distribution function can be calculated as the neighbors around each atom or molecule are sorted into distance and then the number of atoms in each distance is averaged over the entire simulation. This calculation can be done during the simulation or during the analysis of generated data. The radial distribution function can be experimentally measured using X-ray diffraction [104].

Figure 3.10 shows a pattern of peaks that is characteristics of an atomic system. At the beginning, the graph starts from zero for smaller  $r$  values than the atomic diameter as a consequence of the strong repulsive forces. The graph tends to reach unity at very large  $r$ . The peaks in the graph show the shells of neighbor atoms around the reference atoms. Integration of the first coordination shell estimates the number of the nearest neighbors as coordination number. The concept of shell and coordination number is a useful measure for liquids and solids [141].



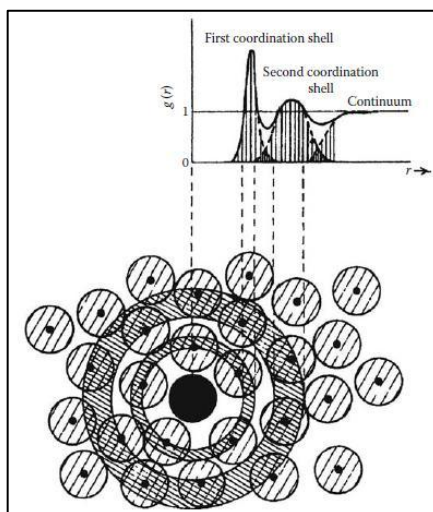


Figure 3.10. The representation of radial distribution function [142]

Radial distribution function is an important measure to obtain several thermodynamic quantities such as energy and pressure. It is a common analysis method however it uses too much computer power to be calculated. Therefore Levine and coworkers presented an implementation of radial distribution histogramming scheme for multiple graphical processing units. The algorithm is executable in VMD that is freely available software package for molecular dynamics [141].

### 3.1.7. Student T-Test

Statistical analysis is performed for understand whether the difference between samples is meaningful or not. T-test is any statistical hypothesis test in which function of the sample follows Student's t distribution if the null hypothesis is supported. Null hypothesis means there is no relationship between the samples. In the significance testing approach of Ronald Fisher [142], a null hypothesis is potentially rejected or disproved on the basis of data that is significantly under its assumption, but never accepted or proved. The p-value is the probability to reject the null hypothesis. This probability reflects the measure of evidence against the null hypothesis. Small p-values correspond to strong evidence. If the p-value is below a predefined limit, the results are designated as statistically significant. The level of significance of 0.05 or 0.01 (or 5%, 1%) is often chosen depending on the size of the data set. If the p-value is less than this limit, the result is significant and it is agreed that the null

hypothesis should be rejected and the alternative hypothesis that there is a difference is accepted. The specification of the level of significance also fixes the probability that the null hypothesis is wrongly rejected [143]. This test is applied to confirm the significance of the results. However the size of data is higher than 2000 data points the significance level is chosen as 0.0001.

### **3.1.8. Docking**

Docking is a computational approach to bind small molecules to macromolecules and score the binding modes to identify the biologically active molecules [144]. This method became popular in 1990s with increasing in the number of X-Ray crystallized structures. The aim of docking is to predict the binding modes and conformations between a ligand and a binding site of a receptor [144].

This method consists of two main parts. These are posing and scoring. In posing part, the algorithms try to place the ligand into the active site of the receptor by all possibilities of different conformations and rotations. A score is calculated for each pose to find the appropriate binding affinity of the ligand. The essential assumption is that the best score belongs to the correct conformation of the ligand and the receptor [145].

The simplest scoring function is based on how good the ligand fits the active site of the receptor. It is a shape-based approach to score the poses. This approach is quicker but results in a less accurate scoring function. Most other scoring functions are based on energy equations. These calculate the score based on Gibbs free energy or binding energy. The most accurate score includes entropy and solvation terms [146]. There are not any docking studies with levan so there is lack of information about these systems. Anticoagulant effect of sulfated levan, similar to heparin is experimentally shown and in this study, docking is used to determine the interactions of levan, sulfated levan and thrombin at the molecular level to computationally show the anticoagulant effect of sulfated levan.

## 3.2. COMPUTATIONAL WORK

The natural chemical and biological properties of oligosaccharides and polysaccharides that provide their biological functions make them one of the most challenging class of molecules for conformational analysis. Computer simulations are performed to understand the structure of polymers and relation between the structure and the biological functions of these polymers. Molecular dynamics is used in this study for conformational analysis of levan based biopolymers. For this method, Xenoview software [147] was chosen because it simplifies creating structures and analyzing simulation results with its graphical user interface and tools. However, for large systems, simulations can be time consuming in Xenoview. All simulations created with Xenoview Software Package have been converted to LAMMPS program [148] and then further simulated. The trajectory files were visualized with Visual Molecular Dynamics (VMD) [149]. SwissDock and UCSF Chimera were used for docking studies [150, 151]. The computational simulations in this study were performed at TUBITAK ULAKBIM, High Performance and Grid Computing Center (TRUBA resources) [152].

### 3.2.1. Xenoview

Xenoview is a free software to create molecular structure, to visualize the structures, to run simulations and to analyze the results. It has Graphical User Interface to see the processes before, during and after the simulations on the screen. After configuration of Xenoview, energy minimization, molecular dynamics and normal mode analysis and some other modules are included. These modules help the users to start Xenoview easily.

In energy minimization and molecular dynamics modules, DISCOVER/CERIUS force fields and data formats are used. When the structure is saved, two text files are created with different file formats. These files are \*.car and \*.mdf that includes atomic positions and description of covalent bonds between atoms respectively. The third file is necessary for run a simulation in molecular dynamics. The input file (\*.inp) is used to start the simulation. The structures can be saved another additional file formats (such as pdb, Imp, lmi, etc.). The structures can be loaded from \*.car and \*.mdf files or converted from other file formats like pdb and ASCII text file with atom coordinates [147].

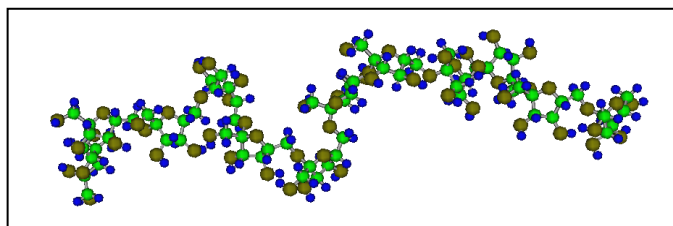


Figure 3.11. Levan Structure in Xenoview

In this study, this computer program is used to prepare and minimize the energy of the systems before simulating. Fructose units were created by choosing appropriate atoms and bonds before creation of levan structure. By bonding these units the levan structure of desired length is formed. The simulation box was chosen as  $60 \times 60 \times 60$  Å and then it was filled with water molecules and approximate number of  $\text{Na}^+$ ,  $\text{Cl}^-$  atoms to obtain the desired medium. After the systems were prepared, energy minimization was applied until the systems energy became stable.

### 3.2.2. LAMMPS

LAMMPS has parallel algorithms that can be used in complex molecular dynamics simulations. These algorithms are on-the-fly computation of thermodynamic quantities and transport coefficients, triggering of neighbor list construction by atom movement, and multiple-timescale methods. Little modifications can be applied to be used for more complex systems such as more sophisticated time integrators, and other statistical ensembles besides the constant NVE ensemble of the benchmark, e.g. constant NPT simulations [148].

LAMMPS simulation program is used to simulate the prepared systems in this study as its parallel algorithms decrease the simulation time and also it is free.

### 3.2.3. Visual Molecular Dynamics (VMD)

VMD is a visualization and analysis software for large biological systems such as proteins, nucleic acids, etc. Molecular dynamic studies are used for biological systems therefore

their results generate large trajectory files which represent dynamic data of the systems. VMD has been developed to visualize and analyze the large trajectory files of biological systems. There are functions in the program to analyze the structures and trajectories. These functions can be used to modify or determine the characteristics of the structures. More complex analysis can also be done such as computing root mean square (RMS) deviation or correlation functions. VMD has a complete graphical user interface and also text interface for program control. By generating input scripts high resolution raster images are produced. This software is designed to animate molecular dynamics trajectories imported from files. It is written in C++ using object-oriented design and is freely available [149].

VMD is used to visualize the simulated systems. This visualization program was chosen because of its compatibility with LAMMPS trajectory files.

#### **3.2.4. Python**

Programming is writing an algorithm and encoding it in a notation to be executed by a computer. Algorithms give a description of the solution in a problem. It is in terms of the needed data to represent the problem and the set of steps to produce the result. There are many programming languages however they must provide a notational way to define the process and the data [153].

Python is a programming language easy to use that was developed by Guido van Rossum in 1991. Python language is easier and closer to human language than other high level languages like C, C++ and Java. The program written in Python is shorter and takes less time to create. Object oriented programming is the best way to write programs about large project. However it is not necessary for short problems. In other languages object oriented programming (OOP) is not optional. In Python, it is optional. It has built-up modules to make easier writing a program [154].

The programs that run a graphical user interface (GUI), process files and incorporate multimedia elements such as graphics, sound and animation are able to be written by Python language. Google, IBM, Hewlett-Packard, Microsoft, Nasa Yahoo, Xerox are some

companies from around the world that Python is used. It is also used by professional game programmers [154].

The codes in this study are written in Python to analyze the systems after the simulation. The trajectory files are large scale to analyze in other programs so Python was chosen that is suitable for long time analysis and it is easy to use.

### **3.2.5. SwissDock**

Recognition of the molecules with each other involves most of the biological processes. Docking method predicts the interactions of biological structures at molecular level. SwissDock is the one of the web based docking service used to dock small molecules on target proteins. It has setup scripts to prepare both ligand and target proteins and it is based on the EADock dihedral space sampling (DSS) engine. Docking with this program does not need any user's computational power because the server performs all the calculations [150].

In this study, SwissDock is used to dock levan and sulfated levans as ligands with thrombin and antithrombin as target proteins.

### **3.2.6. UCSF Chimera**

SwissDock server suggests UCSF Chimera to predict, analyze and visualize the molecular structures and related data including docking results, trajectories and conformational assemblies. It is a free program which generates high quality images and animations. Viewdock is a sub program of UCSF Chimera for visualize and analyze the docked ligand and target orientations. It is available for Microsoft Windows, Linux, Apple Mac OS X [151].

UCSF Chimera is used to visualize and analyze the docking results that were performed in SwissDock in this study.

## 4. RESULTS AND DISCUSSION

### 4.1. SIMULATIONS WITH SINGLE LEVAN CHAIN WITH DIFFERENT LENGTHS IN VACUUM AT 298 K

Simulations were performed in vacuum to understand the internal motions of levan without any solvent effect. Different chain lengths were simulated to choose the most appropriate length of the chain for the simulation box. In all these simulations, number of particles and volume were kept constant with well defined temperature (NVT ensemble). The temperature and the pressure were 298 K and 1 atm respectively. They were controlled with Berendsen thermostat and barostat. Box size of these simulations was set to be 6.0x6.0x6.0 nm to contain a certain amount of levan chains without increasing simulation time with periodic boundary conditions. Polymer Consistent Force Field (PCFF) was applied to the simulations with 0.9 nm cut-off distance. The cut-off distance can be between 0.7 nm and 1.1 nm. While cut-off distance increases, more interactions are considered during simulations. However when cut-off distance increases, the simulation time increases as well [155]. Therefore 0.9 nm cut-off distance was chosen. The simulations performed in vacuum at 298 K for single levan chain of various number of fructose units are shown in Table 4.1.

Table 4.1. Simulated systems with one levan chain of various number of fructose units in vacuum at 298 K

# of levan units	# of fructose units	media	Pressure (atm)	Temp (K)	Dt	duration
1	9	vacuum	1	298	1 ps	1 ns
1	12	vacuum	1	298	1 ps	1 ns
1	18	vacuum	1	298	1 ps	1 ns

First three simulations were performed to compare the length of polymer chain. Fructose units were created by choosing appropriate atoms and bonds before creation of levan structure. By bonding these units, levan with 9, 12 and 18 fructose units were formed. First simulation contained one levan polymer chain with 9 fructose units and was simulated for 1 nanosecond time period with stated parameters using LAMMPS. The trajectory files were visualized with Visual Molecular Dynamics (VMD). The snapshots of the system show that levan assumed a spherical structure during the process (Figure 4.1.).

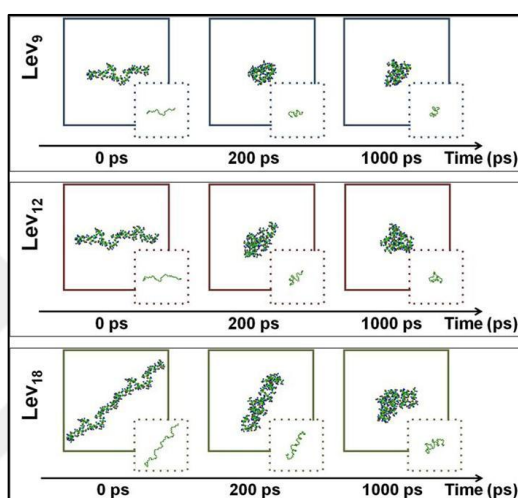


Figure 4.1. Snapshots for 9, 12, 18 fructose rings of levan over 1 ns

#### 4.1.1. End-to-end Distance in Vacuum at 298 K

End-to-end distance is used to calculate the distance between terminal atoms. In vacuum, as there is no solvent effect, the movement occurs due to internal motions of the molecules such as vibration and rotation. With no excluded volume, the only effect is the charges of the atoms. In levan, the terminal atoms attract each other and the size of the chain decreases.

In these results, the end-to-end distance of each chain decreased with respect to time as expected and then it leveled off (Figure 4.2.). Therefore 1 nanosecond is sufficient simulation time for the vacuum systems. The chains became spherical and the terminate atoms of chains were getting closer as was seen in the snapshots (Figure 4.1.). The final shape of the structure was not affected with the length of the chain.



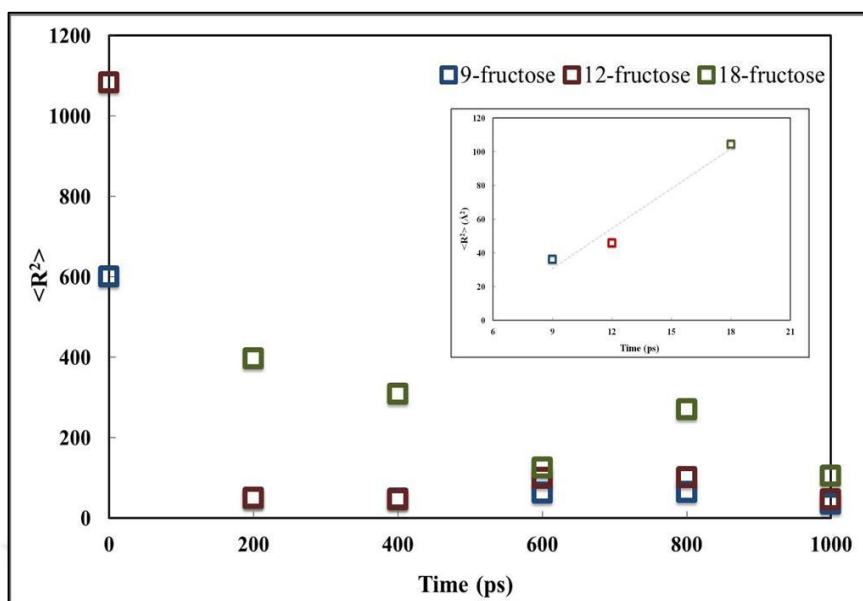


Figure 4.2. End-to-end distance of levan chains with different number of fructose rings in vacuum with respect to time

#### 4.1.2. Radius of Gyration in Vacuum at 298 K

Radius of gyration is an alternative measure to obtain the size of a polymer. It is radial distance from given point to the center of mass; as explained in detail in Section 3. Figure 4.3 shows radius of gyration values of levan chains with different lengths over time.

Radius of gyration values decreased and leveled off with time but when the number of fructose rings was increased, the percentage of the decrement increased. Both the end-to-end distance and radius of gyration values increases with increasing the number of fructose rings on the levan chains as expected.

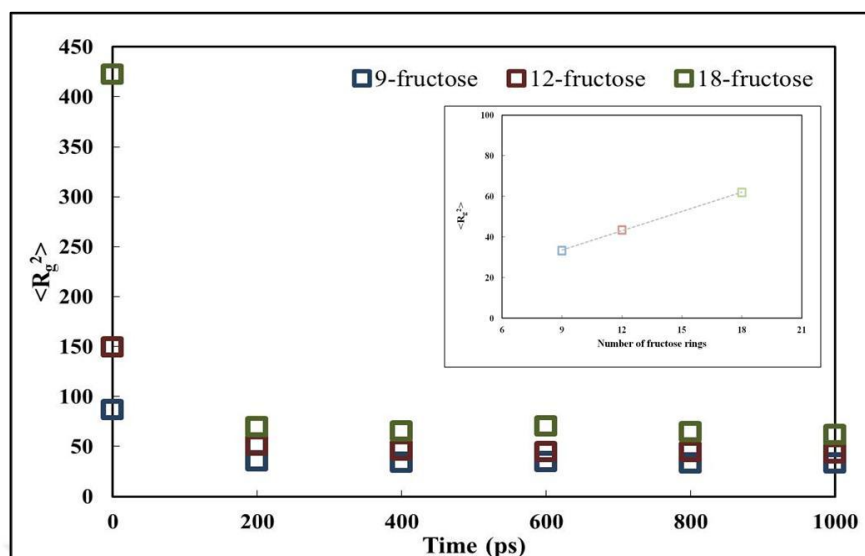


Figure 4.3. Radius of gyration of chains with different number of rings in vacuum with respect to time

All chains folded into globular shape regardless of its molecular weight. The structure should be long as possible to configure the conformational analysis better. However levan with 18 fructose rings can fit the simulation box diagonally. The box may be enlarged for using 18 fructose rings however when the box is enlarged, the systems get larger to simulate and use more computational power. This causes the increase of the simulation time. Levan with 9 fructose rings is not long enough to understand the structural conformation. Therefore levan structure with 12 fructose rings was chosen for the following simulations.

#### 4.2. SIMULATIONS WITH SINGLE LEVAN CHAIN IN DIFFERENT MEDIA AT 298 K AND 310 K

Levan chain with 12 fructose rings was simulated in vacuum, in water and saline solutions with different concentrations to obtain the behavior of single levan chain in these media. Aqueous solutions of levan will be used in applications so the systems were run in water and in saline solution. Salinity of the normal saline is 0.15 M of NaCl and the salt concentration range of these systems is chosen to be well above this concentration to see the effect of high salinity. The number of NaCl molecules was calculated to adjust the

system to be 0.5 M, 1 M and 2 M. The levan chain was placed in the simulation box and then it was filled with many water molecules sufficient the box to be full. After that the mole number of NaCl was calculated to adjust the molarity of the system. The mole number was converted to molecule number with Avogadro's number. The calculated number of NaCl molecules was placed in the box and it got filled with water molecules again to check the molarity of the system. 59 Na<sup>+</sup> and 59 Cl<sup>-</sup> ions were added to 6571 water molecules to adjust the media to be 0.5 M. The number of NaCl molecules were calculated again and added to the box to increase the molarity of the system to be 1 M and 2 M.

Table 4.2. Simulations of one levan chain in different media at 298 K and 310 K

# of levan units	# of fructose units	NaCl conc.(M)	Media	Pressure (atm)	Temp (K)	Dt	Duration
1	12	0	Vacuum	1	298	1 ps	5 ns
1	12	0	Water	1	298	1 ps	5 ns
1	12	0.5	Saline	1	298	1 ps	5 ns
1	12	1	Saline	1	298	1 ps	5 ns
1	12	2	Saline	1	298	1 ps	5 ns
1	12	0	Vacuum	1	310	1 ps	5 ns
1	12	0	Water	1	310	1 ps	5 ns
1	12	0.5	Saline	1	310	1 ps	5 ns
1	12	1	Saline	1	310	1 ps	5 ns
1	12	2	Saline	1	310	1 ps	5 ns

The systems were analyzed as coarse grained model. Each fructose ring was considered as a monomer bead to decrease the total number of atoms in order to decrease the computational work while analyzing the conformation of the structures. Although 1 ns was

sufficient to simulate the system in vacuum, due to the increase in number of atoms, the simulation time was increased to 5 ns to allow sufficient time for the systems to reach equilibrium.

The behavior of single chain resulting in its structure is analyzed at room and body temperature. Levan structure is proposed as a drug carrier candidate therefore the temperature was set to 310 K as well as 298 K to determine the effect of body temperature on the structure and folding behavior single chain levan. The simulations performed are tabulated in Table 4.2.

#### 4.2.1. End-to-end Distance of Single Chain in Different Media at 298 K and 310 K

First of all, vacuum, water and saline systems were compared with each other to understand the effect of solvent molecules on compactness. Figure 4.4 shows end-to-end distance values in vacuum and other systems during 5 ns at 298 K and 310 K. As seen in Figure 4.4, the levan chain became compact in all media however it is more compact in vacuum because of the lack of solvent effect. The levan chain stabilized more rapidly than other media as seen in the inset figures in Figure 4.4.

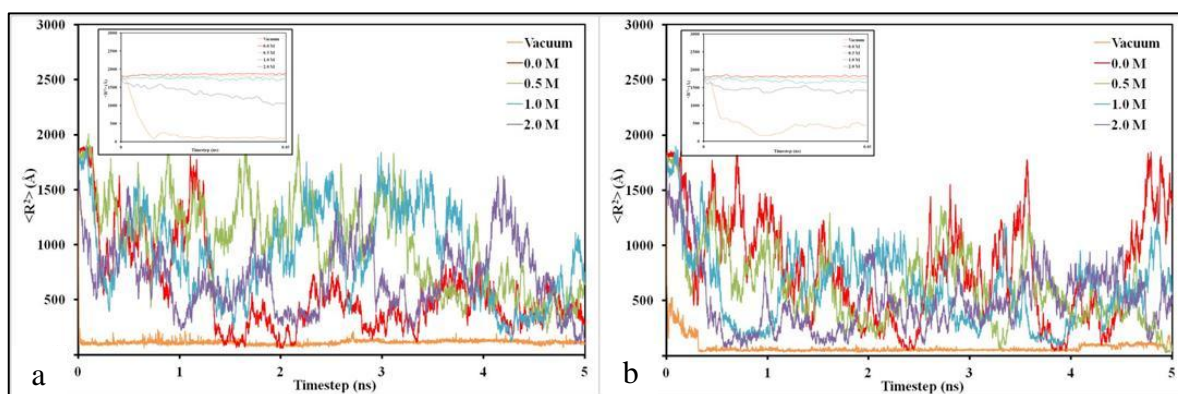


Figure 4.4. End-to-end Distances Comparison for one levan chain of 12 fructose rings in different media over time at a) 298 K and b) 310 K

The solvent quality affects the dynamics of polymer which can be observed with end-to-end distance. The favorable interactions between solvent molecules and levan prevent the terminal atoms from getting closer. The distance between the terminal atoms of single

levan chain was calculated from simulations at body temperature. Water can be considered a suitable medium when compared with vacuum because end-to-end distance is 73 % and 89% larger than the vacuum system at 298 K and 310 K, respectively.

The conformation of the chain fluctuates during the simulations. The fluctuation continues over 5 ns therefore end-to-end distance values were tabulated with respect to the average value after 2 ns to 5 ns (Table 4.3) for comparison. According to these values, the most significant result is the difference between levan in vacuum and in aqueous media. When different temperatures are compared for the vacuum systems, the final structures of levan have the same trend in end-to-end distance after 5 ns. The increment of temperature increases the kinetic energy of atoms therefore the system becomes more mobile. Water hydration is affected by temperature and water molecules caused terminal atoms to become distant from each other. Water becomes a better solvent at higher temperatures, deduced from larger R values obtained.

Table 4.3. Average End-to-end Distance values between 2 ns and 5 ns for all systems at 298 K and 310 K

<b>Media</b>	<b>Average End-to-End value between 2 ns - 5 ns at 298 K (<math>\text{\AA}^2</math>)</b>	<b>Average End-to-End value between 2 ns - 5 ns at 310 K (<math>\text{\AA}^2</math>)</b>
Vacuum	115.33±17.13	74.13±24.80
Water	427.93±159.42	662.48±446.50
0.5 M Salt Solution	853.73±382.69	520.72±271.99
1.0 M Salt Solution	916.07±431.53	542.29±259.57
2.0 M Salt Solution	686.47±327.55	522.12±189.04

The average end-to-end distance between 2 ns and 5 ns is very similar for all saline concentrations at 310 K, where this value is slightly higher, approximately % 25, when there is no salt in the medium. The Student T-test is applied to understand the significance of the difference between data series. For end-to-end distance values for all systems are found to be significantly different from with each other ( $p < 0.0001$ ). At 298 K, up to 1.0 M

salt concentration, the average  $R$  increases, suggesting that the interaction between the polymer and solvent is becoming more favorable. However, at 2.0 M salt concentration,  $R$  is reduced, indicating that above a certain concentration of salt, the interactions are becoming less favorable. At 310 K, that threshold salt concentration is possibly at a much lower value than 0.5 M, such that we are unable to detect it within this data set.

#### **4.2.2. Radius of Gyration of a Single Chain in Different Media at 298 K and at 310 K**

Radius of gyration of levan chain in different media is analyzed to understand the size of the polymer in these environments. Figure 4.5. shows radius of gyration values in vacuum, water and saline systems for 5 ns time span at 298 K and 310 K. The atoms became closer to the center of mass of levan chain in all media during the first nanosecond of the simulations to become equilibrium. However after 5 ns, the levan chain is 42 % and 60% more compact in vacuum at 298 and 310 K respectively, showing similar trend to  $R$  values. It can be also seen that water and saline solutions are better solvent media than vacuum from radius of gyration analysis of single levan chain simulations.

The conformation of the chain fluctuates during the simulations as similar to end-to end distance therefore radius of gyration values were tabulated with respect to the average value after 2 ns to 5 ns for both temperatures (Table 4.4). The vacuum systems became stable sooner and there were lower fluctuations than other systems (Inset figures in Figure 4.5). The results tabulated in Table 4.4 for 298 K are significantly different from each other ( $p < 0.0001$ ). The radius of gyration increases until the concentration of salt solution is 1.0 M and then it started to decrease at 298 K. The radius of gyration values follows the same trend as end-to-end distance. However when they are compared with each other 1.0 M salt solution shows better solvent quality for levan. Good hydration effect of water is also seen in radius of gyration analysis. Very similar to end-to-end distance, the radius of gyration values in vacuum are lower than all those in aqueous medium. Once simulated in the solvent, the radius of gyration values in water is found to be slightly higher at 310 K than those in saline solution however the difference in saline concentration does not seem to have an effect on the radius of gyration. Significance test also shows that salt solutions do not affect the radius of gyration ( $p < 0.0001$ ).

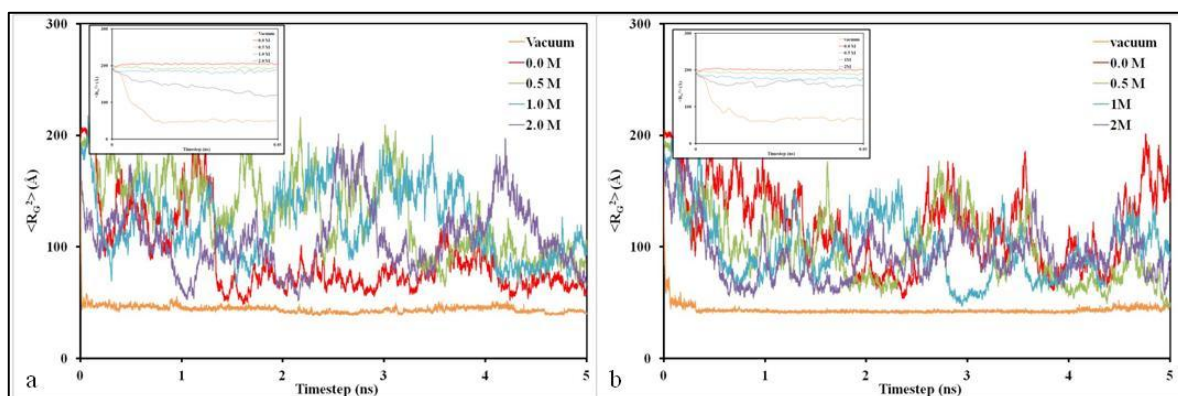


Figure 4.5. Radius of Gyration Comparison for one levan chain of 12 fructose rings in different media over time at a) 298 K and b) 310 K

Table 4.4. Average Radius of Gyration values between 2 ns and 5 ns for all systems at 298 K and 310 K

Media	Average Radius of Gyration value between 2 ns - 5 ns at 298 K ( $\text{\AA}^2$ )	Average Radius of Gyration value between 2 ns - 5 ns at 310 K ( $\text{\AA}^2$ )
Vacuum	42.77 $\pm$ 2.34	42.74 $\pm$ 1.86
Water	74.26 $\pm$ 11.84	107.52 $\pm$ 38.65
0.5 M Salt Solution	116.33 $\pm$ 33.65	90.12 $\pm$ 29.08
1.0 M Salt Solution	124.19 $\pm$ 32.64	94.56 $\pm$ 25.86
2.0 M Salt Solution	112.09 $\pm$ 32.58	94.80 $\pm$ 16.38

Based on the end-to-end and radius of gyration results, it appears that water is a good solvent for levan as it expands in water when compared to vacuum. When the temperature was increased to 310 K, water becomes a better solvent, i.e. hydrates the chains more, resulting in larger end-to-end and radius of gyration values. In both  $R_g$  and  $R$  average values, the common observation is that water becomes a better solvent when temperature is increases. However, upon addition salt, the saline solutions become an even better solvent

up to 1.0 M at 298 K however, the salt tolerance at 310 K is much lower than even the addition of 0.5 M salt results in the contraction of the molecule.

In polymer science, the basic polymer model is Gaussian model where the beads are connected with strings. These strings show harmonic oscillations [156]. Any two points on the chain follow Gaussian distribution in Gaussian chain. If two Gaussian segments are joined together, the final chain also follows Gaussian chain model as a single segment [157]. The ideal polymer chains follow Gaussian model where the polymer chains are considered to have no interaction between the monomers [158]. This model depends on  $R$  and  $R_g$  of chains where there is a relation between these values in Gaussian chain model. The relation between these values can be shown in equation 4.1. [159]

$$R_g^2 = \frac{R^2}{6} \quad (4.1)$$

Where  $R_g$  is the distance of beads to the center of mass of the chain and  $R$  is the distance between the terminal beads of the chain.

To understand the Gaussian model for levan chains, the ratio between end-to-end distance and radius of gyration of these systems are also calculated. As seen in figure, the levan chains are not Gaussian in vacuum system, however in other systems the ratio is close to the value 6, the chains behave more like Gaussian for both temperatures (Figure 4.6.). The average values are given in Table 4.5.

Based on this model, it is concluded that levan curls to its final shape exhibiting ideal chain model where freely joint segments of the polymer perform a random walk in all dimensions.



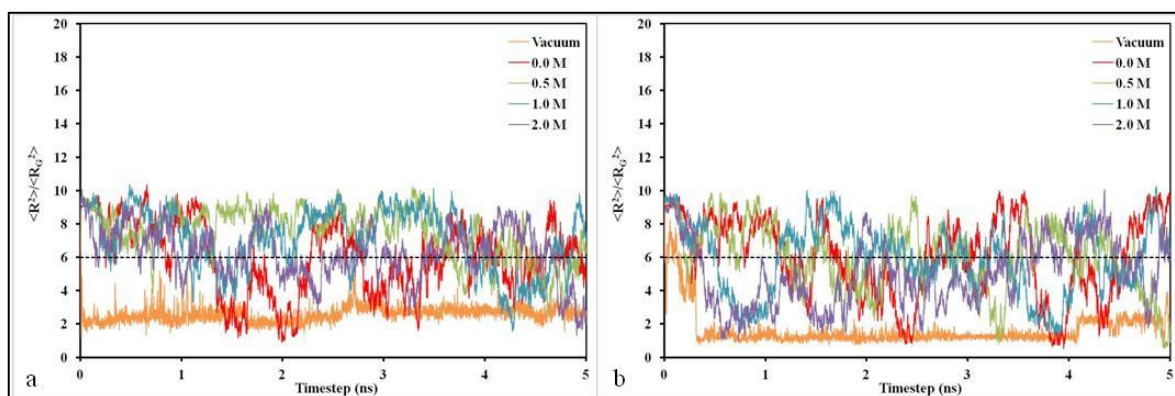


Figure 4.6. End-to-end Distance over Radius of Gyration Values for one levan chain of 12 fructose rings in different media over time at a) 298 K and b) 310 K

Table 4.5. Average End-to-end Distance over Radius of Gyration values between 2 ns and 5 ns for all systems at 298 K and 310 K

Media	Average value between 2 ns - 5 ns at 298 K	Average value between 2 ns - 5 ns at 310 K
Vacuum	2.70±3.66	1.73±1.46
Water	5.76±6.73	6.16±5.78
0.5 M Salt Solution	7.34±5.69	5.78±4.68
1.0 M Salt Solution	7.38±6.61	5.73±5.03
2.0 M Salt Solution	6.12±5.03	5.51±5.77

#### 4.2.3. Chain Characteristics of a Single Chain for Different Media at 298 K and 310 K

Chain characteristics of single chain of levan were analyzed with the calculation of bond length, bond angle, chord length and torsional bond angle considering each fructose rings as a monomer bead. The next figures show these parameters for vacuum, water and saline solutions with different concentrations at 298 K and 310 K.

In Figure 4.7, the bond length between each monomer bead is shown for vacuum and aqueous systems at 298 K and 310 K. As seen in the figure, bond length between monomer beads is shorter in vacuum system. Shorter bond length indicates stronger the interaction between monomer beads. It is also observed that the chain in vacuum stabilizes sooner than the water and the other saline systems (inset of figure 4.7). The bond length of the water and different saline concentrations stabilize after 100 ps and fluctuate between 4.9 Å and 5.2 Å until 5 ns at 298 K. This shows that the monomer beads reach steady state fairly quickly. Temperature does not seem to affect the stabilization time. The graphs fluctuate between 4.9 and 5.2 Å until the end of the simulations for both temperatures.

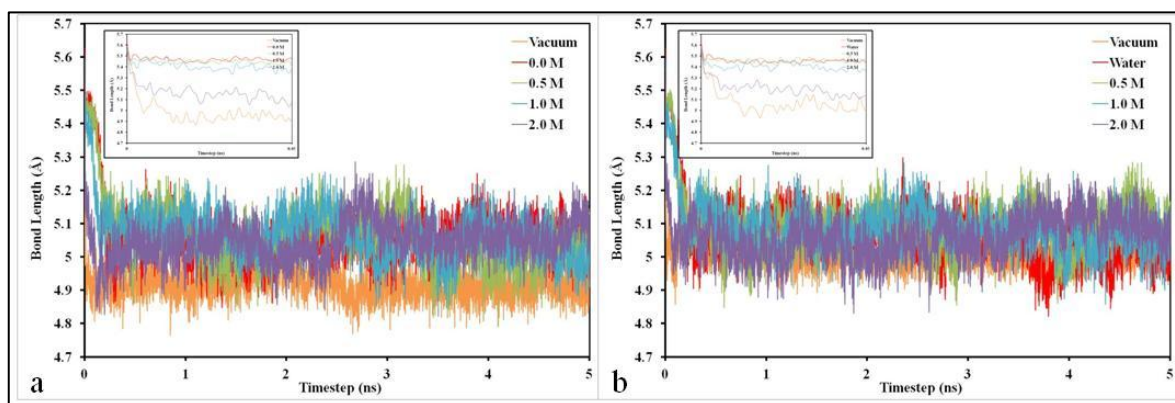


Figure 4.7. Bond length for one levan chain of 12 fructose rings in different media over time at a) 298 K b) 310 K

Table 4.6 shows the averaged bond length values in different media between 2 ns and 5 ns. As seen in the table, bond length between the monomer beads of levan chain in vacuum are % 3 lower than other environments at 298 K. Student T-test evaluated the bond length values are to be the same for aqueous systems ( $p > 0.0001$ ). Whereas the difference between aqueous system and vacuum is significant and is about 3 % higher, showing that water molecules interact with the fructose units, making them slightly weaker. As seen in Figure 4.6 and Table 4.5, the salinity does not appear to affect the bond length ( $p > 0.0001$ ). When compared to 298 K, the bond lengths are not different from each other. Therefore it can be concluded that temperature and salinity do not affect the bond length of the monomer beads of levan chain.

Table 4.6. Average Bond Length values between 2 ns and 5 ns for all systems at 298 K and 310 K

Media	Average Bond Length value between 2 sn - 5 ns at 298 K (Å)	Average Bond Length value between 2 sn - 5 ns at 310 K (Å)
Vacuum	4.91±0.04	5.01±0.04
Water	5.06±0.05	5.04±0.07
0.5 M Salt Solution	5.04±0.07	5.09±0.07
1.0 M Salt Solution	5.05±0.07	5.08±0.06
2.0 M Salt Solution	5.06±0.06	5.07±0.06

Bond angle is the angle between two monomer beads and these angles are shown for different media in the next figure (Fig. 4.8). It shows the flexibility of the polymer chain. Solvent quality influences the flexibility of biopolymers. Dominant solvent affects the flexibility of the biopolymers [1]. In aqueous media, monomer beads bend with respect to each other. However in vacuum medium, they are less flexible than in water for both temperatures.

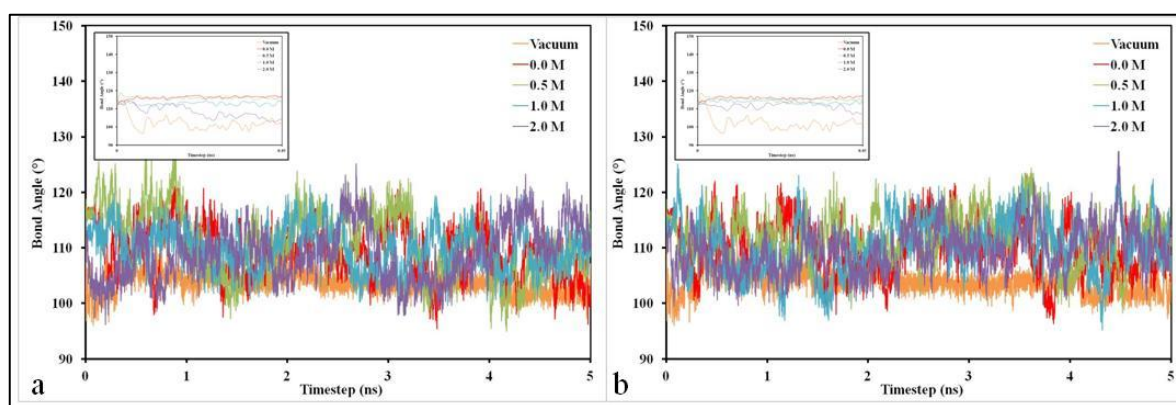


Figure 4.8. Bond angle of 12 fructose single chain in different media with respect to time at a) 298 K and b) 310 K

The saline concentration did not affect the flexibility of the polymer chain. The monomer beads bend between  $100^\circ$  and  $120^\circ$  in all different media except vacuum where fluctuations are between  $100^\circ$  and  $110^\circ$ . Values in vacuum, water and saline solutions are different from each other. Water is slightly different from saline solutions whereas in a vacuum a 5 % different is observed. As far as bond angles, this difference clearly means that aqueous environment makes the chains more flexible. Figure 4.8 (b) shows the bond angle for these systems at 310 K. The monomer beads bend between  $100^\circ$  and  $120^\circ$  in all different media except vacuum. In vacuum system, the monomer beads bend between the angles  $100^\circ$ - $110^\circ$  however the chain is more stable in vacuum system, deduced from less fluctuating values over time.

In Table 4.7 due to fluctuations, the averaged values of bond angle between 2 ns and 5 ns are tabulated for 298 K and 310 K. As seen from the table, the bond angles of monomer beads are % 5 lower in vacuum than water and salt solutions at 298 K. Significance test shows that the bond angle values of saline solutions are the same ( $p>0.0001$ ). It can be also seen that the differences in salinity does not affect the bond angle for 310 K either (Table 4.6) ( $p>0.0001$ ). The bond angle values are compared with 298 K in Table 4.17 and it is seen that bond angle values increase when temperature is increased to 310 K.

Table 4.7. Average Bond Angle values between 2 ns and 5 ns for all systems at 298 K and 310 K

<b>Media</b>	<b>Average Bond Angle value between 2 ns - 5 ns at 298 K (°)</b>	<b>Average Bond Angle value between 2 ns - 5 ns at 310 K (°)</b>
Vacuum	103.32±1.69	103.33±1.70
Water	108.50±4.24	109.58±4.49
0.5 M Salt Solution	110.03±5.43	112.13±4.58
1.0 M Salt Solution	109.63±3.87	111.75±4.29
2.0 M Salt Solution	109.83±5.28	111.23±3.93

Chord length figures also show the folding of levan structures in these systems. In Figure 4.9, levan chain folded in all systems however, the vacuum media increases the folding of levan chain. Saline concentration did not affect the foldings. The systems stabilize between 8 Å and 9 Å in water and saline systems. The vacuum system is at steady state between 7 Å and 7.5 Å. Similar to bond length, chord length values are also statistically the same for all aqueous systems where all are different from vacuum ( $p < 0.0001$ ). As seen in Figure 4.9 (b) the systems fluctuate between 8 Å and 9 Å in water and saline systems at 310 K. The vacuum system is at steady state around 8 Å instead of 7.5 Å as seen also at 298 K.

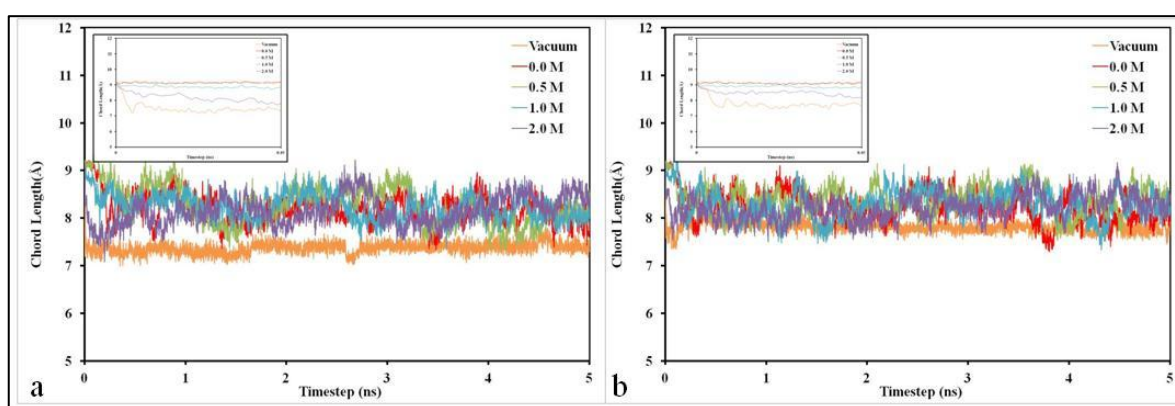


Figure 4.9. Chord length of 12 fructose single chain in different media with respect to time at a) 298 K and b) 310 K

As seen in Figure 4.9 there is fluctuations after 1 ns therefore the averaged values between 2 ns and 5 ns are tabulated (Table 4.8.). The values are similar for water and saline solutions. However in vacuum system, levan chain has the lowest chord length value. Chord length in vacuum system is approximately 10 % lower than the aqueous systems for both temperatures.

As bond length, chord length also slightly increases with temperature and this increase is statistically significant ( $p < 0.0001$ ).

Table 4.8. Average Chord Length values between 2 ns and 5 ns for all systems at 298 K and 310 K

Media	Average Chord Length value between 2 ns - 5 ns at 298 K (Å)	Average Chord Length value between 2 ns - 5 ns at 310 K (Å)
Vacuum	7.39±0.10	7.78±0.09
Water	8.15±0.24	8.19±0.29
0.5 M Salt Solution	8.20±0.36	8.40±0.29
1.0 M Salt Solution	8.18±0.26	8.35±0.27
2.0 M Salt Solution	8.22±0.31	8.30±0.25

Based on the bond length, bond angle and chord length values a schematic representation of levan can be shown as in Figure 4.10.

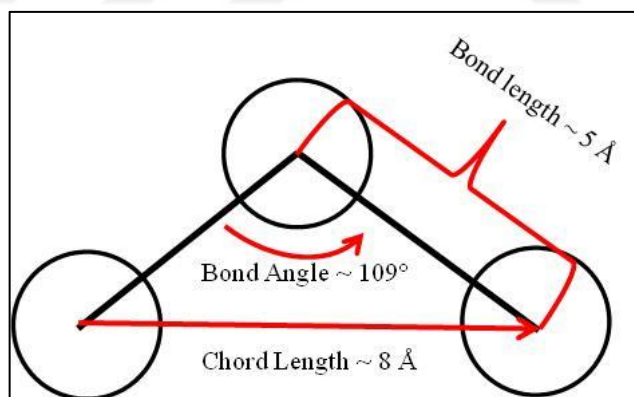


Figure 4.10. Schematic representation of monomer beads at 298 K and 310 K

Chain characteristics are important parameters to define the structural conformation of polymers. End-to-end distance can be calculated as theoretical length of the polymers for freely jointed chains by using the equation below:

$$\langle R^2 \rangle_f^{1/2} = n^{1/2} \times l \quad (4.2)$$

Where  $n$  is the number of bond segments between the monomer beads and  $l$  is the length of these segments which can be called bond length. Table 4.8 shows the theoretical end-to-end distance of single levan chain calculated with using the bond lengths shown in Table 4.6.

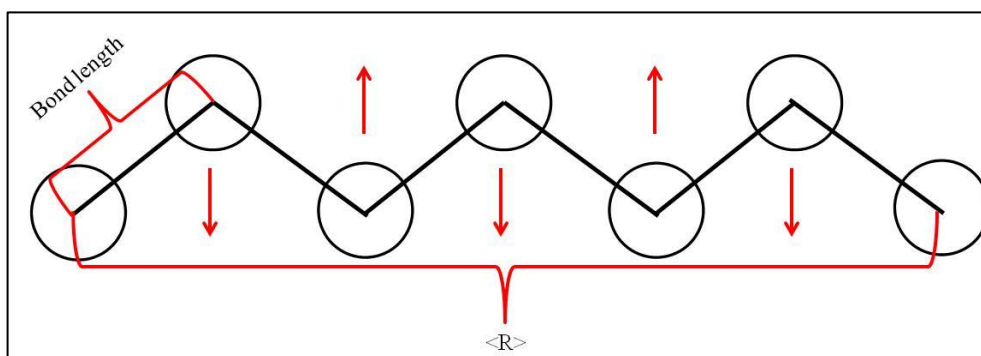


Figure 4.11. Representation of freely joint chain model

As seen from the results, the theoretical values are very different from our calculated end-to-end distances. When the polymers are accepted as freely jointed chains, the effect of bond angles and short range steric interactions (interactions between the neighboring beads) are not considered. Both of these effects cause larger estimation of end-to-end distance values for actual systems.

Table 4.9. Theoretical End-to-End Distance Calculated From Bond Lengths  $\langle R^2 \rangle_f$

Media	Theoretical End-to-end Distance Values at 298 K ( $\text{\AA}^2$ )	Theoretical End-to-end Distance Values at 310 K ( $\text{\AA}^2$ )
Vacuum	265.47	269.52
Water	281.28	284.98
0.5 M Salt Solution	279.75	283.87
1.0 M Salt Solution	280.85	282.75
2.0 M Salt Solution	281.79	283.87

When only bond lengths are considered in the calculations, there is not much difference between water and saline systems and they only differ from the system in vacuum. Temperature does not seem to have an effect.

For modification of freely jointed chain model, the bond angle is fixed between  $90^\circ$  and  $180^\circ$  whilst the allowing free movement of the bonds. As seen from the calculations at above, the bond angle of the monomer beads are between  $90^\circ$  and  $180^\circ$  therefore this modification can be applied to our systems.

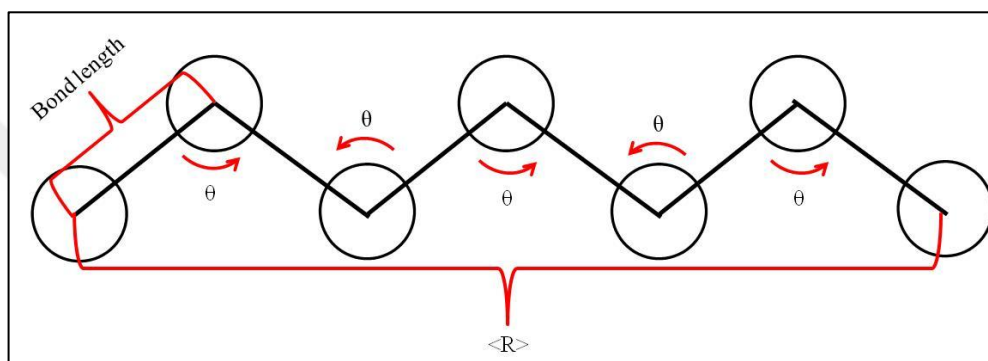


Figure 4.12. Representation of the modified freely joint model

Due to this modification, the end-to-end distance can also be calculated from the equation below:

$$\langle R^2 \rangle_t = nl^2 \left( \frac{1 - \cos \theta}{1 + \cos \theta} \right) \quad (4.3)$$

$\theta$  values are tabulated in Table 4.6 for all simulated systems. By using these bond angle values and bond length values, end-to-end distances are calculated and tabulated in Table 4.10.



Table 4.10. Theoretical End-to-End Distance Calculated From Bond Lengths and Bond Angles  $\langle R^2 \rangle_t$

Media	Theoretical End-to-end Distance Values at 298 K ( $\text{\AA}^2$ )	Theoretical End-to-end Distance Values at 310 K ( $\text{\AA}^2$ )
Vacuum	423.96	441.57
Water	543.44	561.09
0.5 M Salt Solution	570.54	629.48
1.0 M Salt Solution	564.36	618.10
2.0 M Salt Solution	570.82	603.78

When the angles are considered along with the bond lengths, the difference between the vacuum, water and saline becomes more evident. Although saline systems are still similar with each other, temperature now appears to have a more pronounced effect. From these calculated end-to-end distances, the characteristic ratio of levan chain can be calculated from Equation 4.4.

$$C_{\infty} = \frac{\langle R^2 \rangle_t}{\langle R^2 \rangle_f} \quad (4.4)$$

[160,161]

Where  $R_f$  is the end-to-end distance for freely jointed chain model and  $R_t$  is the end-to-end distance calculated for modified freely joint chain model.

The characteristic ratio gives the stiffness of the chains. For real polymer chains this value is higher than 1. Characteristic ratio close to 10 shows the compact structure of the polysaccharides. Increase in characteristic ratio suggests the less stiff conformation of the structures. The characteristic ratios of levan chain in different media are tabulated in Table 4.11. As seen from the results, the characteristic ratio of levan chain is higher than 1 in all different media which supports that levan chain is compact in these solvents. Several

studies that are based on the characteristic ratio of polysaccharides showed that any small differences in geometry of the structure and bond angles affect the characteristic ratio. The bond angle between monomer beads is higher in 310 K therefore the characteristic ratio is higher at 310 K for aqueous systems (Eqn. 4.3).

Table 4.11. Characteristic Ratio of Levan Chain in Different Media at 298 K and 310 K

<b>Media</b>	<b>Characteristic Ratio at 298 K</b>	<b>Characteristic Ratio at 310 K</b>
Vacuum	1.59	1.60
Water	1.93	2.00
0.5 M Salt Solution	2.04	2.20
1.0 M Salt Solution	2.00	2.18
2.0 M Salt Solution	2.02	2.13

There can be different characteristic ratios for the same polysaccharides [162]. Characteristic ratio of amylose which consists of glucose units with  $\alpha(1\rightarrow4)$  glycosidic bonds is calculated between 2.5 and 11.7 [163].

Expansion factor,  $\alpha$ , can be used to identify the excluded volume effect on polymer chain in a solution which is shown at below;

$$\alpha = \sqrt{\frac{\langle R^2 \rangle}{\langle R^2 \rangle_f}} \quad (4.5)$$

Where  $R$  is the end-to-end distance calculated from molecular dynamics simulations and  $R_f$  is the end-to-end distance calculated for freely joint chain model.

The expansion factor gives an idea about the solvent quality as mentioned in Methodology part. In a good solvent where polymer-solvent interactions are stronger the expansion factor is bigger than one ( $\alpha > 1$ ). In a poor solvent, polymer-polymer interactions become more favorable than solvent-polymer interaction therefore the expansion factor is lower

than 1 ( $\alpha < 1$ ) [128]. The expansion factor for levan is calculated for all different media and temperature. The values are tabulated in Table 4.12.

Table 4.12. Expansion Factor for Single Levan Chain in Different Media at 298 K and 310 K

Media	Expansion Factor at 298 K	Expansion Factor at 310 K
Vacuum	0.65	0.51
Water	1.23	1.53
0.5 M Salt Solution	1.74	1.35
1.0 M Salt Solution	1.80	1.38
2.0 M Salt Solution	1.56	1.35

As seen from the results, the vacuum media is in the poor solvent region however water and saline solutions are found to be good solvents for levan. Levan is an amphiphilic structure in nature and it contains hydrophobic parts which consist of  $\text{CH}_2$  groups. Therefore levan forms self-assemble nanoparticles in water [6]. Hydrogen bonding tends to occur between hydrophilic part of the levan and solvent molecules which is responsible for the water solubility of levan.

Probability of torsion angles shows the possible planar conformations of monomer beads. In vacuum system, the possible conformations occurred at  $-120^\circ$ ,  $-40^\circ$ ,  $80^\circ$  and  $140^\circ$  as seen in Figure 4.13 (a). When 310 K is compared with vacuum system at 298 K, the chain preferred to be at a more variety of angles ( $-50^\circ$ ,  $-20^\circ$ ,  $25^\circ$ ,  $70^\circ$ ,  $130^\circ$ ,  $170^\circ$ ) as opposed to  $-120^\circ$ ,  $-40^\circ$ ,  $80^\circ$  and  $140^\circ$  which again is a result of the increase in the mobility of atoms with increasing temperature (Figure 4.13 (b)).

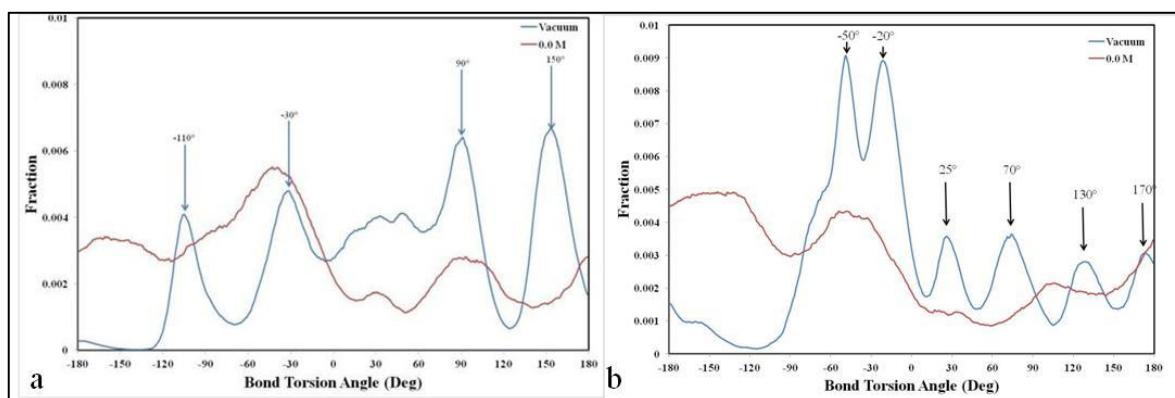


Figure 4.13. Histogram of the distribution of the dihedral angle between monomer bead 12 fructose single chain in vacuum and water systems over 5 ns a) 298 K and b) 310 K

Next figure shows the preferred angles and free energies of levan structures in different saline concentrations. As seen in Figure 4.14, the possible conformations occurred at  $-160^\circ$ ,  $-40^\circ$  and  $100^\circ$ . In saline solutions at 310 K, the chain preferred to be at the same angles with the systems at 298 K. Therefore, in saline solutions the mobility of the atoms is not affected by temperature.

If the structure has side chains, the planar conformation may prefer to be in trans conformation at  $180^\circ$  to minimize the interactions of these side chains [164]. However, levan does not have any side chains and  $180^\circ$  does not appear to be one of its preferred angles. The potential of preferable conformations can be calculated as free energy from the eq. 4.6.

$$\Delta G = -kT \ln \left( \frac{p}{p_{\max}} \right) \quad (4.6)$$

Where  $k$  is the Boltzmann constant ( $1.987 \cdot 10^{-3}$  kcal/mol.K),  $T$  is the temperature (in Kelvin),  $p$  is the probability which is calculated from the histogram of torsion angles and  $\Delta G$  is the free energy (in kcal/mol). This free energy gives information about the energy barrier for the rotation of monomers [165].

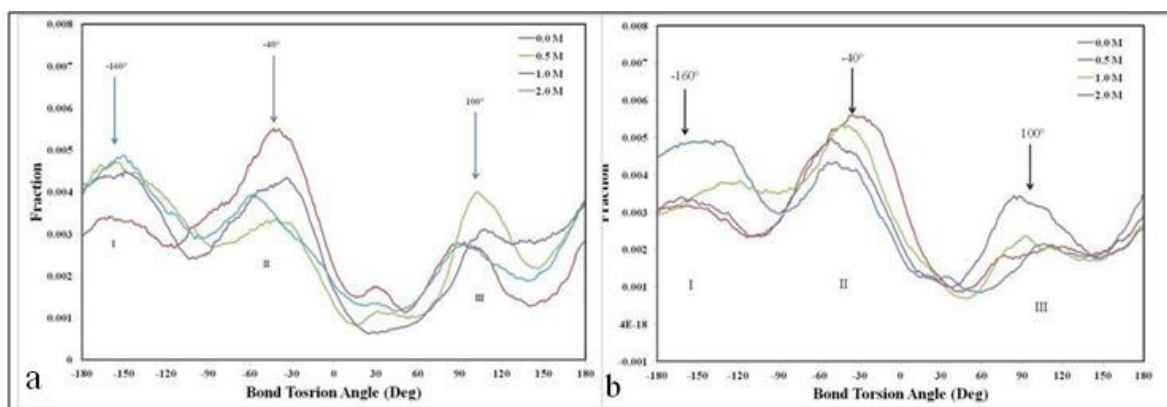


Figure 4.14. Histogram of the distribution of the dihedral angle between monomer beads of 12 fructose single chain in water and saline systems over 5 ns a) 298 K and b) 310 K

Table 4.13. Free Energy values for water and saline systems at 298 K and 310 K

	298 K			310 K		
	Free Energy between I-II (kcal/mol)	Free Energy between I-III (kcal/mol)	Free Energy between II-III (kcal/mol)	Free Energy between I-II (kcal/mol)	Free Energy between I-III (kcal/mol)	Free Energy between II-III (kcal/mol)
0.0 M	0.044	0.143	0.100	0.033	-0.473	-0.440
0.5 M	0.081	-0.284	-0.365	-0.291	-0.260	-0.552
1.0 M	-0.166	-0.043	0.123	0.175	-0.278	-0.453
2.0 M	-0.035	-0.190	-0.154	0.213	0.042	-0.171

The calculated free energies are shown in Table 4.13 for water and saline systems and in vacuum systems, where they have the lowest energy values at the preferred angles in these systems. There are three peaks where levan chain prefers to be the most. The difference between these peaks refers to the energy barrier to change the conformation of levan chain between these three conformations. Negative sign represents the direction of energy which is from highest to lowest peak point. As seen in the table, the change in energy barriers does not depend on medium or temperature. Therefore the rotation of monomers are not affected from medium or temperature.

#### 4.2.4. Radial Distribution Function Analysis (RDF) of a Single Chain in Different Media at 298 K and 310 K

In order to understand how single levan chain in different media fold, radial distribution functions (RDF) (Figure 4.15) are calculated between the monomers of levan structure. The figures show pair distribution function values of a single levan chain in different media with respect to the distance  $r$  at 298 K and 310 K.

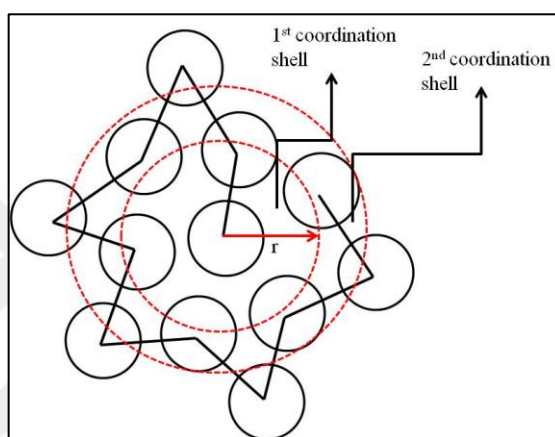


Figure 4.15. Representation of Radial Distribution Function

In the next figures each of fructose rings are accepted as a bead and distances between center of mass of these beads are calculated. Figure 4.16 is for single levan chain system in vacuum media for different temperatures. The first peak in RDF is seen between 5-10 Å because the bond length between the monomer beads is around 5 Å the second coordination shell appears around 7 Å. The second coordination shell shows the neighbor monomer beads around the first coordination shell. In vacuum system, the levan chain gets compact immediately therefore no change in radial distribution function is observed after 1 ns as seen Figure 4.16 at both studied temperatures.

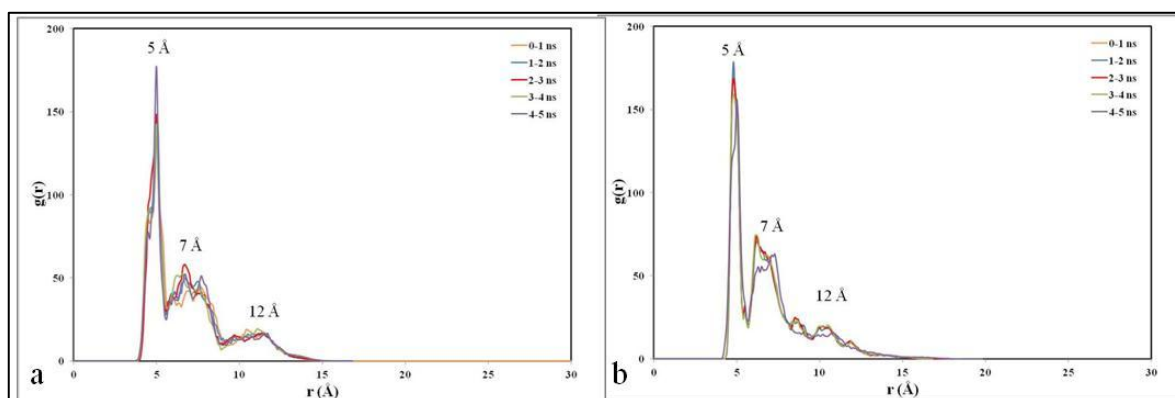


Figure 4.16. RDF for 12 fructose single chain in vacuum with 1 ns intervals a) at 298 K and b) 310 K

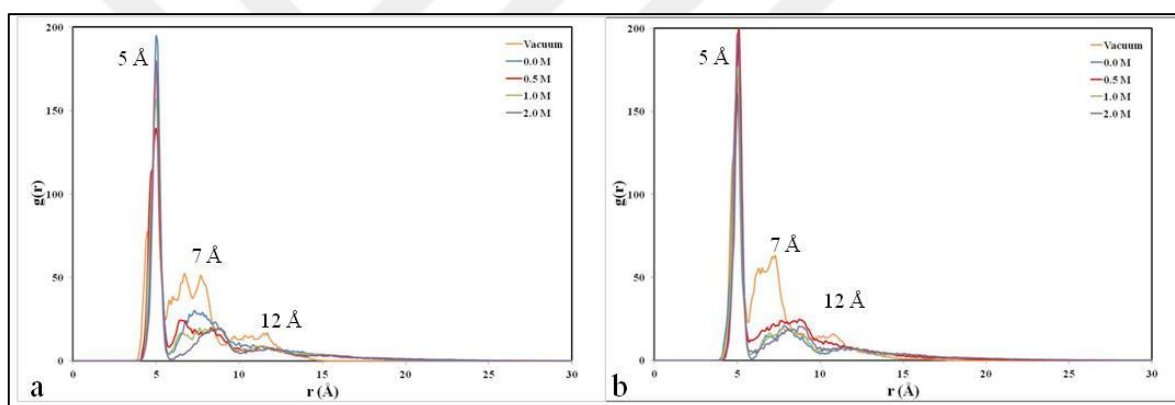


Figure 4.17. RDF for 12 fructose single chain in all media 4 ns-5 ns intervals a) at 298 K and b) 310 K

Figure 4.17 shows RDF results for all systems between 4-5 ns interval at 298 K and 310 K. After 4 ns, the number of monomers increased at the same distance for water and saline systems because of folding. Addition of solvent did not inhibit the structure to fold up. However, the highest and immediate folding was seen in vacuum systems at 298 K and 310 K. Table 4.14 shows the  $g(r)$  values of the systems at their maximums, an increase in number of beads at the distance between 5 and 10 Å was seen for all systems, which is expected as the beads further get closer. Saline concentration did not affect the RDF of levam chain at both temperatures.

Table 4.14. RDF values of the all systems at their peak point at 298 K and at 310 K

	298 K			310 K		
	Peak point (Å)	g(r) at 1 ns	g(r) at 5 ns	Peak point (Å)	g(r) at 1 ns	g(r) at 5 ns
Vacuum	7.30	45.34	51.27	7.30	46.88	63.01
0.0 M	8.00	19.34	27.29	7.80	15.45	20.92
0.5 M	8.30	16.16	19.89	8.70	18.55	24.48
1.0 M	8.40	17.21	20.42	7.70	20.83	19.28
2.0 M	8.30	18.79	19.41	8.70	19.17	20.30

In this part of the study, solvent and temperature effect on the conformation of single levan chain was analyzed. Theoretically, these parameters have a small effect on the conformation of structures. There is a theta temperature at which the polymer has an ideal conformation [166]. At theta temperature, all excluded volume effects are eliminated, and there is no interaction between the polymer chains and the solvent due to the cancellation of attractive and repulsive forces polymer chain stays same. Above the theta temperature, the polymer expands and below the theta temperature, the polymer tends to collapse because excluded volume is negative [167]. Different polymer and solvent systems have their own theta temperature which can be called as ideal temperature. Dextran/water system is an example for polysaccharides/solvent systems that has its own theta temperature around 317 K [168]. From the calculations, water is found to be a good solvent therefore theta temperature of the levan/water system should be lower than 298 K. According to data above which are summarized in Table 4.15., aqueous media can be considered as good solvents for levan chains. However saline concentration did not affect the solvent quality at the both temperatures. As a conclusion of this part, it was understood that levan chain shows the similar conformational properties in all media and studied temperatures. Levan is a stable biopolymer in different conditions.



Table.4.15. Summary of all results of single levan chain simulations

		<b>Vacuum</b>	<b>Water</b>	<b>0.5 M</b>	<b>1.0 M</b>	<b>2.0 M</b>
298 K	$R^2 (\text{Å}^2)$	115.33 $\pm 17.13$	427.93 $\pm 159.42$	853.73 $\pm 382.69$	916.07 $\pm 431.53$	686.47 $\pm 327.55$
	$R_G^2 (\text{Å}^2)$	42.77 $\pm 2.34$	74.26 $\pm 11.84$	116.33 $\pm 33.65$	124.19 $\pm 32.64$	112.09 $\pm 32.58$
	Bond Length (Å)	4.91 $\pm 0.04$	5.06 $\pm 0.05$	5.04 $\pm 0.07$	5.05 $\pm 0.07$	5.06 $\pm 0.06$
	Bond Angle (Å)	103.32 $\pm 1.69$	108.50 $\pm 4.24$	110.03 $\pm 5.43$	109.63 $\pm 3.87$	109.83 $\pm 5.28$
	Chord Length (Å)	7.39 $\pm 0.10$	8.15 $\pm 0.24$	8.20 $\pm 0.36$	8.18 $\pm 0.26$	8.22 $\pm 0.31$
	Free Energy (kcal/mol)	-	0.421	-0.095	0.167	0.143
	Characteristic Ratio	1.93	2.04	2	2.02	1.59
	Expansion Factor	0.65	1.23	1.74	1.8	1.56
310 K	$R^2 (\text{Å}^2)$	74.13 $\pm 24.80$	662.48 $\pm 446.50$	520.72 $\pm 271.99$	542.29 $\pm 259.57$	522.12 $\pm 189.04$
	$R_G^2 (\text{Å}^2)$	42.74 $\pm 1.86$	107.52 $\pm 38.65$	90.12 $\pm 29.08$	94.56 $\pm 25.86$	94.80 $\pm 16.38$
	Bond Length (Å)	5.01 $\pm 0.04$	5.04 $\pm 0.07$	5.09 $\pm 0.07$	5.08 $\pm 0.06$	5.07 $\pm 0.06$
	Bond Angle (Å)	103.33 $\pm 1.70$	109.58 $\pm 4.49$	112.13 $\pm 4.58$	111.75 $\pm 4.29$	111.23 $\pm 3.93$
	Chord Length (Å)	7.78 $\pm 0.09$	8.19 $\pm 0.29$	8.40 $\pm 0.29$	8.35 $\pm 0.27$	8.30 $\pm 0.25$
	Free Energy (kcal/mol)	-	0.276	0.526	0.51	0.233

Table.4.15. Summary of all results of single levan chain simulations cont'd

Characteristic Ratio	1.59	2	2.2	2.17	2.13
Expansion Factor	0.51	1.53	1.35	1.38	1.35

#### 4.3. SIMULATIONS WITH 9 ORIGINAL LEVAN STRUCTURE IN DIFFERENT MEDIA AT 298 K AND 310 K

Conformational analysis of levan was investigated to understand the structure-function relationship of levan as the main objective of the study. In this chapter, nine levan chains are used to understand the behavior of the chains with respect to each other and in each other presences in different media and temperature. Levan was affirmed as a potential nanocarrier in delivery of macromolecular drugs [6]. Levan structures are simulated in different concentration of saline solutions at 298 K which is room temperature and at 310 K to determine the effect of salt ions on conformation of levan at body temperature. For these simulations, 9 of 12 ring fructose chains are used because the volume of the simulation box is kept constant as previous simulations and 9 chains of 12 fructose rings can be placed equidistant with each other in this box. Firstly, 9 levan chains are simulated in vacuum to understand the interaction between chains without any solvent effect. Then the simulation box with 9 levan chains was filled with water molecules, the energy of the system was minimized and the system is simulated for 25 ns with the same parameters. After that, the number of NaCl molecules was calculated as previous systems to adjust the salt concentration of the systems to be 0.5 M, 1 M, 1.5 M and 2 M. 51 Na<sup>+</sup> and 51 Cl<sup>-</sup> ions were added to 5736 water molecules to adjust the system to be 0.5 M. The levan chains were analyzed as coarse grained model. The simulation time was increased to 25 ns because the systems are larger therefore longer times are required to reach equilibrium. The simulation parameters are tabulated in Table 4.16 for multiple chains at 298 K and 310 K. The parameters are averaged over 9 levan chains and the results show the behavior of single chain in multiple chain systems.

Table 4.16. Simulation parameters for 9 chains systems at 298 K and 310 K

# of levan units	# of fructose units	NaCl conc.(M)	media	Pressure (atm)	Temp (K)	dt	duration
9	12	0	vacuum	1	298	1 ps	25 ns
9	12	0	water	1	298	1 ps	25 ns
9	12	0.5	saline	1	298	1 ps	25 ns
9	12	1	saline	1	298	1 ps	25 ns
9	12	1.5	saline	1	298	1 ps	25 ns
9	12	2	saline	1	298	1 ps	25 ns
9	12	0	vacuum	1	310	1 ps	25 ns
9	12	0	water	1	310	1 ps	25 ns
9	12	0.5	saline	1	310	1 ps	25 ns
9	12	1	saline	1	310	1 ps	25 ns
9	12	1.5	saline	1	310	1 ps	25 ns
9	12	2	saline	1	310	1 ps	25 ns

#### 4.3.1. End-to-end Distance for 9 Levan Chains in Different Media at 298 K and 310 K

The effect of different media was analyzed placing the levan chains in vacuum, water and different saline solutions for both temperatures. The purpose was to understand the effect of electrostatic forces on the conformation of chains. The end-to-end distance shows the distance between terminal atoms of a single chain averaged from nine levan chains. As seen in Figure 4.18, the terminal atoms are getting closer with each other immediately in vacuum system (Inset graphs). The levan chains stabilize at around 200 Å without any solvent effect. However, the end-to-end distance of a single levan chain stabilizes at less than 200 Å (Figure 4.4). The end-to-end distance stabilizes in 1-1.2 ns, whereafter fluctuations within a range is observed somewhat suggesting continuing fluctuations to be due to local conformational changes. In the absence of any solvent effect (i.e. vacuum) the

only interactions present are those between levan chains. Due to these electrostatic forces between levan chains in vacuum, in the presence of other levan molecules, levan chains tend to be less compact than if it was the only chain in vacuum. When compared to single levan conformation in the same media at 298 K and 310 K, levan chain is more stable (fluctuations after 1 ns are in a narrower range) when the number of chains increase which is due to favorable electrostatic interactions between the chains due to amphiphilic nature of the biopolymer. The levan chains cannot fluctuate at a wider range of distance because of limited free volume in the simulation box.

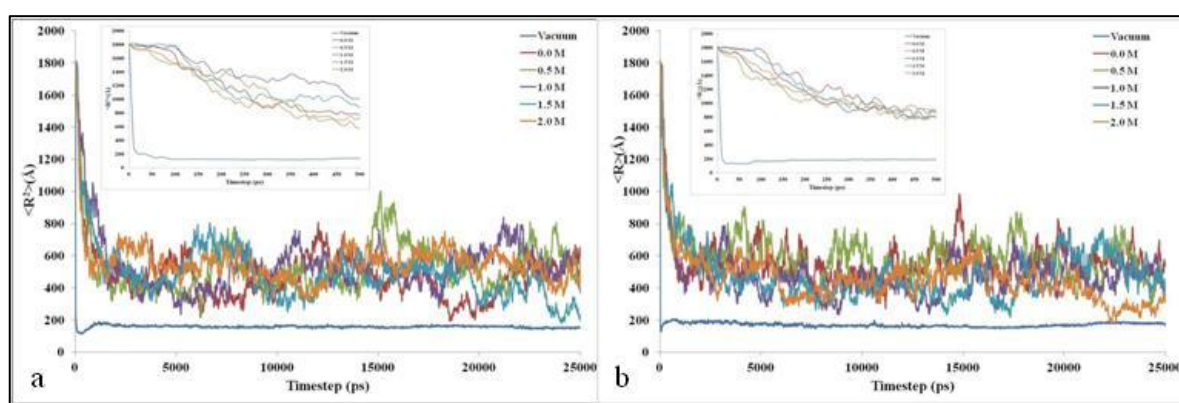


Figure 4.18. End-to-end distance of 9 levan chains with 12 fructose units in different media with respect to time at a) 298 K and b) 310 K

Solvent quality is an important phenomena in polymer science. In these simulations, there is no significant difference between water and saline solutions. However when the average end-to-end values after 5 ns are compared (Table 4.17), the most significant difference is seen between vacuum and aqueous media for both temperatures. End-to-end distances in water systems are % 65 and % 69 larger than vacuum systems at 298 K and 310 K respectively. Therefore water can be considered as a suitable medium for multiple chain systems when compared to vacuum media.

Table 4.17. The Average end-to-end distance values of 9 levan chains at 5 ns - 25 ns at 298 K and 310 K

<b>Media</b>	<b>Average End-to-End value between 5 ns - 25 ns at 298 K (<math>\text{\AA}^2</math>)</b>	<b>Average End-to-End value between 5 ns - 25 ns at 310 K (<math>\text{\AA}^2</math>)</b>
Vacuum	157.36 ± 5.49	166.81 ± 9.80
Water	453.26±117.49	540.89±97.10
0.5 M Salt Solution	533.66±130.44	564.05±106.60
1.0 M Salt Solution	525.39±106.75	455.47±95.00
1.5 M Salt Solution	460.82±125.62	444.44±112.10
2.0 M Salt Solution	536.08±83.71	410.11±93.80

The Student T-test is applied to understand the significance of the difference between vacuum, water and saline systems. According to student T-test, vacuum system is significantly different from all aqueous solutions. At 298 K, addition of salt makes the aqueous systems more favorable, enlarging R. At 310 K, this happened to be case until the addition of 0.5 M NaCl, above which the polymer starts to contract. Further addition of salt does not significantly change the R value ( $p > 0.0001$ )

#### 4.3.2. Radius of Gyration of 9 Levan Chains in Different Media at 298 K and 310 K

Radius of gyration is the distance of atoms to the mass center of the molecule which is a kind of diameter measurement. Figure 4.19. shows the average radius of gyration values of single levan chain amongst 9 levan chains in different media during 25 ns for 298 K and 310 K. As seen in the figure, the radius of gyration values show decreasing trend during the first nanosecond of the simulations. In vacuum, the decrease occurs more rapidly than other systems similar to end-to-end distance (Inset graphs). However after 25 ns, the levan chain is 40 % and 70% more compact in vacuum at 298 and 310 K respectively, showing similar trend to the end-to-end distance values. The reason of the difference is the effect of

solvent and electrostatic forces between the chains. The increase in the number of chains also affects the radius of gyration values. Due to favorable intermolecular interactions with other levan chains, the individual chain now tends to be less compact, resulting in larger radius of gyration values. The radius of gyration of these systems at 310 K fluctuate between 140 Å and 180 Å however the levan chains fluctuate between 80 Å and 120 Å at 298 K. The increase in temperature causes wider fluctuation of the polymer chains which is expected.

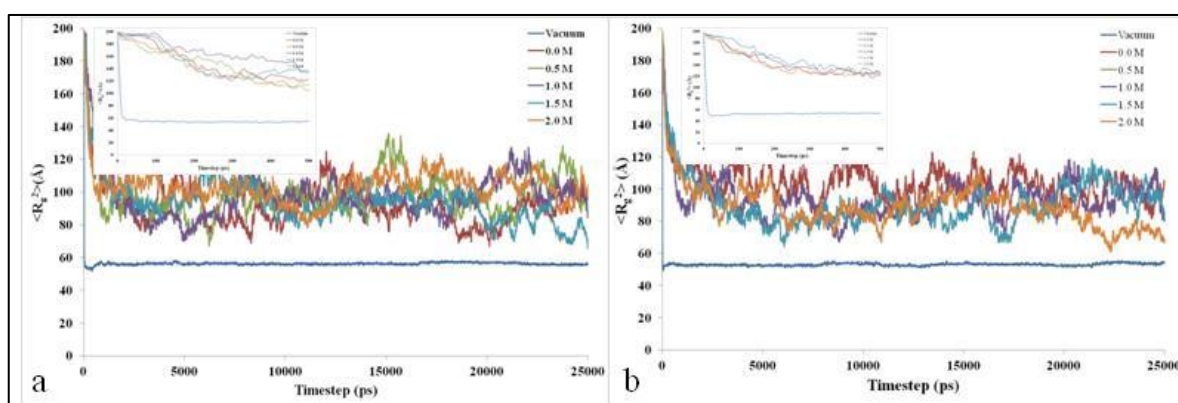


Figure 4.19. Radius of Gyration of 9 levan chains in different media with respect to time at a) 298 K and b) 310 K

Solvent media also affects the radius of gyration values because of the interactions between atoms of solvent and the polymer. Better solvent quality results in an increase in the size of polymer chains [128]. In the single chain system, salt solutions are found to be better solvent than water. In 9 chain systems, based on Rg values at the end of the simulations, again salt solutions are found to be better solvents than water at 298 K (Table 4.18).

Table 4.18. Average Radius of Gyration values of 9 Levan Chains in Different Media at 298 K and 310 K between 5 ns - 25 ns

<b>Media</b>	<b>Average <math>R_G</math> value between 5 ns - 25 ns at 298 K (<math>\text{\AA}^2</math>)</b>	<b>Average <math>R_G</math> value between 5 ns - 25 ns at 310 K (<math>\text{\AA}^2</math>)</b>
Vacuum	56.49±0.61	53.22±0.79
Water	90.25±10.28	99.09±8.64
0.5 M Salt Solution	97.43±11.55	102.25±8.56
1.0 M Salt Solution	95.36±9.40	91.62±8.96
1.5 M Salt Solution	92.27±10.17	88.21±10.54
2.0 M Salt Solution	102.66±8.49	85.62±9.38

At 310 K, all the  $R_g$  values are significantly different from each other and from those at 298 K. At 310 K, the solubility of levan probably increases, resulting in larger  $R_g$  values in water. This increase is observed until a threshold salt concentration (0.5 M) above which levan starts to contract, suggesting some unfavorable interactions, or screening of favorable interactions due to the presence of high salt concentrations which was previously observed for the single chain. The pH effect on the stability of levan solution was studied by Runyon and his colleagues. It is important to measure physicochemical properties for levan because they show how levan chains change as a function of hydrolysis and their stability under different solution conditions. They concluded that acid hydrolysis that result in a decrease in mass and size, occurs at pH lower than 5.5 [89]. The pH value is accepted as 7.00 in our systems and from  $R_g$  results, it can be seen that the levan chains do not disintegrate to form smaller monomers. The levan chains agglomerate with each other but not all the chains agglomerate together.

In the section above, the effect of different media is analyzed according to end-to-end distance and radius of gyration Both at 298 K and 310 K, presence of water (as opposed to vacuum) led to larger  $R_{\text{end-to-end}}$  and  $R_g$  values, indicating favourable interactions between water and levan. This was also observed for the single chain. Comparative results between single and multiple chains is summarized in Table 4.19.

Table 4.19 End-to-end Distance and Radius of Gyration Comparison of Single and Multiple Chain Systems at 298 K and 310 K

Media	Single Chain		Multiple Chain	
	$\langle R \rangle^2$ 298 K ( $\text{\AA}^2$ )	$\langle R \rangle^2$ 310 K ( $\text{\AA}^2$ )	$\langle R \rangle^2$ 298 K ( $\text{\AA}^2$ )	$\langle R \rangle^2$ 310 K ( $\text{\AA}^2$ )
Vacuum	115.33±17.13	74.13±24.80	157.36 ± 5.49	166.81 ± 9.8
Water	427.93±159.42	662.48±446.50	453.26±117.49	540.89±97.1
0.5 M Salt Solution	853.73±382.69	520.72±271.99	533.66±130.44	564.05±106.6
1.0 M Salt Solution	916.07±431.53	542.29±259.57	525.39±106.75	455.47±95.0
1.5 M Salt Solution	-	-	460.82±125.62	444.44±112.1
2.0 M Salt Solution	686.47±327.55	522.12±189.04	536.08±83.71	410.11±93.8
Media	$\langle R_g \rangle^2$ 298 K ( $\text{\AA}^2$ )	$\langle R_g \rangle^2$ 310 K ( $\text{\AA}^2$ )	$\langle R_g \rangle^2$ 298 K ( $\text{\AA}^2$ )	$\langle R_g \rangle^2$ 310 K ( $\text{\AA}^2$ )
Vacuum	42.77±2.34	42.74±1.86	56.49±0.61	53.22±0.79
Water	74.26±11.84	107.52±38.65	90.25±10.28	99.09±8.64
0.5 M Salt Solution	116.33±33.65	90.12±29.08	97.43±11.55	102.25±8.56
1.0 M Salt Solution	124.19±32.64	94.56±25.86	95.36±9.40	91.62±8.96
1.5 M Salt Solution	-	-	92.27±10.17	88.21±10.54
2.0 M Salt Solution	112.09±32.58	94.80±16.38	102.66±8.49	85.62±9.38

When levan is single, it tends to interact better with the aqueous medium, expanding itself more. In the presence of other levan molecules, levan-levan interactions also start to play a role and the levan molecule appears to get more compact. Levan is an amphiphilic molecule where some parts of the molecules favors the interaction with water, whereas other parts do not. In the presence of other levan molecules, levan-levan interactions which may be of hydrophilic or hydrophobic nature also come into play. Temperature effect on the size of the levan molecule is similar for the single and multiple chain systems. Again,



at 298 K all saline solutions are better solvents than water and at 310 K, water or low salt concentrations (0.5 m) are found to be better solvents.

The relation between the end-to-end distance and radius of gyration values can be expressed in Gaussian Model as mentioned before. The expression between these values was shown in Equation 4.1. To understand the Gaussian model for levan chains, the ratio between end-to-end distance and radius of gyration of these systems are also calculated.

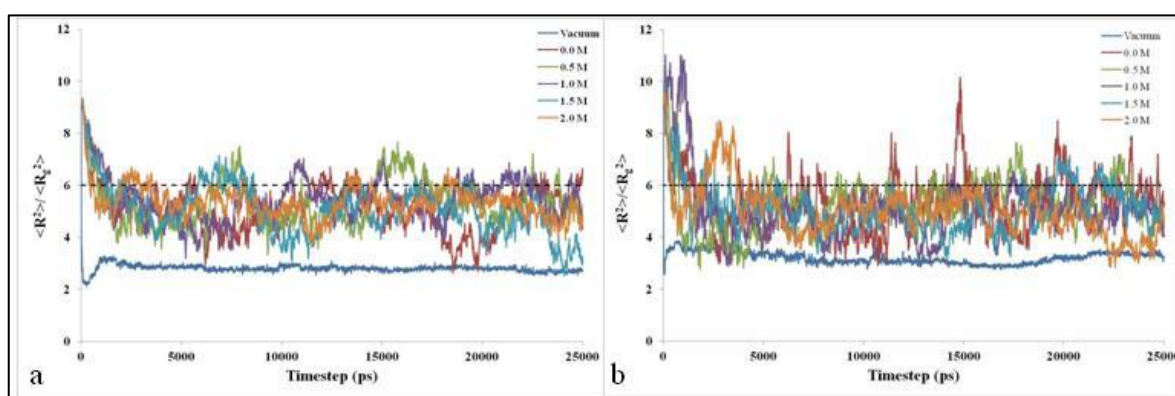


Figure 4.20.  $\langle R^2 \rangle / \langle R_G^2 \rangle$  for 9 levan chains in water and saline solution systems at a) 298 K and b) 310 K

As seen in Figure 4.20, the levan chains are not Gaussian in vacuum system, however in other systems the ratio is close to the value 6, the chains behave more like Gaussian for both temperatures. These results are consistent with those obtained for single chain systems (Figure 4.6.). The average values are tabulated in Table 4.20.

Table 4.20. Average End-to-end Distance over Radius of Gyration values between 2 ns and 5 ns for all systems at 298 K and 310 K

<b>Media</b>	<b>Average value between 2 ns - 5 ns at 298 K</b>	<b>Average value between 2 ns - 5 ns at 310 K</b>
Vacuum	2.78±0.08	3.01±0.09
Water	4.94±0.81	5.35±1.03
0.5 M Salt Solution	5.37±0.80	4.44±0.70
1.0 M Salt Solution	5.37±0.70	4.15±0.68
1.5 M Salt Solution	4.92±0.88	4.49±0.75
2.0 M Salt Solution	5.21±0.50	4.53±0.67

### 4.3.3. Chain Characteristics for 9 Levan Chains in Different Media at 298 K and 310 K

Chain characteristics are analyzed for multiple systems by calculating bond length, bond angle, chord length and bond torsion to understand the effect of multiple levan chains on these structural properties. They were calculated in the same way as in single chain systems.

First of all, bond lengths of the levan chains were analyzed. Figure 4.21 shows the bond length between monomer beads during 25 ns simulations. The inset figure shows the first 500 ps part of the simulations to see the equilibrium stage of the systems.

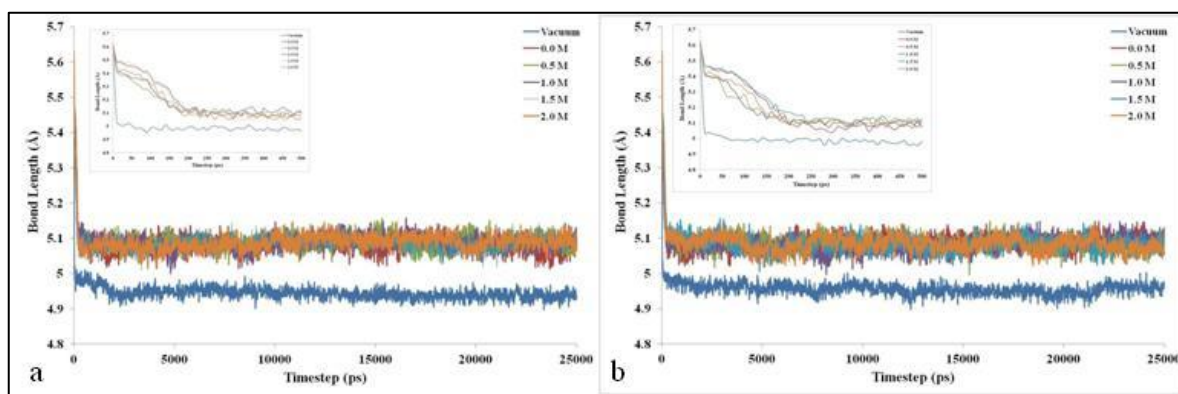


Figure 4.21. Bond Length values of 9 levan chains in different media with respect to time at a) 298 K and b) 310 K

The average bond length values between 5 ns and 25 ns are shown in Table 4.21. As seen in Table 4.21, the values do not change with respect to the saline concentration ( $p < 0.0001$ ).

Table 4.21. Average Bond Length Values of 9 levan chains between 5 ns – 25 ns For All Systems at 298 K and 310 K

Media	Average Bond Length value between 5 ns - 25 ns at 298 K (Å)	Average Bond Length value between 5 ns - 25 ns at 310 K (Å)
Vacuum	4.94±0.01	4.95±0.01
Water	5.08±0.02	5.09±0.02
0.5 M Salt Solution	5.09±0.02	5.08±0.01
1.0 M Salt Solution	5.09±0.02	5.07±0.02
1.5 M Salt Solution	5.09±0.02	5.08±0.02
2.0 M Salt Solution	5.09±0.02	5.08±0.02

As seen in these figures, vacuum system reached equilibrium more rapidly than other systems. And the bond length decreases % 3 more in vacuum system for both 298 K and 310 K which is a considerable decrease. The water and saline solutions have approximately the same trend during simulations. Vacuum system reached equilibrium more quickly than

other systems at 310 K similar to at 298 K. Water and saline systems shows same decreasing trend. When compared to the single chain systems, the values are not quite different with each other but the fluctuation range is different. In single chain systems the bond length values fluctuate with approximately  $\pm 0.08 \text{ \AA}$  and  $\pm 0.06 \text{ \AA}$  at 298 K and 310 K, respectively however in multiple chain systems this value decrease to  $0.02 \text{ \AA}$  for both temperatures. This suggests that the interaction between levan chains make them more stable.

Bond angle between the monomer beads is the next analyzed parameter. As shown in Figure 4.22, the angle between monomer beads is % 7 smaller in vacuum system.

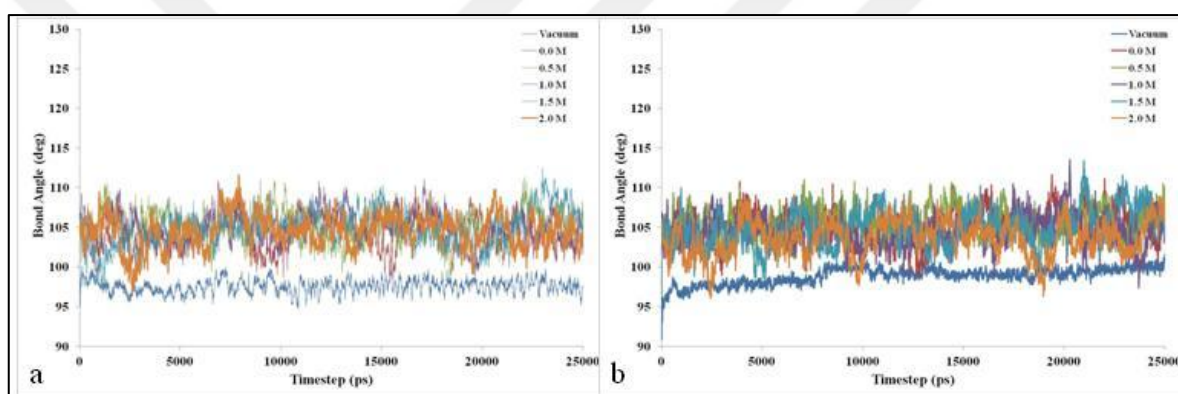


Figure 4.22. Bond Angle Values of 9 levan chains in different media with respect to time  
a) 298 K and b) 310 K

Average bond angle values calculated from Figure 4.23 between 5 ns -25 ns at 298 K and 310 K are tabulated in Table 4.22.

Table 4.22. Average Bond Angle Values of 9 levan chains between 5 ns -25 ns at 298 K and 310 K

<b>Media</b>	<b>Average Bond Angle value between 5 ns - 25 ns at 298 K (°)</b>	<b>Average Bond Angle value between 5 ns - 25 ns at 310 K (°)</b>
Vacuum	97.63±0.85	99.25±0.7
Water	104.55±2.10	105.42±2.0
0.5 M Salt Solution	105.10±2.01	105.48±1.9
1.0 M Salt Solution	104.85±1.98	104.41±2.0
1.5 M Salt Solution	105.44±2.02	105.31±2.3
2.0 M Salt Solution	104.76±1.89	103.78±2.1

When bond angle values are compared to single levan chain systems, the angles are approximately % 3 smaller in multiple systems. The interactions of levan chains with each other affect the flexibility of the monomer beads. Comparison of other values shows the effect of the presence of solvent however the salt concentration appears to be insignificant. Table 4.22 shows that there is no difference ( $p > 0.0001$ ) between water and saline systems in terms of bond angle. The values and the fluctuation range of these systems are not affected from the increase of the temperature to 310 K. In single chain systems at 310 K, the values are higher and the fluctuation range is wider than these systems. The number of chain decreases the free volume in the simulation box and increases the interaction between monomers therefore the bond angle values decrease in multiple chain systems.

Another chain characteristics parameter is the chord length. This parameter also shows the folding of the levan chains. As seen in Figure 4.23, the folding of levan chains in vacuum is much more than other systems. The water and salt concentration do not affect the chord length ( $p > 0.0001$ ). Because of the fluctuations, the average values between 5 ns and 25 ns are tabulated in Table 4.23. It also shows that water and salt solutions are same, the vacuum system is the lowest. As same as other chain characteristics parameters, the values

are almost same with the single chain systems but the fluctuation range is lower in multiple chain systems for both temperatures.

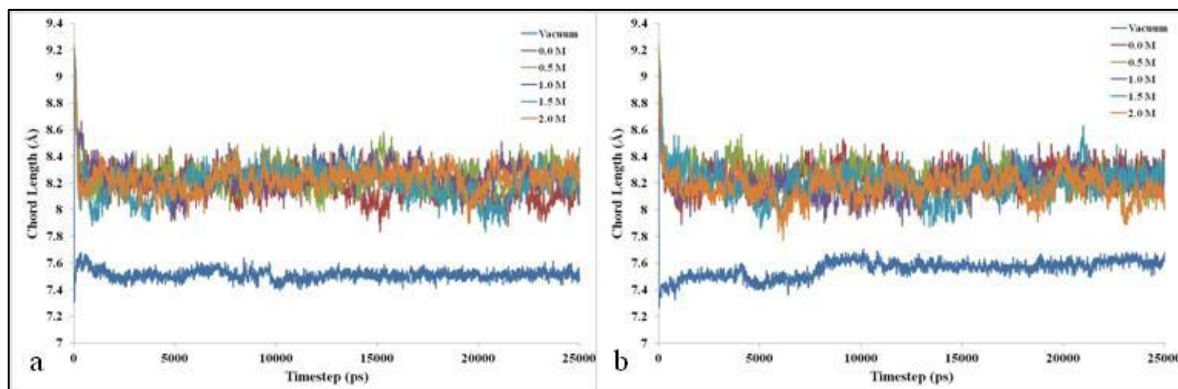


Figure 4.23. Chord Length values of 9 levan chains in different media with respect to time  
a) 298 K and b) 310 K

Table 4.23. Average Chord Length values of 9 levan chains between 5 ns-25 ns at 298 K  
and 310 K

Media	Average Chord Length value between 5 ns - 25 ns at 298 K (Å)	Average Chord Length value between 5 ns - 25 ns at 310 K (Å)
Vacuum	7.51±0.03	7.57±0.05
Water	8.16±0.09	8.25±0.09
0.5 M Salt Solution	8.25±0.09	8.23±0.08
1.0 M Salt Solution	8.25±0.09	8.19±0.10
1.5 M Salt Solution	8.22±0.10	8.19±0.11
2.0 M Salt Solution	8.24±0.08	8.16±0.10

Based on the bond length, bond angle and chord length values a schematic representation of levan in multiple chain systems can be shown as in Figure 4.25.

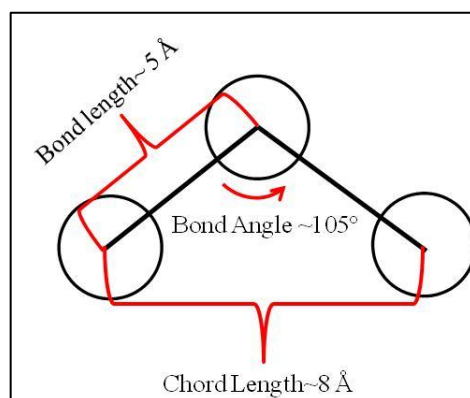


Figure 4.24. Schematic representation of monomer beads in multiple chain systems at 298 K and 310 K

Chain characteristics are important parameters to define the structural conformation of polymers. End-to-end distance can be calculated as theoretical length of the polymers for freely jointed chains by using the equation 4.2. Table 4.24 shows the theoretical end-to-end distance of multiple levan chains calculated with using the bond lengths. As seen from the results, the theoretical values are not affected from the increase in temperature.

Table 4.24. Theoretical End-to-End Distance Calculated From Bond Lengths at 298 K and 310 K

Media	Theoretical End-to-end Distance Values at 298 K ( $\text{\AA}^2$ )	Theoretical End-to-end Distance Values at 310 K ( $\text{\AA}^2$ )
Vacuum	268.43	269.52
Water	283.87	284.98
0.5 M Salt Solution	284.98	283.87
1.0 M Salt Solution	284.98	282.75
1.5 M Salt Solution	284.98	283.87
2.0 M Salt Solution	284.98	283.87

By using bond length values in Table 4.21 and the bond angle values in Table 4.22, end-to-end distance for this model is calculated and tabulated in Table 4.25. As seen from the

results, increase in temperature increases the theoretical end-to-end distance in vacuum, water and 0.5 M salt solution however decreases the theoretical end-to-end distance in 1.0 M, 1.5 M and 2.0 M salt solution.

Table 4.25. Theoretical End-to-End Distance Calculated From Bond Lengths and Bond Angles

<b>Media</b>	<b>Theoretical End-to-end Distance Values at 298 K (<math>\text{\AA}^2</math>)</b>	<b>Theoretical End-to-end Distance Values at 310 K (<math>\text{\AA}^2</math>)</b>
Vacuum	350.08	372.96
Water	474.12	491.54
0.5 M Salt Solution	485.25	490.67
1.0 M Salt Solution	481.11	470.25
1.5 M Salt Solution	491.54	487.51
2.0 M Salt Solution	480.08	461.19

From these calculated end-to-end distances, the characteristic ratio of levan chain can be calculated from Equation 4.4. Table 4.26 tabulates the characteristic ratio of levan chain in different media. As seen from the results, the characteristic ratio of levan chains is lower than the single chains which shows more stiff conformation in the presence of other levan chains. The levan chains are stiffer in vacuum than in water and in saline solutions.



Table 4.26. Characteristic Ratio of Levan Chain in Different Media at 298 K and 310 K

<b>Media</b>	<b>Characteristic Ratio at 298 K</b>	<b>Characteristic Ratio at 310 K</b>
Vacuum	1.30	1.38
Water	1.67	1.72
0.5 M Salt Solution	1.70	1.72
1.0 M Salt Solution	1.68	1.66
1.5 M Salt Solution	1.72	1.71
2.0 M Salt Solution	1.68	1.62

Solvent quality can be expressed in terms of expansion factor which can be calculated from Equation 4.5. Expansion factor is tabulated in Table 4.25 for multiple chain systems for both temperatures.

Table 4.27. Expansion Factor for Multiple Levan Chains in Different Media at 298 K and 310 K

<b>Media</b>	<b>Expansion Factor at 298 K</b>	<b>Expansion Factor at 310 K</b>
Vacuum	0.76	0.78
Water	1.26	1.38
0.5 M Salt Solution	1.37	1.41
1.0 M Salt Solution	1.36	1.27
1.5 M Salt Solution	1.27	1.25
2.0 M Salt Solution	1.37	1.20

As seen in the table, the expansion factor is less than one for vacuum systems which shows that vacuum is a poor environment for levan solubility. Water and saline solutions are good solvents ( $\alpha > 1$ ) however when these values are compared with each other, water became a

better solvent than saline solutions at 310 K except 0.5 M which is in agreement with the previous results. The expansion factor of single chain systems is similar with multiple chain systems. Water and saline systems are good solvents for levan solutions even if the concentration of levan changes.

Torsional angles are calculated to understand planar conformations of levan chains in different media. Figure 4.25 shows the probability of bond torsion angles which the monomer beads prefer to be. The conformations at the peak of the graph have the lowest free energy. In vacuum system, there are five peak points that correspond the minimum energy for 298 K and 310 K (-150°, -80°, 20°, 90°, 120° and -120°, -40°, -20°, 60°, 110° respectively). However levan chains prefer to be at only three conformations when they are in a solvent for both temperatures (-150°, -50°, 100° and -150°, -50°, 95°). In vacuum, there are no solvent effects so the mobility of the chains increases. The planar conformations of levan chains are the same in solvent media. In water and saline solutions, they prefer to be at three conformations at 310 K. The solvent effect decreases the mobility of the chains leading to a preferred conformation.

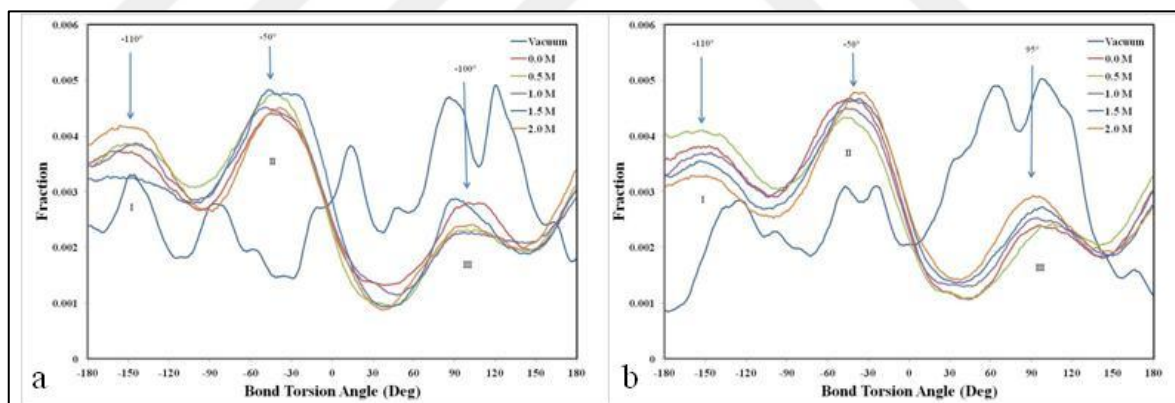


Figure 4.25. Torsion Angle of 9 levan chains in different media with respect to time at a) 298 K and b) 310 K

Table 4.28. Free Energy values for water and saline systems at 298 K and 310 K

	298 K			310 K		
	Free Energy between I-II (kcal/mol)	Free Energy between I-III (kcal/mol)	Free Energy between II-III (kcal/mol)	Free Energy between I-II (kcal/mol)	Free Energy between I-III (kcal/mol)	Free Energy between II-III (kcal/mol)
0.0 M	0.118	-0.113	-0.231	0.135	-0.270	-0.405
0.5 M	0.122	-0.298	-0.420	0.040	-0.268	-0.308
1.0 M	0.100	-0.318	-0.418	0.114	-0.255	-0.368
1.5 M	0.266	-0.080	-0.345	0.147	-0.180	-0.327
2.0 M	0.015	-0.350	-0.366	0.198	-0.062	-0.260

Table 4.28 shows the free energy barrier that needed to switch between these three conformations. Low salinity and high polymer charge cause a fall in free energy barrier [7]. Levan has no charge so only saline concentration affects the energy barrier in our systems. As seen from the table, free energy values do not depend on media and temperature similar to single chain systems.

#### 4.3.4. Radial Distribution Function Analysis (RDF) for Levan Chains at 298 K and 310 K

Radial distribution function was analyzed in three ways. In the first part, each fructose ring was accepted as a bead and distances between center of mass of these beads were calculated. Figure 4.26 shows the RDF for vacuum system with 5 ns intervals. The first nanosecond of the simulation is the equilibrium stage therefore that part is not shown in the figure. It can be seen that in vacuum system, the monomers are collected around 5 Å, 7 Å and 11 Å. Levan chains folded immediately in vacuum therefore no change is observed between the figures. Figure 4.27 shows the last nanosecond of the simulations for all systems. In this figure, it is understood that the salinity of the medium do not affect the

approach of the levan chains, and that presence of water molecules is the main contributor to the observed difference between vacuum and aqueous systems.

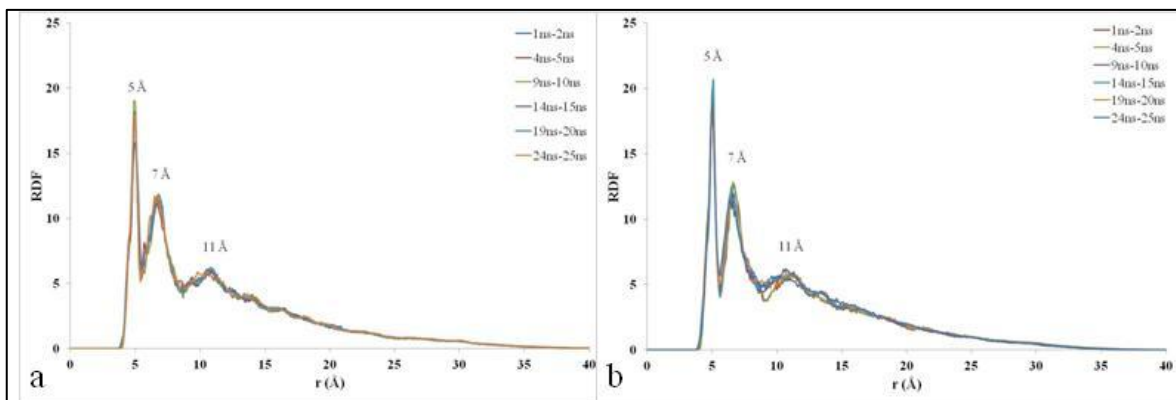


Figure 4.26. RDF of all monomer beads with each other in vacuum at a) 298 K and b) 310 K

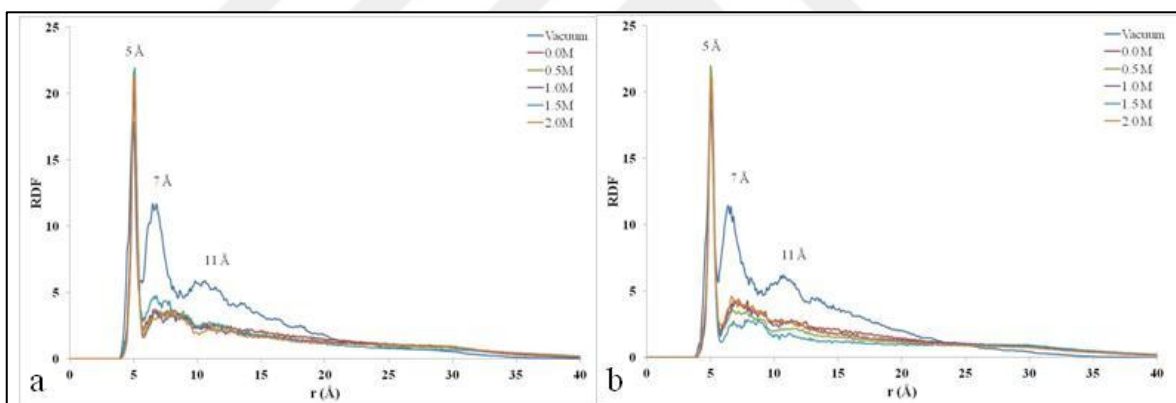


Figure 4.27. RDF of all monomer beads for all systems between 24 ns and 25 ns at a) 298 K and b) 310 K

Table 4.29 shows the radial distribution function values of the systems at their maximums. As seen from the table, the most compactness is seen in vacuum for both temperatures. The values are consistent with expansion factor values.

Table 4.29. RDF values of the all systems at their peak point at 298 K and at 310 K

	298 K				310 K			
	Peak (Å)	g(r) 1 ns	Peak (Å)	g(r) 25 ns	Peak (Å)	g(r) 1 ns	Peak (Å)	g(r) 25 ns
Vacuum	6.70	11.60	6.80	11.71	6.60	12.76	6.40	11.43
0.0 M	6.70	4.02	6.70	3.69	7.70	3.39	7.90	4.22
0.5 M	7.80	3.11	7.90	3.82	7.80	3.65	6.70	3.65
1.0 M	7.80	2.93	6.90	3.57	8.00	2.66	7.00	4.20
1.5 M	7.60	2.87	6.80	4.77	9.00	2.78	7.90	2.83
2.0 M	6.70	3.26	7.90	3.56	7.10	3.42	6.60	4.59

The second part shows the distribution of distance of beads from each other on the same chain which is called  $RDF_{\text{INTRA}}$ . This gives the radial distribution of monomer beads to understand the interactions in the levan chains. Figure 4.28 is plotted for vacuum system with 5 ns intervals. As seen in the figure, the monomer beads get closer and are collected between 5 Å and 10 Å. The vacuum system stabilized before 1 ns therefore the RDF of vacuum system does not change during the simulation.

Figure 4.29 shows the last nanosecond of the simulations for all systems. This figure also shows that the levan chains get closest in vacuum system. Table 4.30 gives the values at the peak points. Major change is observed in the presence of water molecules. Addition of salt does not seem to have much of an effect on the interaction of levan. These results are consistent with those obtained from single chain.

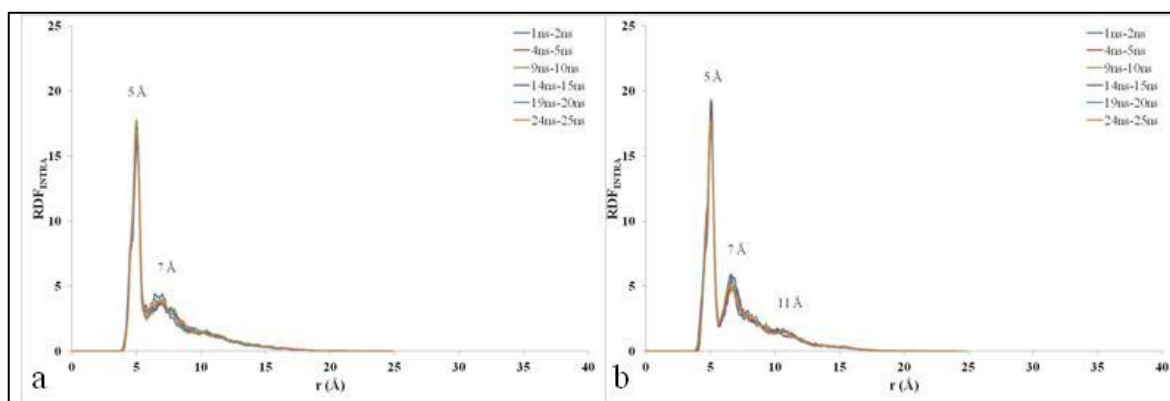


Figure 4.28. Intra-RDF of vacuum system with 1 ns intervals at a) 298 K and b) 310 K

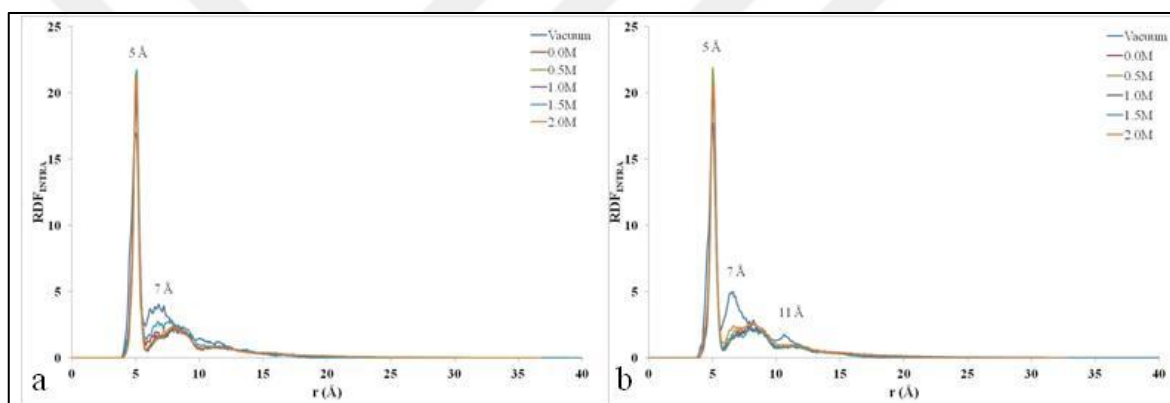


Figure 4.29. Intra-RDF of all systems between 24 ns and 25 ns at a) 298 K and b) 310 K

Table 4.30. RDF-Intra values of the all systems at their peak point at 298 K and at 310 K

	298 K				310 K			
	Peak (Å)	g(r) 1 ns	Peak (Å)	g(r) 25 ns	Peak (Å)	g(r) 1 ns	Peak (Å)	g(r) 25 ns
Vacuum	6.40	4.41	6.80	4.05	6.70	5.39	6.60	5.02
0.0 M	7.60	2.36	8.20	2.29	7.70	2.64	7.90	2.56
0.5 M	7.80	2.52	7.90	2.39	8.10	2.38	7.90	2.49
1.0 M	8.10	2.36	7.90	2.27	8.00	2.19	7.80	2.32
1.5 M	7.60	2.26	7.80	2.91	8.80	2.11	7.90	2.21
2.0 M	8.00	2.33	7.90	2.40	7.90	2.44	8.30	2.68

On the other hand,  $RDF_{INTER}$  shows the distribution of distances between beads of other chains.  $RDF_{INTER}$  of the chains gives an idea about the permeation of the chains into each other. Figure 4.30 is plotted for vacuum system. The peak between 5 Å and 15 Å shows the agglomeration of levan chains.

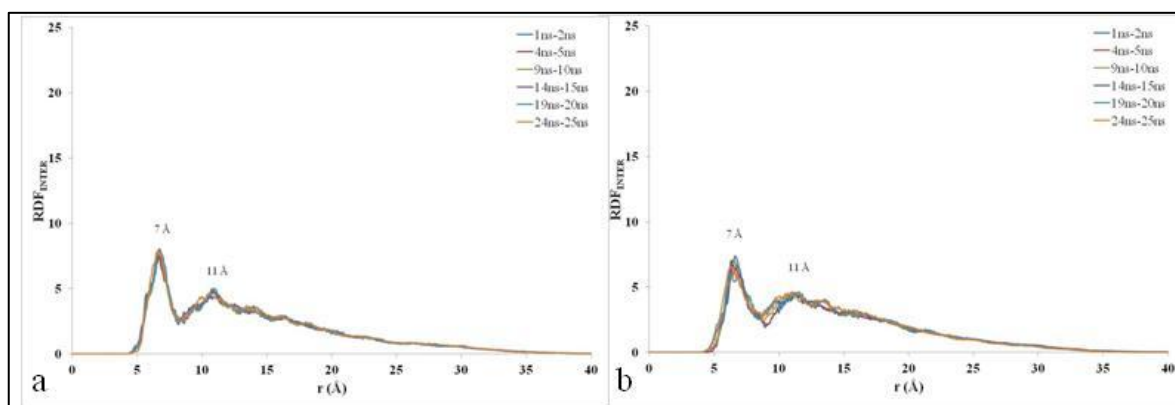


Figure 4.30. Inter-RDF of vacuum system with 1 ns intervals at a) 298 K and b) 310 K

Figure 4.31 is plotted for all systems and Table 4.31 shows the values at peak points. It is understood that the agglomeration is the highest in vacuum system after 25 ns. In other systems, the agglomeration decrease in the presence of water and salt molecules. However,

neither the temperature, nor the salt concentration significantly affects the agglomeration of levan chains.

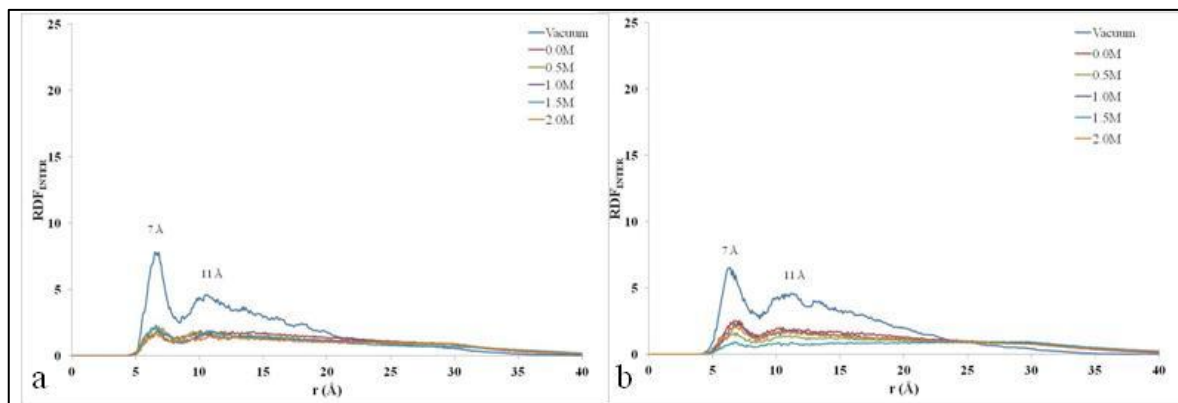


Figure 4.31. Inter-RDF of all systems between 24 ns and 25 ns at a) 298 K and b) 310 K

Table 4.31. RDF-Inter values of the all systems at their peak point at 298 K and at 310 K

	298 K				310 K			
	Peak (Å)	g(r) 1 ns	Peak (Å)	g(r) 25 ns	Peak (Å)	g(r) 1 ns	Peak (Å)	g(r) 25 ns
Vacuum	6.70	7.59	6.50	7.82	6.60	7.39	6.40	6.50
0.0 M	6.70	1.95	6.70	1.83	6.80	1.20	7.10	2.56
0.5 M	6.60	0.86	6.80	2.18	6.50	2.25	6.90	1.62
1.0 M	6.80	1.19	6.70	2.02	6.70	0.71	6.70	2.35
1.5 M	6.50	1.07	6.60	2.31	6.40	1.18	6.70	0.92
2.0 M	6.70	1.45	6.50	1.74	6.60	1.38	6.60	2.18



### 4.3.5. Diffusivity Coefficients for 9 Levan Chains in Different Media at 298 K and 310 K

Mean square displacement (MSD) of levan chains are calculated as mentioned in Methodology part to compare their diffusivity coefficients. Mean square displacement graphs of 9 levan chains in water system are shown in Figure 4.32. As a definition,  $g_2(t)$  and  $g_5(t)$  correspond to the square of end-to-end distance and radius of gyration. End-to-end distance and radius of gyration approach to 10 Å and 25 Å respectively after 25 ns (Figure 4.19 and 4.20.). Similarly,  $g_2(t)$  and  $g_5(t)$  approach to their maximum values 90 Å<sup>2</sup> and 450 Å<sup>2</sup> for 298 K, 100 Å<sup>2</sup> and 625 Å<sup>2</sup> for 310 K as seen in Figure 4.32.

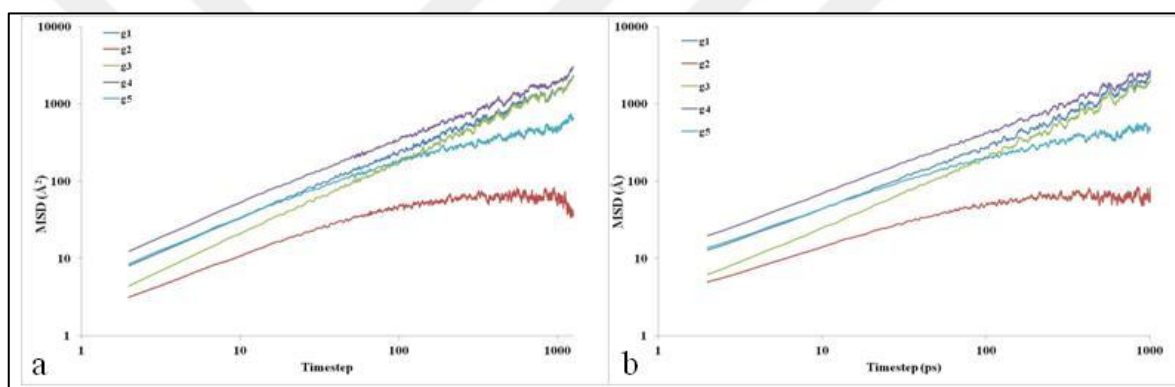


Figure 4.32. MSD graphs for 9 levan chains in water with respect to time at a) 298 K and b) 310 K

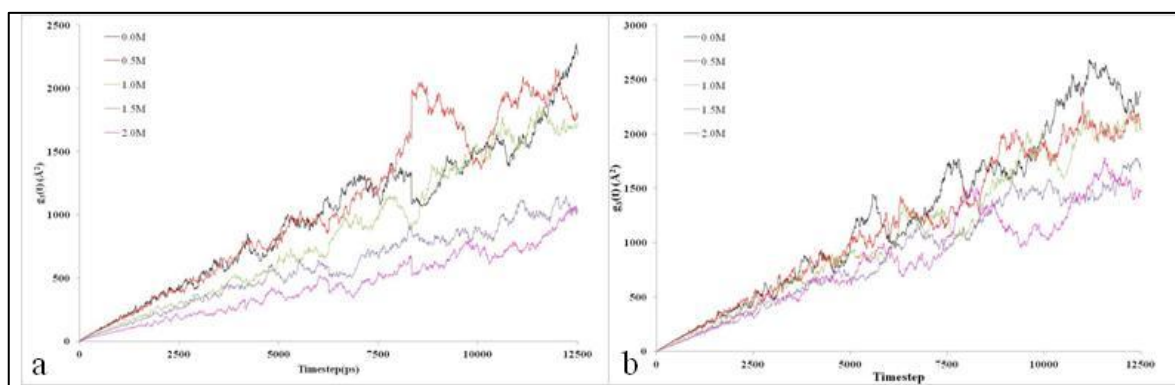


Figure 4.33.  $g_3(t)$  graphs for 9 levan chains in water and saline systems with respect to time at a) 298 K and b) 310 K

As mentioned before,  $g_3(t)$  is the time dependent displacement of the center of mass of levan chains and it is related to the diffusivity coefficient [140]. Figure 4.33 shows the time dependent displacements at different concentrations of saline solutions. The mobility of levan chains decreases with increase of saline concentration. The diffusion coefficients for these systems can be calculated from the slope of these graphs. They are tabulated in Table 4.32 for both temperatures.

Table 4.32. Diffusion Coefficients for 9 Levan Chains in Water and Saline Systems at 298 K and 310 K

	298 K				310 K			
	Diff. Coef. at 298 K (cm <sup>2</sup> /s)	R <sub>H</sub> (Stokes Einstein Eqn.) (Å)	R <sub>G</sub> (If $\alpha > 1$ ) (Å)	R <sub>G</sub> (MD sim.) (Å)	Diff. Coef. at 310 K (cm <sup>2</sup> /s)	R <sub>H</sub> (Stokes Einstein Eqn.) (Å)	R <sub>G</sub> (If $\alpha > 1$ ) (Å)	R <sub>G</sub> (MD sim.) (Å)
0.0 M	2.83x10 <sup>-6</sup>	7.69	14.25	9.50	3.44x10 <sup>-6</sup>	6.58	12.19	9.95
0.5 M	2.68x10 <sup>-6</sup>	7.74	14.33	9.87	2.97x10 <sup>-6</sup>	7.26	13.45	10.11
1.0 M	2.12x10 <sup>-6</sup>	9.32	17.27	9.76	2.92x10 <sup>-6</sup>	7.04	13.04	9.57
1.5 M	1.46x10 <sup>-6</sup>	12.80	23.70	9.61	2.28x10 <sup>-6</sup>	8.52	15.79	9.39
2.0 M	1.06x10 <sup>-6</sup>	16.47	30.50	10.13	2.06x10 <sup>-6</sup>	8.82	16.33	9.25

Diffusion coefficients of 9 levan chains depend on center of mass displacements in different solvents. As seen in Table 4.32., the diffusion coefficients decrease with respect to the salt concentrations. It is understood that salt ions prevents the mobility of the levan chains. The diffusion coefficients are higher at 310 K. The increase of temperature increase the kinetic energy of the chains and this causes high diffusivity in the simulation box.

The conformational and dynamical properties of a polymer chain depend on chain architecture and molecular weight. In linear polymer chains, if each monomer moves into the solvent, friction will occur between the monomer and the solvent molecules. The friction of a linear chain is less than single unbonded monomers. This friction affects the

polymers dynamic properties such as diffusion. Hydrodynamic radius which is another radius type of a polymer chain, includes the hydration shell as well (Figure 4.34).

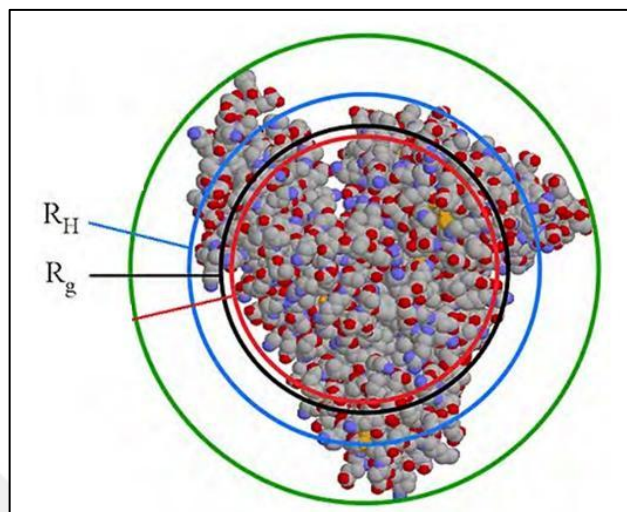


Figure 4.34. Hydrodynamic radius of a polymer [169]

This is the radius that is used in the calculation of diffusion coefficients as the polymer moves within its hydration shell.

$$R_H = \frac{k_b T}{6\eta\pi D} \quad 4.3$$

where  $k_b$  is the Boltzmann constant,  $T$  is temperature,  $\eta$  is the viscosity and  $D$  is the diffusion coefficient.

As seen in Equation 4.3., diffusion coefficient and the size of the linear polymer chain are inversely proportional with each other [170]. As seen in Stokes-Einstein equation (Eq. 4.3) the diffusion coefficient is directly proportional with temperature. When the temperature increases, the increase in diffusion coefficient is expected.

Hydrodynamic radius of levan chains are calculated from the calculated diffusion coefficient from Equation 4.3. The viscosity values and Boltzmann constant are found in the literature [171, 172]. Hydrodynamic radius ratio over radius of gyration is 0.67 for theta solutions and 0.54 for good solvents [173]. Aqueous media is found to be good solvent for levan chains therefore hydrodynamic radius also calculated by using literature data. The  $R_G$  values obtained using  $R_H$  is tabulated in Table 4.32 together with  $R_G$  values obtained from prior MD simulations. Table 4.33 shows the ratio between  $R_G$  calculated from

diffusion coefficient and  $R_G$  from MD simulations. The ratio between these values is considered to give information about agglomeration. As can be seen salt induces agglomeration of levan chains. However, this is much less pronounced at 310 K, indicating that higher temperature helps disperse levan even in saline medium.

Table 4.33. Agglomeration values for multiple chain systems at 298 K and 310 K

<b>System</b>	<b>Agglomeration at 298 K</b>	<b>Agglomeration at 310 K</b>
0.0 M	1.50	1.23
0.5 M	1.45	1.33
1.0 M	1.77	1.36
1.5 M	2.46	1.68
2.0 M	3.01	1.76

In this part of the study, multiple chains of levan were used in different media with the same simulation parameters to understand the interaction of chains with each other. The calculated parameters showed that, the different media do not affect the folding even if the number of levan chains is increased. Agglomeration of levan chains is also observed during the simulations. The levan chains can be considered as Gaussian in all aqueous media. Only vacuum medium affects the Gaussian behavior of the chains. The diffusion coefficients of polymers are calculated from Einstein's Equation as mentioned in Methodology part. Diffusion of polymer chains decreases with the increase of salt concentration. Diffusion coefficient of fructose in water at 298 K is found to be  $6.8 \times 10^{-6}$  cm<sup>2</sup>/s where  $R_G$  value is calculated as 6.61 Å [174]. The diffusion coefficient is higher than the values found in this study however when the radius of gyration increases, the diffusion coefficient decreases. Our  $R_G$  is 9.50 Å, therefore our values are consistent with theoretical values.

The chain characteristics, bond angle, bond length, chord length and torsion angle are very similar for aqueous systems regardless of temperature. Only bond angle decreases slightly when multiple levan chains are present. For all systems, conformation change takes place

immediately (i.e. in the 1<sup>st</sup> ns), followed by a stable region. This happens even faster in vacuum (~100 ps) and always results in a more compact configuration. Based on  $R_G$  and  $R_{\text{end-to-end}}$  results, water is shown to be a suitable solvent whereas addition of salt appears to induce agglomeration of levan chains although the individual properties are not much affected by the presence of salt.

#### 4.4. SIMULATIONS WITH 9 SULFATED LEVAN IN DIFFERENT MEDIA AT 310 K

Sulfated polysaccharide (SPS) is a kind of polysaccharide with sulfated groups in its hydroxyls and comprises a complex group of macromolecules with a range of important biological properties [175, 176]. SPS can be found in two types such as naturally formed or chemically formed. SPSs are used in treatment of various diseases and industrial applications [177]. For example, cellulose sulfate shows anticoagulant and antiviral functions [178]. Bioactivity of sulfated polysaccharides depends on several structural variables such as sugar composition, molecular weight, type of glycosidic bond of the main chain and degree of sulfation. Degree of sulfation is the principle component that affects bioactivity of the polymers. There is positive correlation between degree of sulfation and bioactivity. Erginer, et. al., studied biological activities of sulfated levan produced from *Halomonas* sp. AAD6 [179]. Anticoagulant activity of sulfated levan was found to be similar to heparin in that study. Therefore the simulations were performed for sulfated levan (Fig. 4.35) at body temperature, 310 K, to see the difference between the conformations of native levan and sulfated levan which may lead to functional changes. All rings were sulfated in the structure to obtain higher degree of sulfation. Table 4.34 shows the simulations done with the sulfated levan structure.

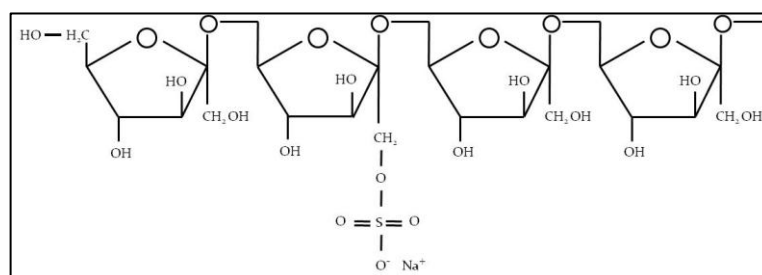


Figure 4.35. Sulfated Levan Structure

Table 4.34. Simulation Parameters of Sulfated Levan Structure Systems

# of levan	# of fructose	NaCl conc. (M)	Media	Pressure (atm)	Temp. (K)	Time step	Duration
9	12	0.0 M	Water	1	310	1	25 ns
9	12	0.5 M	Saline	1	310	1	25 ns
9	12	1.0 M	Saline	1	310	1	25 ns
9	12	1.5 M	Saline	1	310	1	25 ns
9	12	2.0 M	Saline	1	310	1	25 ns

#### 4.3.1. End-to-end Distance for 9 Sulfated Levan Chains in Different Media at 310 K

End-to-end distance was analyzed as previous parts of the study to obtain the change in conformation depending on different media. This parameter is the distance between the terminal monomer beads of levan chains. Average end-to-end distance of 9 sulfated levan chains was plotted with respect to time. As seen in Figure 4.36, the end-to-end distance follows the same trend for different media. They show a sudden decrease in the first nanosecond and then they reach equilibrium. The inset figure shows the first 500 ps of the simulation. It is seen that the sulfated levan structure closes in vacuum more rapidly than in other solvents. Original levan structures decrease to 600 Å approximately but sulfated levan structures decrease to 1000 Å approximately in aqueous media. The levan chains fluctuate between the same range of values during the simulations in different media. The end-to-end distance decreases for all concentrations however end-to-end distance of original levan decreases more than sulfated levan after 25 ns. The sulfate groups at the two end of the chains which are negatively charged repel each other preventing the ends to come closer as much as in original levan structure. Sulfated levan chain is an ionic structure therefore the interactions between the solvent and the molecule is more favorable in aqueous media.

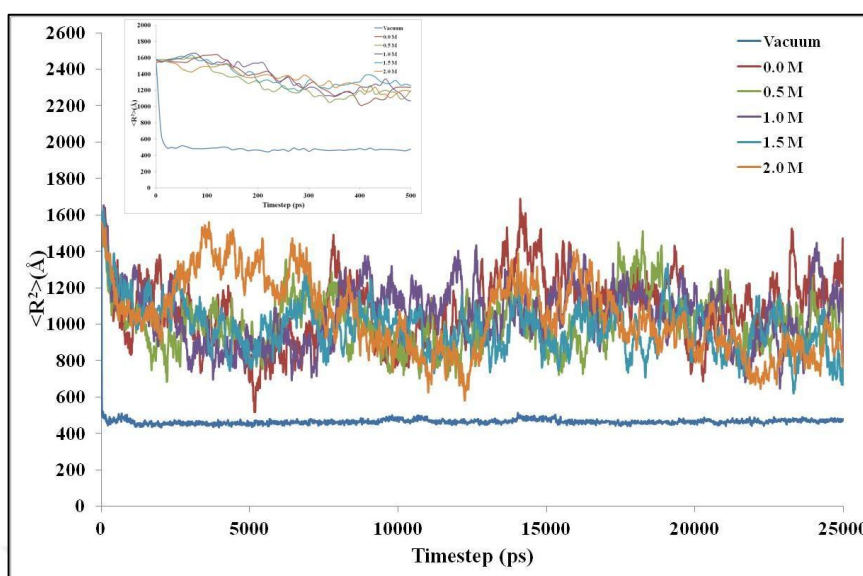


Figure 4.36. End-to-end distance of 9 sulfated levan chains with 12 fructose units in different media at 310 K with respect to time

Table 4.35 shows the averaged end-to-end values between 5 ns and 25 ns of the levan chains in different media. When Table 4.35 is compared to Table 4.16, the values are % 55 higher than the end-to-end distance of original levan structure at the same temperature. The sulfated levan structures show significantly different behavior to original levan in different media at 310 K ( $p < 0.0001$ ). Difference in the salinity of the environment does not seem to have an effect on end-to-end distance. Both water and saline solutions are better solvents for sulfated levan than original levan structures. The force of repulsion between sulfate groups is stronger than interaction between levan and the solvent molecules. Salt screening effect on ions at the end groups probably takes place allowing the end groups to approach each other. It should be noted that the structure now fluctuates more than the original levan.

Table 4.35. The Average end-to-end distance values of 9 sulfated levan chains at 5 ns - 25 ns at 310 K

	<b>Original Levan</b>	<b>Sulfated Levan</b>
<b>Media</b>	<b>Average End-to-End value between 5 ns - 25 ns (<math>\text{\AA}^2</math>)</b>	<b>Average End-to-End value between 5 ns - 25 ns (<math>\text{\AA}^2</math>)</b>
Vacuum	166.81 ± 9.8	465.96±10.27
Water	540.89±97.1	1087.57±186.44
0.5 M Salt Solution	564.05±106.6	1012.10±144.42
1.0 M Salt Solution	455.47±95.0	1059.60±149.09
1.5 M Salt Solution	444.44±112.1	956.49±112.95
2.0 M Salt Solution	410.11±93.8	997.38±181.90

#### 4.3.2. Radius of Gyration of 9 Sulfated Levan Chains in Different Media at 310 K

Radius of gyration is analyzed as the next property of the sulfated levan chains to understand the conformation. As seen in end-to-end distance analysis, the sulfated levan structures do not fold as original structure because of the repulsion of sulfate groups. As other sulfate groups are also present within the structure higher radius of gyration values than original levans are also expected. Higher radius of gyration is expected not only because of the repulsion of sulfate groups, but also because sulfated levan is more hydrophilic than the original levan structure. Due to favorable interactions between the sulfate groups and water, radius of gyration is expected to be larger. Figure 4.37 shows the radius of gyration values over 25 ns simulations. In the figure, there is a sudden decrease during the first nanosecond and then they become equilibrium as seen in end-to-end distance. The radius of gyration values of original levan chains fluctuate between 80 Å and 120 Å however they fluctuate between 140 Å and 180 Å in sulfated levan simulations. This confirms the sulfate groups prevent the folding of levan chains.



The averaged radius of gyration values between 5 ns and 25 ns are tabulated in Table 4.36. As seen from the table, the values are higher than the radius of gyration of original levan.

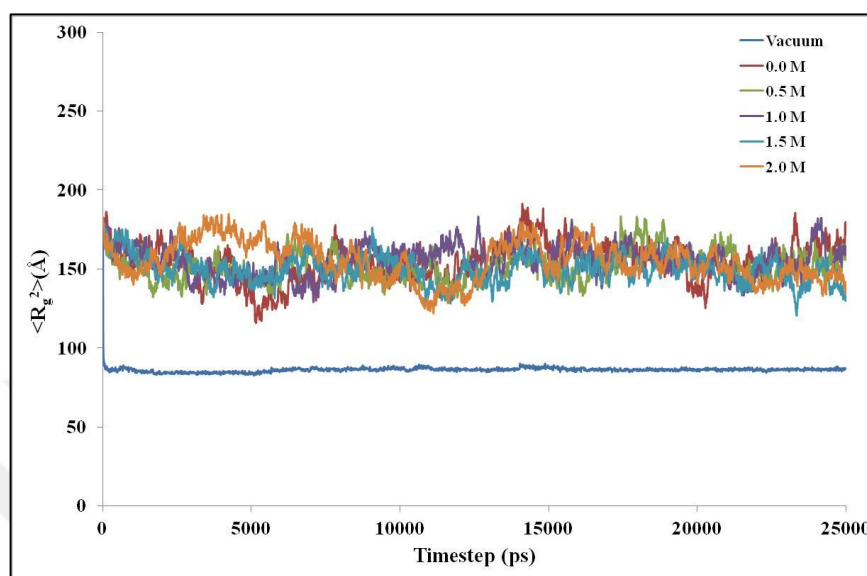


Figure 4.37. Radius of Gyration values of 9 Sulfated Levan Chains in Different Media at 310 K with respect to time

When significance test is applied to understand the different between the values, the conformation of levan chains in all aqueous media can be considered to be the same except for 1.5 M, which can not be explained ( $p > 0.0001$ ). The significant difference is obtained between the aqueous systems and vacuum.

Table 4.36. Average Radius of Gyration values of 9 Sulfated Levan Chains in Different Media at 310 K between 5 ns - 25 ns

	<b>Original Levan</b>	<b>Sulfated Levan</b>
<b>Media</b>	<b>Average <math>R_G</math> value between 5 ns - 25 ns (<math>\text{\AA}^2</math>)</b>	<b>Average <math>R_G</math> value between 5 ns - 25 ns (<math>\text{\AA}^2</math>)</b>
Vacuum	53.22±0.79	86.34±0.87
Water	99.09±8.64	154.99±12.24
0.5 M Salt Solution	102.25±8.56	152.52±9.24
1.0 M Salt Solution	91.62±8.96	155.76±9.37
1.5 M Salt Solution	88.21±10.54	148.72±8.04
2.0 M Salt Solution	85.62±9.38	153.34±11.74

Solvent quality is understood with the size of the polymers. If a polymer is in a good solvent, it expands and its size increases [128]. Water and saline solutions show better solvent effects to sulfated levan chains than original levan because of the ionic groups. The first nanosecond of the simulations is the equilibrium stage therefore the solvent quality is interpreted according to the rest of the simulations.

Gaussian model is also analyzed for the sulfated levan structures to understand the compatibility of the model to these polymers. The proportion between the end-to-end distance and radius of gyration gives an idea about the model of the polymer solutions (Eqn. 4.2). Figure 4.38 shows the  $\langle R^2 \rangle / \langle R_g^2 \rangle$  over time and this value reaches 6 approximately during the simulations. Therefore the chains behave more like Gaussian as original levan systems. Sulfation did not affect the compatibility of Gaussian model for these systems.

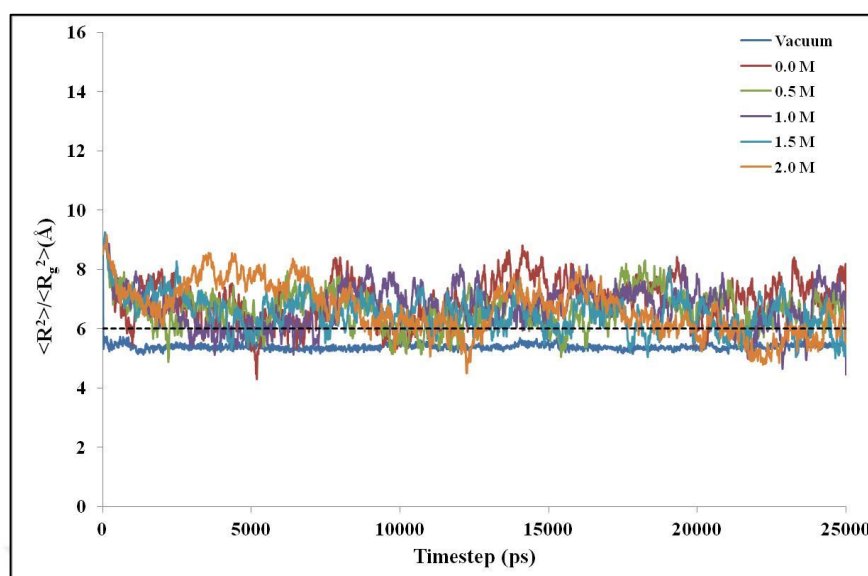


Figure 4.38.  $\langle R^2 \rangle / \langle R_g^2 \rangle$  values of 9 sulfated levan chains at 310 K with respect to time

Table 4.37. Average  $\langle R^2 \rangle / \langle R_g^2 \rangle$  values of 9 original and sulfated levan chains at 310 K

Media	Average value for original levan between 2 ns - 5 ns at 310 K	Average value for sulfated levan between 2 ns - 5 ns at 310 K
Vacuum	3.01±0.09	5.87±0.08
Water	5.35±1.03	6.97±0.73
0.5 M Salt Solution	4.44±0.70	6.61±0.60
1.0 M Salt Solution	4.15±0.68	6.77±0.64
1.5 M Salt Solution	4.49±0.75	6.42±0.50
2.0 M Salt Solution	4.53±0.67	6.46±0.75

### 4.3.3. Chain Characteristics for 9 Sulfated Levan Chains at 310 K in Different Media

The monomers of sulfated levan chains are analyzed in terms of bond angle, bond length, chord length and torsion angle to understand the effect of sulfation on conformation. As in

other parts of the study, the analysis is started with calculating the bond length between monomer beads. Figure 4.39 shows the calculated the bond length over 25 ns. As seen in the figure, bond length values decrease in the first nanosecond of the simulations as in other simulations however they do not show a sudden decrease (Inset figure). Bond length of the levan chains decrease and become stable in vacuum more rapidly than in aqueous medium similar to unsulfated levan. All the systems fluctuate between 5.8 Å and 6 Å approximately. In vacuum system, the distance between monomer beads of native levan decrease 16 % more than sulfated levan at 310 K because of the sulfate groups in the monomer beads.

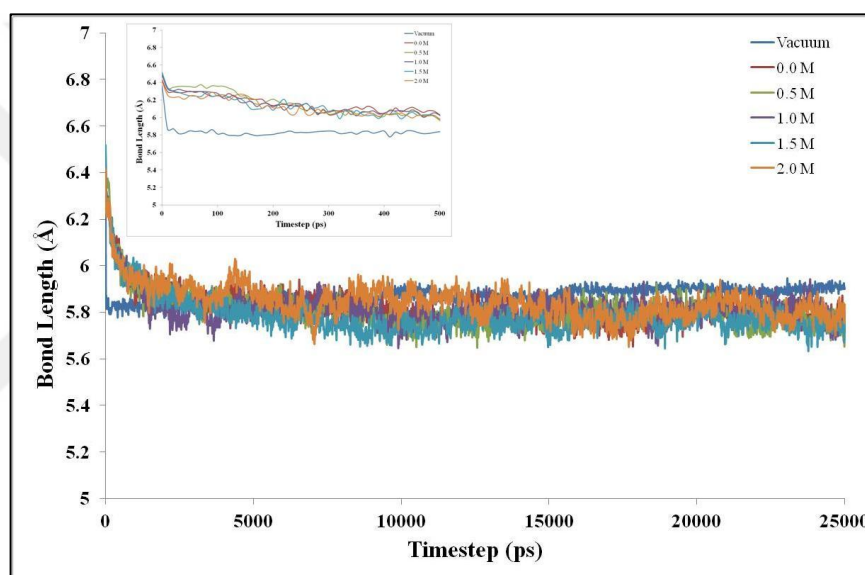


Figure 4.39. Bond Length values for 9 Sulfated Levan Chain Systems at 310 K during 25 ns

As compared to original levan (Figure 4.48), the monomer beads do not get close as much as in original levan chains because of the repulsion between the negatively charged groups in the monomer beads. Table 4.38 is tabulated with the average bond length values between 5 ns and 25 ns. The fluctuations are between 5.8 Å and 6 Å and the range of the fluctuation is 0.04 Å approximately. These values are 5.0 Å and 5.2 Å with 0.2 Å fluctuation range for original levan, where both values and the range of the fluctuation are higher. This shows that the sulfate groups affect the flexibility of the monomer beads.

Table 4.38. Average Bond Length Values of 9 sulfated levan chains Between 5 ns – 25 ns  
For All Systems at 310 K

	<b>Original Levan</b>	<b>Sulfated Levan</b>
<b>Media</b>	<b>Average Bond Length value between (Å) 5 ns - 25 ns</b>	<b>Average Bond Length value between (Å) 5 ns - 25 ns</b>
Vacuum	4.95±0.01	5.88±0.02
Water	5.09±0.02	5.79±0.04
0.5 M Salt Solution	5.08±0.01	5.78±0.04
1.0 M Salt Solution	5.07±0.02	5.81±0.04
1.5 M Salt Solution	5.08±0.02	5.76±0.04
2.0 M Salt Solution	5.08±0.02	5.82±0.05

Bond angle is another parameter to understand the conformation of monomer beads including sulfate groups. It is calculated as an angle between two monomers. Figure 4.40 shows the trend of bond angle values over 25 ns. The angles increase in water and saline solutions. The vacuum medium does not change the bond angles of sulfated monomer beads. The values are about % 5 higher than original levan structures at 310 K in water and salt solution systems.

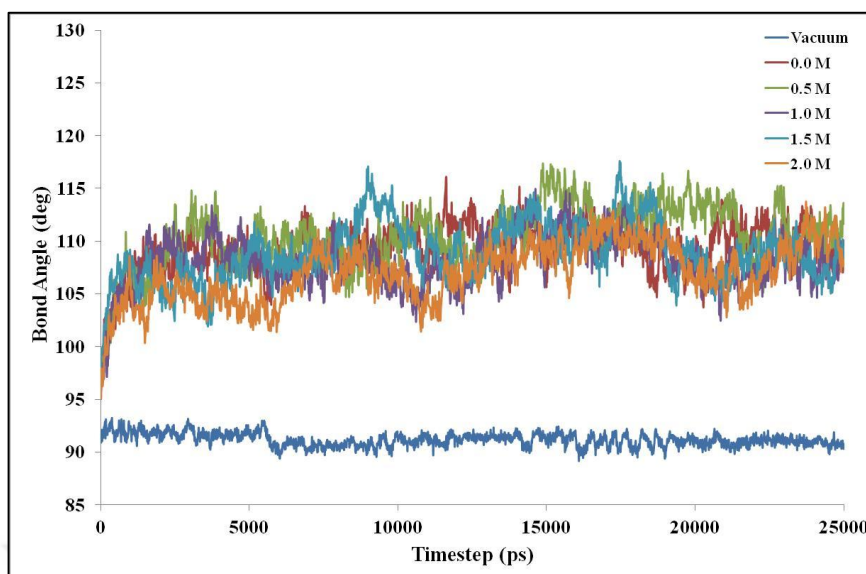


Figure 4.40. Bond angle values for 9 Sulfated Levan Chain Systems at 310 K during 25 ns

Table 4.39. Average Bond Angle Values of 9 sulfated levan chains between 5 ns -25 ns at 310 K

Media	Original Levan	Sulfated Levan
	Average Bond Angle value between 5 ns - 25 ns (°)	Average Bond Angle value between 5 ns - 25 ns (°)
Vacuum	99.25±0.7	91.01±0.55
Water	105.42±2.0	109.81±1.84
0.5 M Salt Solution	105.48±1.9	111.07±2.34
1.0 M Salt Solution	104.41±2.0	108.23±2.17
1.5 M Salt Solution	105.31±2.3	109.63±2.40
2.0 M Salt Solution	103.78±2.1	107.73±2.37

Table 4.39 is tabulated to show the average values between 5 ns and 25 ns for all systems. The average bond angle values increase with respect to the original levan structure. Sulfate groups repel each other therefore the angle between these groups increase.

Figure 4.41 shows the chord length values over 25 ns for all systems to see the behavior of the chains. They show decrease in the first nanosecond and then they become equilibrium. After equilibrium stage, they fluctuate between 8.8 Å and 9.4 Å. The values are about % 9 higher than the original levan systems at the same temperature.

The average chord length values are averaged over 5 ns - 25 ns and tabulated in Table 4.40. The increase in chord length values between original levan and sulfated levan structures are also shown in Table 4.40. The chord length values of original levan fluctuate between 8.2 Å and 8.3 Å with 0.09 range at 310 K however these values are 8.9 Å and 9.1 Å with 0.12 range approximately. It is once again understood that sulfate groups prevent the folding of the levan chains.

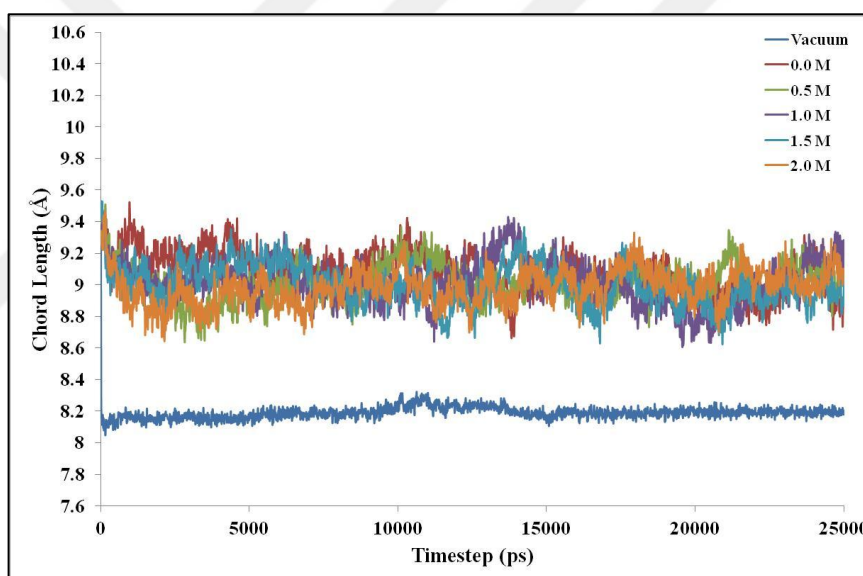


Figure 4.41. Chord Length values for 9 Sulfated Levan Chain Systems at 310 K during 25 ns

Chain characteristics are important parameters to define the structural conformation of polymers. End-to-end distance can be calculated as theoretical length of the polymers for freely jointed chains and tabulated in Table 4.41. Theoretical end-to-end distance of sulfated levan chains calculated from bond lengths are % 40 higher for vacuum and % 30 higher for water and saline systems than original levan structure at 310 K.

Table 4.40. Average Chord Length values of 9 sulfated levan chains between 5 ns-25 ns at 310 K

	<b>Original Levan</b>	<b>Sulfated Levan</b>
<b>Media</b>	<b>Average Chord Length value between 5 ns - 25 ns (Å)</b>	<b>Average Chord Length value between 5 ns - 25 ns (Å)</b>
Vacuum	7.57±0.05	8.19±0.03
Water	8.25±0.09	9.05±0.11
0.5 M Salt Solution	8.23±0.08	9.02±0.10
1.0 M Salt Solution	8.19±0.10	9.00±0.15
1.5 M Salt Solution	8.19±0.11	8.98±0.12
2.0 M Salt Solution	8.16±0.10	8.99±0.10

Table 4.41. Theoretical End-to-End Distance Calculated From Bond Lengths at 310 K

	<b>Original Levan</b>	<b>Sulfated Levan</b>
<b>Media</b>	<b>Theoretical End-to-end Distance Values (Å<sup>2</sup>)</b>	<b>Theoretical End-to-end Distance Values (Å<sup>2</sup>)</b>
Vacuum	269.52	380.31
Water	284.98	368.76
0.5 M Salt Solution	283.87	367.49
1.0 M Salt Solution	282.75	371.31
1.5 M Salt Solution	283.87	364.95
2.0 M Salt Solution	283.87	372.59



Table 4.42. Theoretical End-to-End Distance Calculated From Bond Lengths and Bond Angles

	<b>Original Levan</b>	<b>Sulfated Levan</b>
<b>Media</b>	<b>Theoretical End-to-end Distance Values (<math>\text{\AA}^2</math>)</b>	<b>Theoretical End-to-end Distance Values (<math>\text{\AA}^2</math>)</b>
Vacuum	372.96	393.47
Water	491.54	747.01
0.5 M Salt Solution	490.67	779.12
1.0 M Salt Solution	470.25	709.66
1.5 M Salt Solution	487.51	734.30
2.0 M Salt Solution	461.19	699.62

End-to-end distance is also calculated from bond lengths and bond angles. The values are tabulated in Table 4.42 and it shows that these values are approximately % 35 more than 310 K.

These values are calculated to understand the stiffness of polymers from characteristic ratio. The characteristic ratio is calculated from the ratio of these theoretical end-to-end distances and tabulated in Table 4.43 for sulfated levan chain systems. As seen from Table 4.43, the characteristic ratio is higher than 310 K which shows the sulfated levan chains are less stiff in water and saline solutions, which would be expected from a more hydrophilic structure.

Table 4.43. Characteristic Ratio of Levan Chain in Different Media at 310 K

	<b>Original Levan</b>	<b>Sulfated Levan</b>
<b>Media</b>	<b>Characteristic Ratio</b>	<b>Characteristic Ratio</b>
Vacuum	1.38	1.03
Water	1.72	2.02
0.5 M Salt Solution	1.72	2.12
1.0 M Salt Solution	1.66	1.91
1.5 M Salt Solution	1.71	2.01
2.0 M Salt Solution	1.62	1.87

Expansion factor is also calculated to understand the sulfation effect on solvent quality in levan solutions. The values are tabulated in Table 4.44 for sulfated levan chain systems. When this table is compared to the original levan, it is clearly seen that the expansion factors are higher for sulfated systems. However the aqueous media is a good solvent for levan chains in both conditions.

The most significant change is seen in vacuum systems. Vacuum is considered as poor solvent for original chains but the expansion factor for sulfated levan in vacuum is higher than one which defines the vacuum as a good solvent. This shows the repulsion of sulfate groups from each other even in the absence of any solvent effect.

Table 4.44. Expansion Factor for Sulfated Levan Chains in Different Media at 310 K

<b>Media</b>	<b>Original Levan Expansion Factor at 310 K</b>	<b>Sulfated Levan Expansion Factor at 310 K</b>
Vacuum	0.62	1.22
Water	1.90	2.95
0.5 M Salt Solution	1.99	2.75
1.0 M Salt Solution	1.61	2.85
1.5 M Salt Solution	1.56	2.62
2.0 M Salt Solution	1.44	2.67

The torsional angles between monomer beads are analyzed as histogram of conformations where the monomer beads choose to be. Figure 4.42 shows the histogram to understand the planar conformation of sulfate groups. The highest fraction of torsional angle shows the angle of monomer beads prefer to be at most. The monomer beads have the lowest energy at these points. In vacuum system, the conformation of monomer beads is very flexible as seen in the figure 4.42. In other media, the monomer beads do not move as much as in vacuum system. The peak points are not exact as in original levan systems.  $-110^\circ$  and  $170^\circ$  can be considered as the most preferred angles for sulfated levan chains in aqueous media. The conformation of sulfated levan chains remain more stable because the number of preferred angles is less than original levan. The sulfate groups affect the mobility of monomer beads.

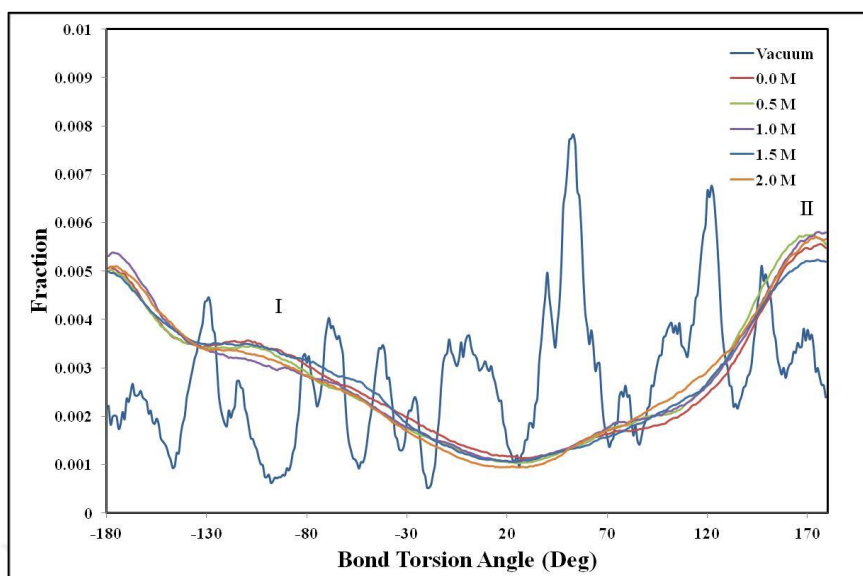


Figure 4.42. Histogram of Torsion Angle values for 9 Sulfated Levan Chain Systems at 310 K during 25 ns

Table 4.45 shows the free energies calculated from the maximum points of the figure 4.42. Table 4.45 shows the free energy of the original levan at the same temperature, the increase in free energy levels can be considered.

Table 4.45. Free Energy values for water and saline systems at 310 K for 9 Sulfated Levan chains

	<b>Free Energy between I-II (kcal/mol)</b>
0.0 M	0.279
0.5 M	0.327
1.0 M	0.394
1.5 M	0.266
2.0 M	0.351

The monomer beads are more flexible when the needed free energy between the conformations is lower, therefore sulfated levan is less flexible than the original structure deduced from the higher free energy between the conformations compared with native levan.

#### **4.4.4. Radial Distribution Function Analysis (RDF) for Sulfated Levan Chain Systems at 310 K**

In this part of the study, the sulfation effect on radial distribution function is analyzed. RDF of the systems are investigated in three ways similar to the previous parts. The first nanosecond of the simulations are not considered, only equilibrium stage of the simulations are analyzed in RDF. First of all, the RDF of the distances between each monomer beads of all chains are shown. Figure 4.43 is plotted for vacuum system with 5 nanoseconds intervals. As seen in the figures displaying almost perfect overlap the sulfated levan chains are in equilibrium after 1 ns. In Figure 4.43, the RDF shows two peaks between 5 Å-10Å and 10 Å-15 Å. The sulfate groups provide better dispersion of levan chains in vacuum than original levan because the peak points are not sharp as original levan. Figure 4.44 is plotted to compare RDF during the last nanosecond of the simulations for all systems. The agglomeration of the chains is seen in all media however, the solvent prevents the agglomeration of the chains. The type or concentration of the medium and sulfation do not affect the trend of the graph.

The inset figure of Figure 4.44 shows the RDF values of original levan and sulfated levan in aqueous medium. As seen in the figure, the interaction of monomers are seen in the larger radius for sulfated levan structure. Table 4.46 shows the radial distribution function values of the systems at their maximums. As seen from the table the peak points are at larger radius values and the radial distribution function values are less than at 310 K which shows the sulfated levan beads do not approach each other as much as original levan chains.

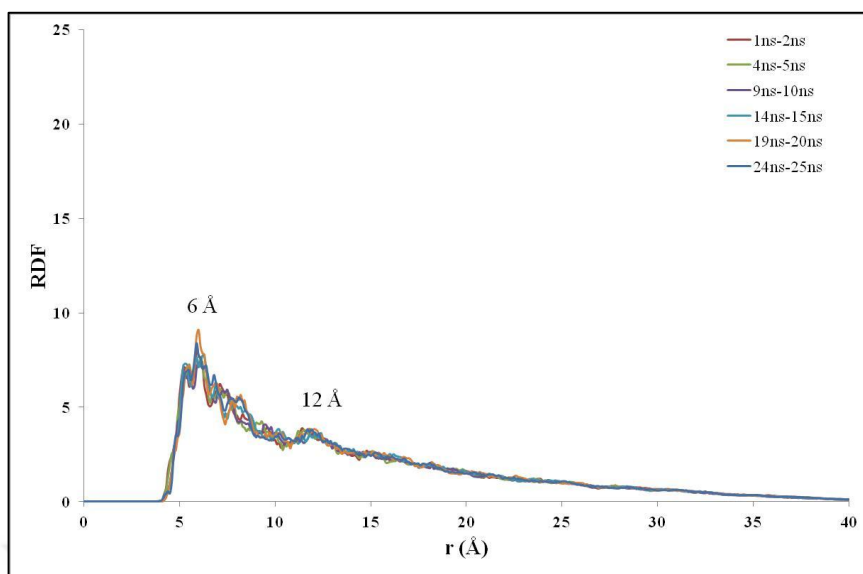


Figure 4.43. RDF of all monomer beads in sulfated levan chains with each other in vacuum at 310 K

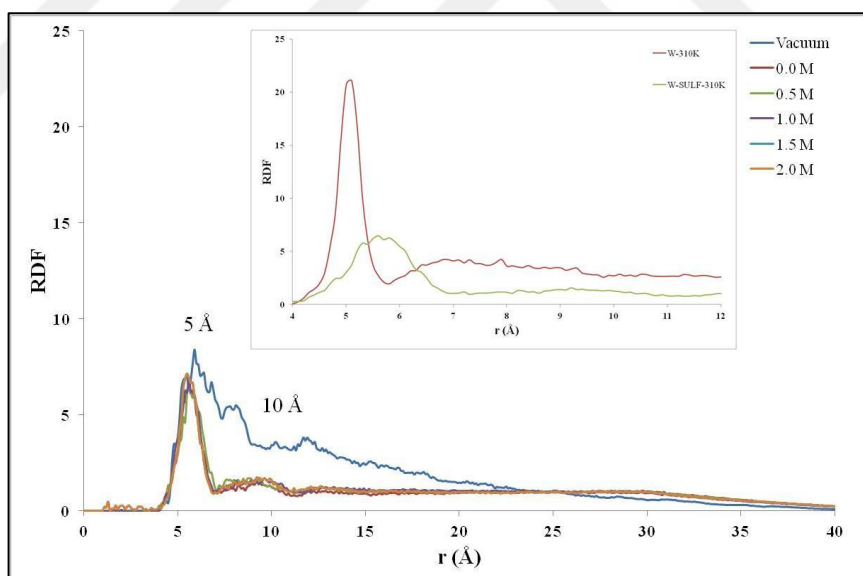


Figure 4.44. RDF of all monomer beads of 9 sulfated levan chains for all systems between 24 ns and 25 ns at 310 K

Table 4.46. RDF values of the all sulfated levan systems at their peak point at 310 K

	Original Levan				Sulfated Levan			
	Peak (Å)	g(r) 1 ns	Peak (Å)	g(r) 25 ns	Peak (Å)	g(r) 1 ns	Peak (Å)	g(r) 5 ns
Vacuum	6.60	12.76	6.40	11.43	11.7	3.84	9.6	1.47
0.0 M	7.70	3.39	7.90	4.22	9.2	1.56	9.0	1.46
0.5 M	7.80	3.65	6.70	3.65	9.3	1.65	9.1	1.46
1.0 M	8.00	2.66	7.00	4.20	9.6	1.69	9.2	1.68
1.5 M	9.00	2.78	7.90	2.83	9.3	1.96	9.3	1.78
2.0 M	7.10	3.42	6.60	4.59	9.2	1.74	9.0	1.84

As RDF shows the interactions between all beads with each other,  $RDF_{\text{INTRA}}$  and  $RDF_{\text{INTER}}$  should be evaluated to obtain more information. Intra RDF shows the distribution of distance of beads from each other on the same chain. Figure 4.45 shows the  $RDF_{\text{INTRA}}$  for vacuum system with 5 ns intervals. The monomer beads approach each other between 5 Å and 10 Å. However they disperse more than the monomer beads of original levan appears to be more compact because g(r) value is lower than original levan in vacuum.

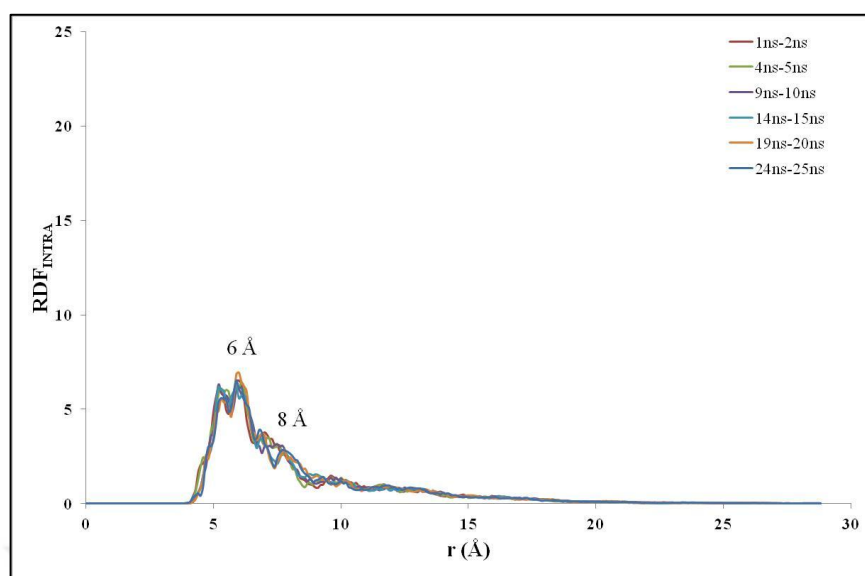


Figure 4.45. Intra-RDF of 9 sulfated levan chains in vacuum system at 310 K

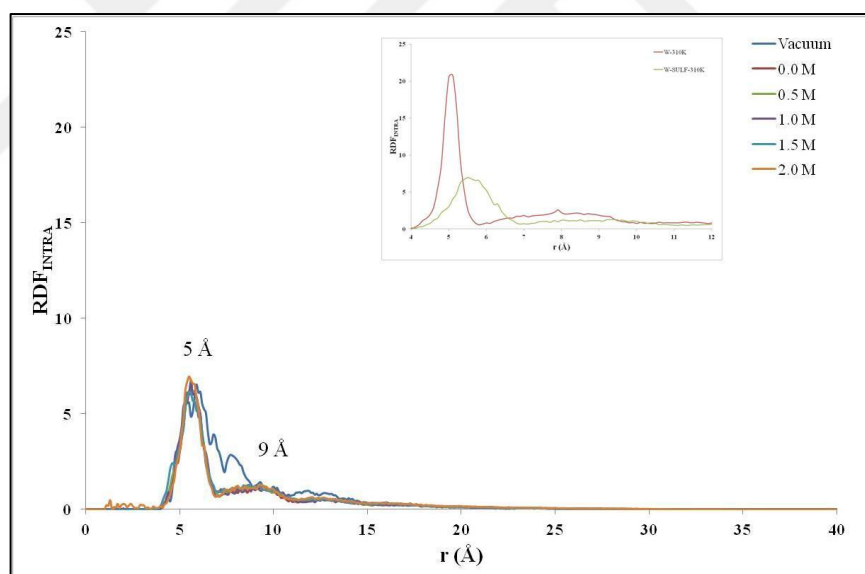


Figure 4.46. Intra-RDF of 9 sulfated levan chains in different media between 24 ns and 25 ns at 310 K

Figure 4.46 is plotted to compare the systems in different media. As seen in the figure, the highest folding is seen in vacuum system (blue line). The intra RDF of sulfated levan in water media is compared to the original levan in water media at 310 K (Inset figure 4.46).



As seen in the figure, the original levan beads are more tightly packed, as understood from lower radius values.

Table 4.47 is tabulated for the peak points for  $RDF_{INTRA}$ . These values are compared with Table 4.28 and it is seen that the peak points are at larger radius with low radial distribution function values for sulfated levan chains. This shows that the sulfated levan chains is less compact than original levan.

Table 4.47. Intra-RDF values of the all sulfated levan systems at their peak point at 310 K

	Original Levan				Sulfated Levan			
	Peak (Å)	g(r) 1 ns	Peak (Å)	g(r) 25 ns	Peak (Å)	g(r) 1 ns	Peak (Å)	g(r) 5 ns
Vacuum	6.70	5.39	6.60	5.02	9.6	1.47	9.3	1.42
0.0 M	7.70	2.64	7.90	2.56	9.0	1.14	9.2	1.22
0.5 M	8.10	2.38	7.90	2.49	9.0	1.16	9.3	1.26
1.0 M	8.00	2.19	7.80	2.32	9.1	1.11	9.5	1.18
1.5 M	8.80	2.11	7.90	2.21	9.3	1.16	9.2	1.24
2.0 M	7.90	2.44	8.30	2.68	9.0	1.22	9.4	1.28

$RDF_{INTER}$  is plotted to understand the distance between one monomer bead of one levan with the beads in other chains. The  $RDF_{INTER}$  of vacuum system is plotted in the next figure with 5 ns intervals. As seen in Figure 4.47, permeation has occurred between the chains. Compared to the original levan structure, the sulfated levan chains are more disperse (less sharp peaks overlapping) in vacuum at 310 K (Inset fig. 4.47) in accordance with characteristic ratio. Figure 4.48 is plotted for all systems. The sulfated levan chains do not permeate with each other in water and saline solutions. Change in the salinity of the medium has no effect on  $RDF_{INTER}$  of sulfated levan chains.

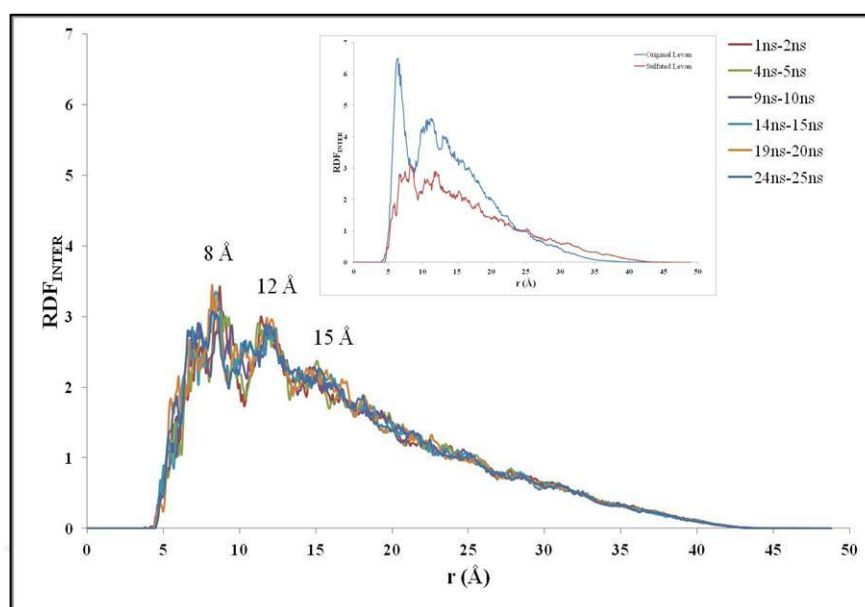


Figure 4.47. Inter-RDF of 9 sulfated levan chains in vacuum system at 310 K

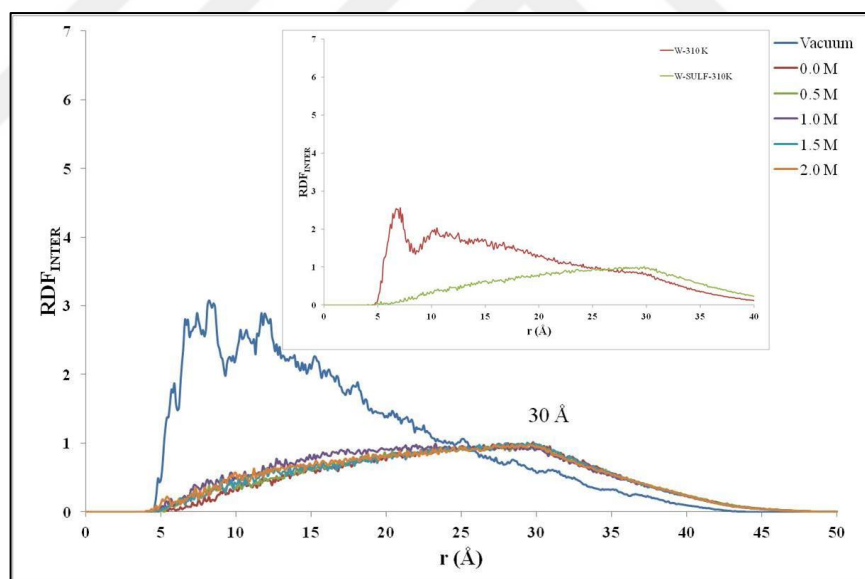


Figure 4.48. Inter-RDF of 9 sulfated levan chains in different media between 24 ns and 25 ns at 310 K

Table 4.48 shows the  $RDF_{INTER}$  values of all sulfated levan systems at their peak points. When compared to the original levan structures in the same media at 310 K, agglomeration appears not to take place in sulfated levan chain systems deduced from peak points being at larger radius.

Table 4.48. Inter-RDF values of the all sulfated levan systems at their peak point at 310 K

	Original Levan				Sulfated Levan			
	Peak (Å)	g(r) 1 ns	Peak (Å)	g(r) 25 ns	Peak (Å)	g(r) 1 ns	Peak (Å)	g(r) 5 ns
Vacuum	6.60	7.39	6.40	6.50	8.7	3.43	11.7	2.89
0.0 M	6.80	1.20	7.10	2.56	26.9	0.98	29.8	1.01
0.5 M	6.50	2.25	6.90	1.62	28.6	0.98	28.8	0.97
1.0 M	6.70	0.71	6.70	2.35	21.2	1.09	29.0	0.95
1.5 M	6.40	1.18	6.70	0.92	23.9	1.08	29.4	1.01
2.0 M	6.60	1.38	6.60	2.18	21.2	1.16	28.4	0.98

#### 4.4.5. Diffusivity Coefficients for 9 Sulfated Levan Chains in Different Media at 310 K

The diffusion coefficients of polymer solutions are related to mean square displacements (MSD) of polymer chains. Figure 4.49 depicts the mean square displacements of 9 sulfated levan chains with 12 monomer units in water. As mentioned before,  $g_2(t)$  and  $g_5(t)$  correspond to the square of end-to-end distance and radius of gyration. End-to-end distance and radius of gyration approach to 12 Å and 32 Å, respectively after 25 ns (Figure 4.37 and Figure 4.38). However,  $g_2(t)$  and  $g_5(t)$  approach to their maximum values 100 Å<sup>2</sup> and 900 Å<sup>2</sup>, respectively as seen in Figure 4.49.

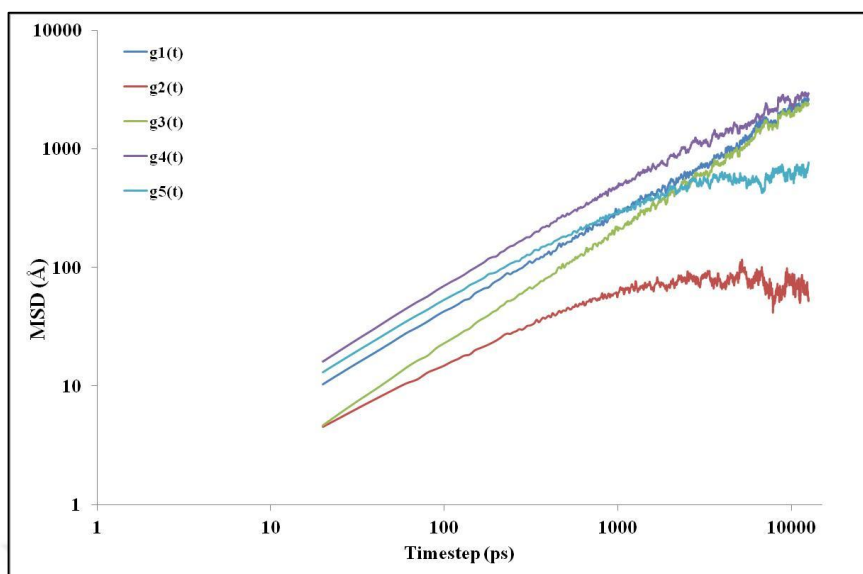


Figure 4.49. MSD of 9 sulfated levan chains in water at 310 K with respect to time

Figure 4.51 shows the  $g_3(t)$  in different concentration of saline solutions to calculate the diffusivity coefficients for sulfated levan chain systems. Diffusivity coefficients can be calculated from the slope of these graphs.

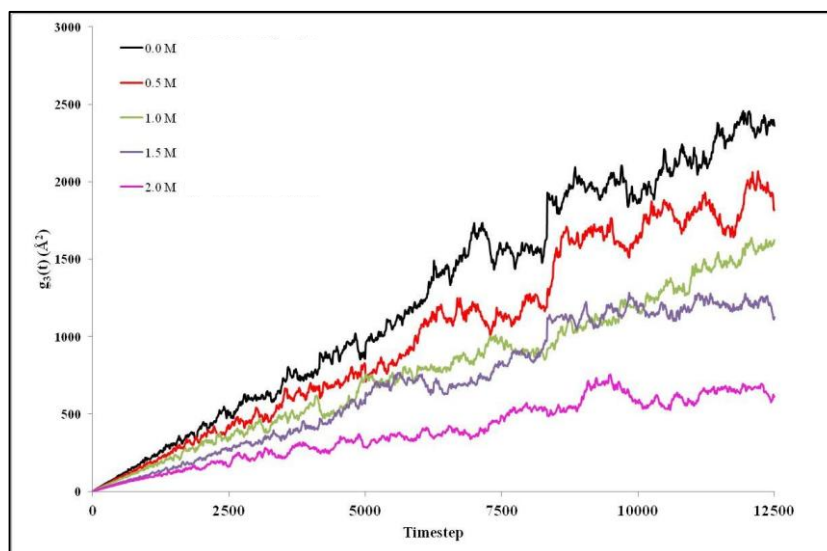


Figure 4.50. MSD  $g_3(t)$  of 9 sulfated levan chains in different media at 310 K with respect to time

The calculated diffusion coefficients are tabulated in Table 4.49. The mobility of sulfated levan chains decreases with increase of saline concentration. Diffusivity values follow decreasing trend with respect to salt concentration. These values follow the same trend with respect to the salt concentration for original levan systems. However diffusivity coefficients of sulfated levan systems are smaller than original levan systems which may be due to larger size of sulfated levan.

Table 4.49. Diffusion Coefficients for 9 Sulfated Levan Chains in Water and Saline Systems at 310 K

System	Diffusion Coefficients at 310 K (cm <sup>2</sup> /s)	R <sub>H</sub> from Stokes Einstein Equation (Å)	R <sub>G</sub> (If good solvent is assumed) (Å)	R <sub>G</sub> (From MD sim.) (Å)
0.0 M	3.32x10 <sup>-6</sup>	6.82	12.64	12.45
0.5 M	2.71x10 <sup>-6</sup>	7.96	14.74	12.35
1.0 M	2.01x10 <sup>-6</sup>	10.23	18.94	12.48
1.5 M	1.83x10 <sup>-6</sup>	10.62	19.67	12.19
2.0 M	8.97x10 <sup>-7</sup>	20.25	37.50	12.38

Heparin is an anticoagulant which is composed of highly sulfated monosaccharides. The diffusion coefficient of heparin with 10-20 kDa molecular weight was found to be approximately 1.2x10<sup>-8</sup> cm<sup>2</sup>/s in aqueous medium at room temperature [180]. Molecular weight of our sulfated levan is 2.8 kDa. The diffusion coefficient of heparin is lower because the molecular weight is higher than sulfated levan which is expected. According to Stokes-Einstein equation (Eq. 4.3), increase in temperature cause an increase in diffusion coefficient. And also according to equation 4.3., hydrodynamic radius also affects the diffusion coefficients. Sulfated levan is anionic structure and higher hydrodynamic radius than original levan is expected. By using equation 4.3., hydrodynamic radius is calculated from the diffusion coefficients and radius of gyration values. The ratio between R<sub>G</sub>

obtained from diffusion coefficient and  $R_G$  from MD simulations is tabulated in Table 4.50 and these values are considered as agglomeration. These values are less than the original levan systems at 310 K which indicated that agglomeration is also less than original levan systems which is in accordance with  $RDF_{INTER}$  and  $RDF_{INTRA}$  results.

Table 4.50. Agglomeration values for sulfated multiple chain systems at 298 K and 310 K

System	Agglomeration of original levan	Agglomeration of sulfated levan
0.0 M	1.23	1.01
0.5 M	1.33	1.19
1.0 M	1.36	1.51
1.5 M	1.68	1.61
2.0 M	1.76	3.03

Sulfated glycans are possible alternatives to heparin due to their structural homogeneity. Linear levan was synthesized from *Halomonas smyrnensis* AAD6<sup>T</sup> and sulfated. Increasing of thrombin inhibitor activity of levan sulfate with increasing of sulfation degree was determined [179]. For the biological activity, the sulphate groups of levan should be situated on the exterior of the structure. The less compact and larger conformation of sulfated levan suggests that the required exposure of sulphate groups is satisfied.

In this part, the systems were simulated with sulfated levan structures for 25 ns at 310 K. Levan chains were analyzed as coarse-grained model assuming each fructose as one unit (bead). Structural properties of these systems were calculated and summarized in Table 4.51. The structural properties were not affected by salt concentration and these systems equilibrated after 1 ns. By comparing end-to-end distance and radius of gyration ratio, it is seen that the levan chains behave like Gaussian after ~1 ns as original levan structures. Sulfation did not affect the model of the polymer. Bond angle, bond length, chord length, bond torsion and  $g_n(t)$  parameters were calculated to obtain information about dynamical properties of the systems. These parameters were also stabilized after ~1 ns resulting in slightly larger bond length, chord length and bond angle which is expected. Diffusion

coefficients decrease as salt concentration increase suggesting agglomeration in the presence of salt. Multiple levan chains folded into a globular shape regardless of the presence of sulfate groups. Because sulfated groups have charges, sulfated levan chains did not form as compact globules as unmodified levan chains. Static and dynamic differences between unmodified and sulfated levan may explain the enhanced biological activity of sulfated levan.

Table 4.51. Summarized results for all systems with 9 levan chains

		<b>Vacuum</b>	<b>Water</b>	<b>0.5 M</b>	<b>1.0 M</b>	<b>1.5 M</b>	<b>2.0 M</b>
OL	$R^2 (\text{Å}^2)$	166.81 ± 9.8	540.89 ±97.1	564.05 ±106.6	455.47 ±95.0	444.44 ±112.1	410.11 ±93.8
	$R_G^2 (\text{Å}^2)$	53.22 ±0.79	99.09 ±8.64	102.25 ±8.56	91.62 ±8.96	88.21 ±10.54	85.62 ±9.38
	Bond Length (Å)	4.95 ±0.01	5.09 ±0.02	5.08 ±0.01	5.07 ±0.02	5.08 ±0.02	5.08 ±0.02
	Bond Angle (Å)	99.25 ±0.7	105.42 ±2.0	105.48 ±1.9	104.41 ±2.0	105.31 ±2.3	103.78 ±2.1
	Chord Length (Å)	7.57 ±0.05	8.25 ±0.09	8.23 ±0.08	8.19 ±0.10	8.19 ±0.11	8.16 ±0.10
	Characteristic Ratio	1.38	1.72	1.72	1.66	1.71	1.62
	Expansion Factor	0.62	1.9	1.99	1.61	1.56	1.44
	Diff. Coeff.	-	$3.44 \times 10^{-6}$	$2.97 \times 10^{-6}$	$2.92 \times 10^{-6}$	$2.28 \times 10^{-6}$	$2.06 \times 10^{-6}$
	Agglomeration	-	1.23	1.33	1.36	1.68	1.76
SL	$R^2 (\text{Å}^2)$	465.96 ±10.27	1087.57 ±186.44	1012.10 ±144.42	1059.60 ±149.09	956.49 ±112.95	997.38 ±181.90
	$R_G^2 (\text{Å}^2)$	86.34 ±0.87	154.99 ±12.24	152.52 ±9.24	155.76 ±9.37	148.72 ±8.04	153.34 ±11.74
	Bond Length (Å)	5.88 ±0.02	5.79 ±0.04	5.78 ±0.04	5.81 ±0.04	5.76 ±0.04	5.82 ±0.05

Table 4.51. Summarized results for all systems with 9 levan chains Cont'd

Bond Angle (Å)	91.01 ±0.55	109.81 ±1.84	111.07 ±2.34	108.23 ±2.17	109.63 ±2.40	107.73 ±2.37
Chord Length (Å)	8.19 ±0.03	9.05 ±0.11	9.02 ±0.10	9.00 ±0.15	8.98 ±0.12	8.99 ±0.10
Characteristic Ratio	1.03	2.02	2.12	1.91	2.01	1.87
Expansion Factor	1.22	2.95	2.75	2.85	2.62	2.67
Diff. Coeff.	-	$3.32 \times 10^{-6}$	$2.71 \times 10^{-6}$	$2.01 \times 10^{-6}$	$1.83 \times 10^{-6}$	$8.97 \times 10^{-7}$
Agglomeration	-	1.01	1.19	1.51	1.61	3.03

The potential biological activity of levan similar to heparin is studied by docking studies where binding energies are compared.

## 4.5. DOCKING STUDIES

### 4.5.1. Coagulation

Coagulation is the transformation of the phase of the blood from liquid to gel. This occurs due to damage to a vessel, which consequently cause blood loss. Homeostasis is the ability to control the flow of the blood during vascular injury in the body. Blood clotting followed by the dissolution of the clot is the homeostasis process. It is important to protect the vasculature of the body [181]. Prior to damage on the vascular system, homeostasis depends on a dynamic balance between coagulation and fibrinolysis. Formation of homeostatic plug and degradation of the fibrin is always in balance. Perturbation of the balance between coagulation and fibrinolysis can lead to thrombosis, which is unwanted blood clotting, which is bleeding [182, 183, 184].



### 4.5.2. Thrombin

Thrombin is a serine proteinase which has a central role in thrombosis and homeostasis. It is located on the step after intersection of extrinsic and intrinsic pathways. This means, if thrombin gets inhibited, it will surpass both of the pathways. Its major role is conversion of fibrinogen to fibrin which forms part of the blood clot. In addition to this, it activates other blood coagulation factors such as V, VIII, XIII and protein C [185]. Several characteristic structural features enable thrombin to accomplish these divergent functions with high specificity. Its active-site cleft is restrictive by two large insertion loops the rigid 60 loop (contains Trp60 amino acid residues), and at the opposite, the more flexible 149 loop (contains Ala149A-Asn149B amino acid residues) [186]. The active-site residues are at the edge of a negatively charged surface area. A positively charged surface which is called fibrinogen recognition exosite patch is situated at the carboxyterminal exit of the active-site cleft. This exosite interacts with negatively charged groups of many specific thrombin substrates and inhibitors [187], and another positive site is called heparin binding site that is implicated in heparin binding [188, 189]. Figure 4.51. shows the structure of thrombin.

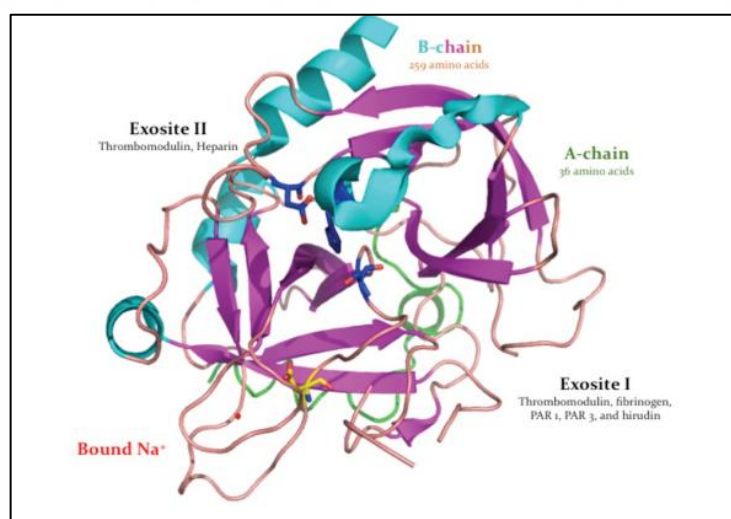


Figure 4.51. Structure of Thrombin [190]

### 4.5.3. Heparin Glycosaminoglycan

Over a half decade, Heparin (which is a type of glycosaminoglycan (GAG)) is the popular drug that is used for curing thromboembolic disorders [101]. Unfractionated (UF) heparin is a naturally occurring mucopolysaccharide, which has high negative charge because of the sulfate groups in its structure and is water soluble [192,193]. It is a heterogeneous mixture of linear polysaccharide chains composed of 15–100 alternating (1→4)-linked mucosaccharide units of D-glucosamine and L-iduronic acid or D-glucuronic acid [192,194]. In Figure 4.52., the repeating disaccharide unit of heparin is shown. The left part is D-glucosamine and the right part is L-iduronic acid [195].

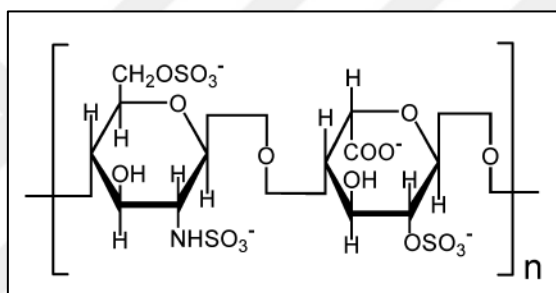


Figure 4.52. Chemical structure of the disaccharide repeating unit of heparin [195]

The molecular weight of unfractionated heparin ranges from 5 to 40 kDa with an average of 14 kDa. Low molecular weight (LMW) heparins are much smaller (mean MW, 5 kDa) and are produced from unfractionated heparin by chemical or enzymatic depolymerization [190].

The unfractionated and low molecular weight heparins are the current anticoagulant polysaccharides drugs [196]. However, heparin has limitations due to serious effects as an anticoagulant such as heparin-induced thrombocytopenia-II (HIT), bleeding, osteoporosis, skin rashes, contact dermatitis, urticarial and skin necrosis, eosinophilia, among others [196, 197].

#### 4.5.4. Docking Studies

Predicting binding modes of small molecules and target proteins is an important issue in drug development. Docking softwares are used to predict these binding modes. In recent years, some different softwares are developed ranging from friendly and fast user program to algorithmically flexible and accurate. EADock is one of the developed software with multiobjective scoring function [198].

Carbohydrate modeling is a challenging research area because of diversity in their structures. They can have high number of monomers with possible linkages and they are flexible structures. Starting structure of carbohydrates can be obtained from Protein Data Bank for analyzing protein carbohydrate interaction. Molecular docking simulations are used to determine carbohydrate-protein complex when experimental data are not available. To decrease the inaccuracies in the docking process, the results may be merged with molecular dynamics simulations [199].

The extracellular polysaccharide with (1→3)/(1→6) linked  $\alpha$ -glucan and (1→3)/(1→6) linked  $\alpha$ -galactose obtained from *Ganoderma lacidum* is first simulated. After simulations, the polysaccharide exists in random coil conformation. The sulfated derivation of this structure is more extensive and stiffer. This polysaccharide is docked with human serum albumin with ZDOCK module. According to ZDOCK score results, sulfated derivative exhibited lower affinity to human serum albumin than the original polysaccharide [200].

Molecular docking is used to determine the relation between sulfated fucose and cancer associated protein. Sulfated fucose is a monomer of a fucodian polysaccharide. The results indicate that bioactive marine compound that is sulfated fucose may serve as a drug candidate for cancer types or other ailments [201].

Modified xyclofucan sulfate obtained from the brown alga *Punctaria plantaginea* has anticoagulant and antithrombic activities. Docking method is used to evaluate the possible binding modes of fucodian with thrombin and antithrombin. The fucooligosaccharides with different number of fucose residues were used in docking studies. All studied structures are found to bind both thrombin and antithrombin [202].

Anionic polysaccharides called glycosaminoglycans participate in important processes in extracellular matrix. They interact with proteins. The electrostatic and water mediated interactions should be considered accurately to understand glycosaminoglycans binding properties. The abundance of solvent in glycosaminoglycans-protein interfaces and effect of adding solvent are analyzed with docking methods. Glycosaminoglycans-protein interfaces are more hydrated than protein-protein interfaces. It is estimated with molecular dynamics approaches. Solvent inclusion effect is analyzed with different docking softwares. Solvent molecules are placed at the binding site before docking. GRID predicts the positions of water and locates them into possible areas upon ligand binding. The results are compared with solvent position in crystal structures. The addition of solvent improves the results to understand the interactions [203].

Many proteins have different functions and structures to bind heparin and heparan sulfate. Docking is a useful method to understand interactions of protein-heparin complexes. Mottarella et. al. integrates the PIPER docking program to use in heparin docking. Other programs are developed for small molecules rather than polysaccharides that are highly charged. The automated protein-protein docking server ClusPro is used. The highest protein-ligand contacts are chosen to predict heparin binding site. The center of the most populated clusters is found to be close to the orientation of native heparin. [204].

In immune system, heparin-protein interactions have an important role. Three programs are used to predict heparin binding sites because the high charge density and weak surface complementarity for sulfated chains are challenging tasks in docking process. The target proteins are antithrombin, basic fibroblast growth factor and three proteins which their complexes with heparin is available. The heparin binding sites of these target proteins are obtained. This method is used to predict the heparin binding site of Interleukin-8, which has a central role in immune response[205].

A highly sulfated pyranosic (1→3)- $\beta$ -L- Arabinan is studied with docking method to evaluate direct interaction with thrombin to understand the mechanism of its anticoagulant activity. The results of these study showed that noval pyranosic sulfated arabinan has a different mechanism from other sulfated polysaccharides for its anticoagulant activity. A highly sulfated pyranosic (1→3)- $\beta$ -L- arabinan is proposed as direct thrombin inhibitor by interaction with exosite 2 to inactivate the thrombin without antithrombin [206].

Erginer et. al. studied the production of sulfated levan from *Halomonas smyrnensis* AAD6<sup>T</sup> and its biological activities in her master thesis. She found that sulfated levan has anticoagulant activity and also levan sulfate showed a better inhibitor activity than heparin. Levan sulfate showed no coagulation after 1 µg/mL concentration, which means that fibrin formation time is above 500 seconds while heparin showed the same results after 5 µg/mL concentration. This clearly indicates that bioactivity of sulfated levan that is significantly better than heparin [179].

In this study, native levan structure obtained from *Halomonas smyrnensis* AAD6<sup>T</sup> and its sulfated form are computationally constructed and docking simulations are performed to understand the effect of sulfation on levan binding to thrombin and to distinguish it from the binding of heparin binding.

#### 4.5.5. Docking Results

To associate structural features to the experimentally observed interaction of SHL-H with thrombin, docking studies are conducted using equilibrated structures obtained from fully atomistic MD simulations as ligands. For this, first, equilibrated structures are obtained for both native and sulfated (SHL-1, SHL-5 and SHL-9) levans by running simulations in physiological saline at 310 K and for 25 ns duration (Fig. 4.53).

In this part of the study, fully atomistic Molecular Dynamics simulations are carried out with polymer consistent force field (PCFF) to construct native and sulfated levan structures. The constructed levan structures had 9 fructose rings per chain. Sulfated levan structures are obtained by sulfation of one ring [SHL-1, Fru<sub>f</sub> 1S-β(2→6)-(Fru<sub>f</sub> -β(2→6)-Fru<sub>f</sub>)<sub>8</sub>], five [SHL-5, Fru<sub>f</sub> 1S-β(2→6)-(Fru<sub>f</sub> -b(2→6)-Fru<sub>f</sub> 1S)<sub>4</sub>] and all rings [SHL-9, (Fru<sub>f</sub> 1S-β(2→6)-Fru<sub>f</sub> 1S)<sub>9</sub>] of native levan [HL, (Fru<sub>f</sub>-β(2→6)-Fru<sub>f</sub>)<sub>9</sub>]. All structures are simulated in physiological saline solution (0.9% NaCl) at 310 K and for 25 ns duration to obtain equilibrated structures. The systems are constructed and energy minimized with Xenoview Simulation Package [147] with 0.9 nm cut-off distance. Production runs are performed with LAMMPS [148]. During the production runs, number of particles, volume and temperature (NVT ensemble) are kept constant. Temperature is set to 310 K with

Berendsen thermostat and the volume of the simulation box is set to be 6x6x6 nm with periodic boundary conditions.

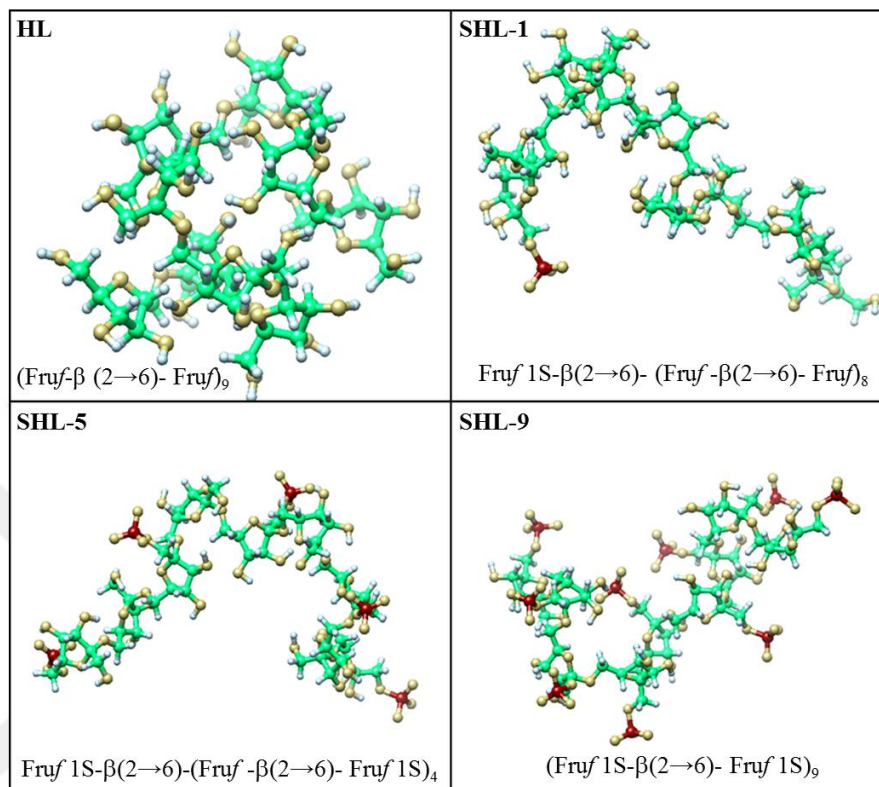


Figure 4.53. Levan structures obtained from MD simulations

For the docking studies, bovine thrombin structure (1TBQ) is obtained from Protein Data Bank [207], whereas the final structures of levan and sulfated levan are obtained from MD simulations and heparin structure is extracted from ClusPro server [208]. All calculations are performed in Swissdock server, the results are analyzed with UCSF Chimera [151] and the binding modes are visualized with ViewDock plugin [198].

After being simulated in physiological saline solution at 310 K for 25 ns, HL, SHL-1, SHL-5 and SHL-9 are docked with thrombin individually and results are tabulated in  $\Delta G$  (kcal/mol). Heparin is used as control in docking studies because it is known that heparin binds like a bridge between antithrombin and exosite II of thrombin [206]. Docking results showed that the complex of heparin and thrombin had the lowest  $\Delta G$  value when heparin was bound to exosite II (Arg93, Lys126, Lys230 and Lys240) of thrombin as expected (Figure 4.54) [206].

Whereas levan, SHL-1 and SHL-5 structures showed a tendency to bind to the active site of thrombin (Hsd57, Asp102 and Ser195), SHL-9 was found to bind to Exosite II, similar to heparin (Fig. 4.54.).

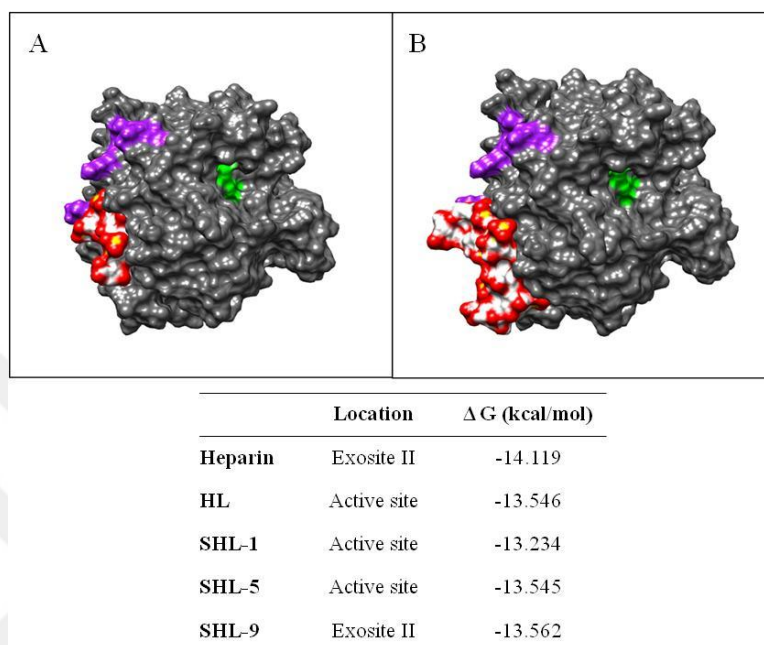


Figure 4.54. The structures of Thrombin (Purple region: Exosite II; green region: Active site) with **A.** Heparin (red structure) **B.** SHL-9 (red structure) with lowest  $\Delta G$

Unsulfated or low sulfated levan structures showed a tendency to bind to the active site of thrombin unlike heparin, but similar to the way direct inhibitors work. Direct inhibitors block the active site of thrombin and enable glycosaminoglycans to achieve a higher rate of activation [209].

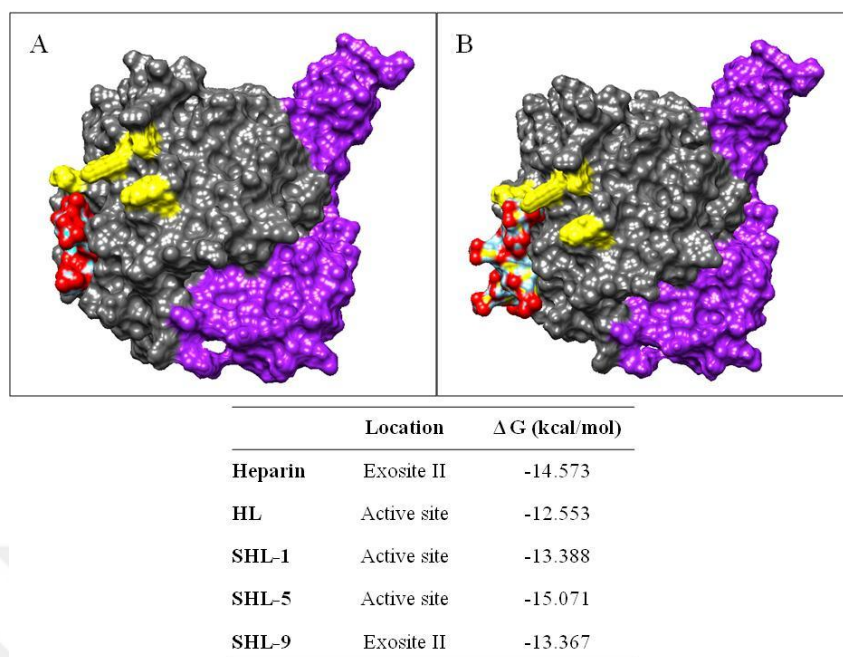


Figure 4.55. The structures of inhibited Thrombin (Yellow region: Exosite II; purple region: Active site closed with rhodniin) with **A.** Heparin (red structure) **B.** SHL-9 (red structure) with lowest  $\Delta G$

To understand the effect of closeness of active site, docking studies were performed again with a thrombin structure inhibited by rhodniin which is a highly specific inhibitor of thrombin [207]. All structures were still found to bind to the active site with the exception of SHL-9. SHL-9 was found to bind to exosite II, similar to heparin (Figure 4.55.). These docking results show that highly sulfated levan exhibits anticoagulation mechanism similar to heparin, quite different from the unsulfated or low sulfated levans which exhibit the mechanism of direct inhibitors. These calculations support the observed experimental data.



## 5. CONCLUSION AND FUTURE WORK

Development and characterization of biopolymers is a promising research area blossoming in the recent years to understand the mechanisms of biological activities. Oligo and polysaccharides are considered to be potential biopolymers that will be used in biological activities such as drug delivery. Levan is a natural polymer that consists of  $\beta$  (2 $\rightarrow$ 6) glycosidic linkages between its  $\beta$ -D-fructofuranose which is an important research area for biological activities. Polysaccharides have plenty of conformation variations therefore their analysis using molecular dynamics is employed to obtain comprehensive information about their conformations. In this study, the aim was to obtain various information about the structure-function relation of levan chains in different media and temperatures with using molecular dynamics studies.

In the first part of this study, the original levan was created with the computational method Xenoview. Different length of levan chains are simulated in vacuum to obtain the effect of length and to decide the optimum length of chain to be used in the following simulations. The end-to-end distances of different number of rings were not different from each other, however, the radius of gyration values were affected by the number of rings. For the following simulations, only levan with 12 fructose units was chosen as it fits in the control unit diagonally. In this part of the study the effects of solvent and temperature were analyzed. Vacuum, water and aqueous solutions with different salt concentrations were chosen as media and 298 K and 310 K were chosen as temperatures. These systems were analyzed with respect to their end-to-end distance, radius of gyration and chain characteristics which are bond length, bond angle, chord length and torsional angles and radial distribution functions. According to these results, aqueous media are generally considered to be good solvents for single levan chains at both 298 K and 310 K. High salinity and temperature difference did not have a significant effect on the conformation of a single levan chain.

In the other part of the study, the multiple levan chains were used to understand the interaction of levan chains with each other. The same parameters were analyzed and additionally their diffusion coefficients were calculated for both temperatures. In multiple

chain systems, agglomeration was seen in all investigated media and temperature. The chains were considered as Gaussian in all aqueous media however the behavior of the chains were not Gaussian in vacuum. Multiple number of chains affected the bond angle of levan chain when compared to single chain systems. The other chain characteristic parameters remained almost same in both single and multiple chain systems. Aqueous media were still considered as good solvent even if the number of chains increased. According to diffusion coefficient values of the systems, the increase of salt induced a decrease of diffusion coefficients. Assuming good solvent,  $R_g$  values are calculated from  $R_H$  (obtained from diffusion coefficient) and the ratio of radius of gyration values obtained from diffusion coefficient to radius of gyration from MD simulations were calculated to give information about agglomeration. Agglomeration was induced upon addition of salt and the highest aggregation was seen in 2 M salt solution. The temperature does not seem to have any effect on the chain characteristics but increase in temperature is observed to reduce the agglomeration of chains in all investigated media.

Levan was sulfated for further molecular dynamic simulations because experimentally sulfated levan was found to be a thrombin inhibitor, similar to heparin. These systems were compared to original levan at 310 K to understand the difference between their conformations that may be related to their biological activity. The most important difference is sulfated levan is an anionic structure therefore its hydrodynamic radius is larger than original levan. Therefore the diffusion coefficients were found to be lower from molecular dynamics simulations which was expected. Due to the presence of anionic groups, in the absence of salt, no aggregation of chains was observed. However, addition of salt strongly induced agglomeration resulting in even higher agglomeration values than the unsulfated chains. According to chain characteristic parameters, it can be understood that sulphate groups did not form as compact globules as original levan. The sulphate groups were situated on the exterior part of the structure which increased the biological activity of levan.

The biological activity of original levan and sulfated levan was analyzed with docking studies. Experimentally, sulfated levan showed the same binding tendency to thrombin as heparin experimentally. Original levan and sulfated levan with different degree of sulphation were used. According to docking results, it was clearly seen that original levan and sulfated levan with less sulphate groups did not show any tendency to binding the

exosite II site of thrombin which is the binding site for heparin. Only the structure with all sulfated fructose rings showed tendency to bind exosite II in thrombin even when the active site of the thrombin is available, unlike all the other lesser sulfated levans which preferentially bind to the active site. The highly sulfated levan exhibits the anticoagulant mechanism similar to heparin which corresponded with the experimental results.

In the further studies, the different modified levan structures can be obtained such as oxidized or phosphated to understand the effect of different active groups on biological activity by docking studies. After that, if the effect of active groups is clarified with docking studies, the difference in conformations of these structures can be analyzed by using molecular dynamics simulations. The methods employed in this thesis can easily be extended to other biopolymers.

## REFERENCES

1. D.P. Livingston, D.K. Hinch and A.G. Heyer, Fructan and Its Relationship to Abiotic Stress Tolerance in Plants, *Cellular and Molecular Life Sciences*, 66:2007-2023, 2009.
2. I.J. Vereyken, J.A.V. Kuik, T.H. Evers, P.J. Rijken and B. de Kruijff, Structural Requirements of The Fructan-Lipid Interaction, *Biophysical Journal*, 84:3147–3154, 2003.
3. M. Frank and S. Schloissnig, Bioinformatics And Molecular Modeling In Glycobiology, *Cellular and Molecular Life Sciences*, 67:2749–2772, 2010.
4. R.J. Woods and M.B. Tessier, Computational Glycoscience: Characterizing The Spatial And Temporal Properties Of Glycans And Glycan–Protein Complexes, *Current Opinion in Structural Biology*, 20:575-583, 2010.
5. F. Sima, E.C. Mutlu, M.S. Eroglu, L.E. Sima, N. Serban, C. Ristoscu, S.M. Petrescu, E.T. Oner and I.N. Mihailescu, Levan Nanostructured Thin Films by MAPLE Assembling, *Biomacromolecules*, 9:66-71, 2011.
6. A.D. Sezer, H. Kazak, E.T. Oner and J. Akbuğa, Levan-Based Nanocarrier System For Peptide And Protein Drug Delivery: Optimization And Influence Of Experimental Parameters On The Nanoparticle Characteristics, *Carbohydrate Polymers*, 84:358-363, 2011.
7. R. Valluru and W. Van den Ende, Plant Fructans In Stress Environments: Emerging Concepts And Future Prospects, *Journal of Experimental Botany*, 59:2905-2916, 2008.
8. I.J. Vereyken, C. Vladimir, A.D. Rudy, C.M.S. Sjeff and D.K. Ben, Fructans Insert Between The Headgroups Of Phospholipids, *Biochimica et Biophysica Acta (BBA) – Biomembranes*, 1510:307-320, 2001.

9. T. Ritsema and S. Smeekens, Fructans: Beneficial For Plants And Humans, *Current Opinion in Plant Biology*, 6:223–230, 2003.
10. M.B. Roberfroid, Inulin-Type Fructans: Functional Food Ingredients, *Journal of Nutrition*, 137: 2493–2502, 2007.
11. S. Cimini, V. Locato, R. Vergauwen, A. Paradiso, C. Cecchini, L. Vandenkoel, J. Verspreet, C. M. Courtin, M. G. D'Egidio, W. V. den Ende and L. De Gara, Fructan Biosynthesis and Degradation as Part of Plant Metabolism Controlling Sugar Fluxes During Durum Wheat Kernel Maturation, *Frontiers in Plant Science*, 6: 89, 2015.
12. A. Franck and D.L. Leen , Inulin, *Biopolymers Online*, 6:439-448, 2006.
13. K. R. Niness, Inulin and Oligofructose: What Are They?, *Journal of Nutrition*, 129:1402-1406, 1999.
14. A. D. Sezer, H.K. Sarılmışer, E. Rayaman, A. Çevikbaş, E.T. Oner and J. Akbuğa, Development and Characterization of Vancomycin-Loaded Levan-Based Microparticulate System for Drug Delivery, *Pharmaceutical Development and Technology*, 1-8, 2015.
15. M. Bekers, J. Laukevics, D. Uprite, E. Kaminska, A. Vigants, U. Viesturs and A. Danilevics, Fructooligosaccharide and Levan Producing Activity of *Zymomonas Mobilis* Extracellular Levansucrase, *Process Biochemistry*, 38:701–706, 2002.
16. A. Poli, H. Kazak, B. Gürleyendağ, G. Tommonaro, G. Pieretti, E. T. Öner and B. Nicolaus, High Level Synthesis of Levan by a Novel *Halomonas* Species Growing On Defined Media, *Carbohydrate Polymers*, 78:651-657, 2011.
17. S.H. Yoo, E.J. Yoon, J. Cha and H.G. Lee, Antitumor Activity of Levan Polysaccharides from Selected Microorganisms, *International Journal of Biological Macromolecules*, 34:37-41, 2004.

18. N. Sapay, A. Nurisso and A. Imberty, Simulation of Carbohydrates, from Molecular Docking to Dynamics in Water, *Methods in Molecular Biology*, 924:469-483, 2013.
19. S.L. Chaplot, Parallelization in Classical Molecular Dynamics Simulation and Applications, *Computational Materials Science*, 37:146-151, 2006.
20. A. Palleschia, G. Bocchinfusa, T. Coviello and F. Alhaique, Molecular Dynamics Investigations of The Polysaccharide Scleroglucan: First Study on The Triple Helix Structure, *Carbohydrate Research*, 340:2154-62, 2005.
21. C. S. Pereira, D. Kony, R. Baron, M. Müller, W. F. van Gunsteren and P. H. Hünenberger, Conformational and Dynamical Properties of Disaccharides in Water: a Molecular Dynamics Study, *Biophysical Journal*, 90:4337-4344, 2006.
22. S. N. Ha, L. J. Madsen and J. W. Brady, Conformational Analysis and Molecular Dynamics Simulations of Maltose, *Biopolymers*, 27:1927:1952, 1988.
23. A. Almond and J. K. Sheehan, Predicting The Molecular Shape of Polysaccharides From Dynamic Interactions With Water, *Glycobiology*, 13:255-264, 2003.
24. L. Gwangorg, W. Nowak, J. Jaronic, Q. Zhang and P. E. Marszalek, Molecular Dynamics Simulations of Forced Conformational Transition in 1,6 Linked Polysaccharides, *Biophysical Journal*, 87:1456-1465, 2004.
25. H. Verli and J. A. Guimaraes, Molecular Dynamics Simulation of a Decasaccharide Fragment of Heparin in Aqueous Solution, *Carbohydrate Research*, 339:281-290, 2004.
26. C. F. Becker, J. A. Guimaraes and H. Verli, Molecular Dynamics and Atomic Charge Calculations in The Study of Heparin Conformation in Aqueous Solution, *Carbohydrate Research*, 340:1499-1507, 2005.

27. J. C. Munoz-Garcia, F. Corzana, J. L. De Paz, J. Angulo and P. M. Nieto, Conformations of The Iduronate Ring in Short Heparin Fragments Described By Time Averaged Distance Restrained Molecular Dynamics, *Glycobiology*, 23:1220-1229, 2013.
28. S. Markutsya, A. Devarajan, J. Y. Baluyut, T. L. Windus, M. S. Gordon and M. H. Lamm, Evaluation of Coarse-Grained Mapping Schemes For Polysaccharide Chains in Cellulose, *The Journal of Chemical Physics*, 138:214108, 2013.
29. University of Twente, 'Polymer Dynamics', <https://www.utwente.nl/tnw/ccp/research/PolymerDynamics.html> [retrieved 1 January 2016].
30. L. K. Tolonen, M. Bergensträhle-Wohlert, H. Sixta, and J. Wohlert, Solubility of Cellulose in Supercritical Water Studied by Molecular Dynamics Simulations, *The Journal of Physical Chemistry B*, 119:4739–4748, 2015
31. H. Liu, K. L. Sale, B. A. Simmons, and S. Singh, Molecular Dynamics Study of Polysaccharides in Binary Solvent Mixtures of an Ionic Liquid and Water, *The Journal of Physical Chemistry B*, 115:10251–10258, 2011.
32. H. B. Mayes, J. Tian, M. W. Nolte, B. H. Shanks, G. T. Beckham<sup>1</sup>, S. Gnanakaran, and L. J. Broadbelt, Sodium Ion Interactions with Aqueous Glucose: Insights from Quantum Mechanics, Molecular Dynamics, and Experiment, *The Journal of Physical Chemistry B*, 118:1990–2000, 2014.
33. J. Einfeldt, D. Meißner and A. Kwasniewski, Comparison of The Molecular Dynamics of Celluloses and Related Polysaccharides in Wet and Dried States by Means of Dielectric Spectroscopy, *Macromolecular Chemistry and Physics*, 201:1969-1975, 2000.
34. D. B. Kony, W. Damm, S. Stoll, W. F. van Gunsteren and P. H. Hünenberger, Explicit-Solvent Molecular Dynamics Simulations of the Polysaccharide Schizophyllan in Water, *Biophysical Journal*, 93:442–455, 2007.

35. M. D. Battistel, R. Pendrill, G. Widmalm, and D. I. Freedberg, Direct Evidence for Hydrogen Bonding in Glycans: A Combined NMR and Molecular Dynamics Study, *The Journal of Physical Chemistry*, 117:4860–4869, 2013.
36. G. S. Grest and M. Murat, Structure of Grafted Polymeric Brushes in Solvents of Varying Quality: A Molecular Dynamics Study, *Macromolecules*, 26:3108–3117, 1993.
37. D. E. Dischera, V. Ortizb, G. Srinivasb, M. L. Kleinb, Y. Kima, D. Christiana, S. Caia, P. Photosa and F. Ahmed, Emerging Applications of Polymersomes in Delivery: From Molecular Dynamics to Shrinkage of Tumors, *Progress in Polymer Science*, 32:838–857, 2007.
38. K. Kremer and G.S. Grest, Dynamics of Entangled Linear Polymer Melts: A Molecular-Dynamics Simulation, *The Journal of Chemical Physics*, 92:5057-5086, 1990.
39. J. T. Padding and W. J. Briels, Time And Length Scales Of Polymer Melts Studied By Coarse-Grained Molecular Dynamics Simulations, *The Journal of Physical Chemistry*, 117:925-943, 2002.
40. F. W. Starr, T. B. Schröder and S. C. Glotzer, Molecular Dynamics Simulation of a Polymer Melt with a Nanoscopic Particle, *Macromolecules*, 35:4481–4492, 2002.
41. G.S. Grest and K. Kremer, Molecular Dynamics Simulation For Polymers In The Presence Of A Heat Bath, *Physical Review A*, 33:3628-3631, 1986.
42. F. Müller-Plathe, Diffusion of Penetrants in Amorphous Polymers: A Molecular Dynamics Study, *The Journal of Chemical Physics*, 94:3192-9, 1991.
43. D.C. Rapaport, Molecular Dynamics Simulation of Polymer Chains With Excluded Volume, *Journal of Physics A: Mathematical and General*, 11:213-217, 1978.



44. S. Silbira, S. Dagbaglib, S. Yegina, T. Baysala and Y. Goksungur, Levan Production by *Zymomonas Mobilis* in Batch and Continuous Fermentation Systems, *Carbohydrate Polymers*, 99:454–461, 2014.
45. R. R. J. Borsari, M. Antonia, P. C. Celligoi, J. B. Buzato, R. S. d. Santos and F. da Silva, Influence of Carbon Source and The Fermentation Process on Levan Production by *Zymomonas Mobilis* Analyzed by The Surface Response Method, *Ciência e Tecnologia de Alimentos*, 26:1-5, 2006.
46. M. Reissa and W. Hartmeier, Levan Production with a Flocculent Strain of *Zymomonas Mobilis*, *Food Biotechnology*, 4:69-75, 1990.
47. K. S. Belghith, I. Dahech, H. Belghith and H. Mejdou, Microbial Production of Levansucrase for Synthesis of Fructooligosaccharides and Levan, *International Journal of Biological Macromolecules*, 50:451-458, 2012.
48. M. A. Esawya, A. M. Abdel-Fattaha, M. M. Alib, W. A. Helmya, B. M. Salamaa, H. A.A. Taiec, A. M. Hashema and G. E.A. Awad, Levansucrase Optimization Using Solid State Fermentation and Levan Biological Activities Studies, *Carbohydrate Polymers*, 96:332-341, 2013.
49. A. Poli, H. Kazak, B. Gürleyendağ, G. Tommonaro, G. Pieretti, E. T. Öner and B. Nicolaus, High Level Synthesis of Levan by a Novel *Halomonas* Species Growing On Defined Media, *Carbohydrate Polymers*, 78:651-657, 2011.
50. F. Küçükaşık, H. Kazak, D. Güney, I. Finore, A. Poli, O. Yenigün, B. Nicolaus and E. T. Öner, Molasses as Fermentation Substrate for Levan Production by *Halomonas* sp., *Applied Microbiology and Biotechnology*, 89:1729-40, 2011.
51. H. K. Sarilmiser, O. Ates, G. Ozdemir, K. Y. Arga and E. T. Oner, Effective Stimulating Factors for Microbial Levan Production by *Halomonas Smyrnensis* AAD6T, *Journal of Bioscience and Bioengineering*, 119:455–463, 2015.

52. O. Kırte1, Zymomonas Mobilis ile Melastan Levan Polimerinin Üretimi, MsC Thesis, Ege University, Food engineering, Bornova, İzmir, 2015.
53. M. R. de Oliveiraa, R. S. Santos, F. da Silvab, J. B. Buzatoa, M. A. Pedrine and C. Celligoi, Study of Levam Production by Zymomonas Mobilis Using Regional Low-Cost Carbohydrate Sources, *Biochemical Engineering Journal*, 37:177–183, 2007.
54. B. Y. Byun, S.J. Lee and J.H. Mah, Antipathogenic Activity and Preservative Effect of Levam (B-2,6-Fructan), A Multifunctional Polysaccharide, *International Journal of Food Science and Technology*, 49:238-245, 2014.
55. J. A. Ramsayab, D.G. Coopera and R. J. Neufeld, Effects of Oil Reservoir Conditions on The Production of Water-Insoluble Levam by Bacillus Licheniformis, *Geomicrobiology Journal*, 1989.
56. I. Kazuoki, Antihyperlipidemic and Antiobesity Agent Comprising Levam or Hydrolysis Products Thereof Obtained From Streptococcus Salivarius, *United states patent*, No: 5,527,784, 1996
57. F. D. Bello, J. Walter, C. Hertel and W. P. Hammes, In vitro study of Prebiotic Properties of Levam-type Exopolysaccharides from Lactobacilli and Non-digestible Carbohydrates Using Denaturing Gradient Gel Electrophoresis, *Systematic and Applied Microbiology*, 24:232-237, 2001.
58. K.H. Kim, C.B. Chung, Y.H. Kim, K.S. Kim, C.S. Han and C.H. Kim, Cosmeceutical Properties of Levam Produced by Zymomonas Mobilis, *International Journal of Cosmetic Science*, 56:395-406, 2005.
59. F. M, Tsuboi, Beautifully Whitening Agent, *Japanese Patent*, No: 2006052146, 2006.
60. K. Jo, and Y. Kikkai, Allergy Inhibitory Compositions, *Japanese Patent*, No: 2006001922, 2006.

61. G.A. Hughes, Nanostructure-mediated Drug Delivery, *Nanomedicine: Nanotechnology, Biology and Medicine*, 1: 22–30, 2005.
62. K. K. Jain, *Drug Delivery Systems*, Springer-Verlag New York, Inc., New York, 2008.
63. V.P. Torchilin, Structure and Design of Polymeric Surfactant-Based Drug Delivery Systems, *Journal of Controlled Release*, 73:137–172, 2001.
64. D. R. Karsa and R. A. Stephenson, *Chemical Aspects of Drug Delivery Systems*, RSC Special Publications, New York, 1996.
65. G.A. Hughes, Nanostructure-mediated Drug Delivery, *Nanomedicine: Nanotechnology, Biology and Medicine*, 1: 22–30, 2005.
66. V.P. Torchilin, Structure and Design of Polymeric Surfactant-Based Drug Delivery Systems, *Journal of Controlled Release*, 73:137–172, 2001.
67. Z. Liu, Y. Jiao, Y. Wang, C. Zhou and Z. Zhang, Polysaccharides-Based Nanoparticles as Drug Delivery Systems, *Advanced Drug Delivery Reviews*, 60:1650–1662, 2008.
68. T. Okano, N. Yui, M. Yokoyama and R. Yoshida, *Advances in Polymeric Systems for Drug Delivery*, Gordon and Breach Science Publishers, USA, 1994.
69. J. K. Mills and D. Needham, Targeted Drug Delivery, *Journal Expert Opinion on Therapeutic Patents*, 9:1499-1513, 2005.
70. L. B. Peppas and J. O. Blanchette, Nanoparticle and Targeted Systems for Cancer Therapy, *Advanced Drug Delivery Reviews*, 56:1649-1659, 2004.

71. S. Ummadi, B. Shravani, N. G. R. Rao, M. S. Reddy and B. S. Nayak, Overview on Controlled Release Dosage Form, *International Journal of Pharma Sciences*, 3:258-269, 2013.
72. D. Bhowmik, H. Gopinath, B. P. Kumar, S. Duraiavel and K. P. S. Kumar, Controlled Release Drug Delivery Systems, *The Pharma Innovation*, 1:24-32, 2012.
73. C. G. Pitt, T. A. Marks and A. Schindler, Biodegradable Drug Delivery Systems Based on Aliphatic Polyesters: Application to Contraceptives and Narcotic Antagonists, *NIDA Research Monograph Journal*, 28:232-253, 1980.
74. L. Fan and S. K. Singh, *Controlled Release: A Quantitative Treatment*, Springer-Verlag Berlin Heidelberg, Berlin, 1989.
75. R. A. Siegel and M. J. Rathbone, Overview of Controlled Release Mechanisms, *Fundamentals and Applications of Controlled Release*, Springer, New York, 2012.
76. C.G. Wilson and P.J. Crowley, *Advances in Delivery Science and Technology*, CRS Springer, New York, 2015.
77. D. Jones, *Pharmaceutical Applications of Polymers for Drug Delivery*, Rapra Review Reports, Belfast, 2004.
78. P. J. Tarcha, *Polymers for Controlled Drug Delivery*, CRC Press, Florida, 1991.
79. A. Nokhodchi and G. P. Martin, *Pulmonary Drug Delivery: Advances and Challenges*, Wiley and Sons, United Kingdom, 2015.
80. W. Wang, X. Liu, Y. Xie, H. Zhang, W. Yu, Y. Xiong, W. Xiea and X. Ma, Microencapsulation Using Natural Polysaccharides for Drug Delivery and Cell Implantation, *Journal of Materials Chemistry*, 16:3252-3267, 2006.

81. L. N. Hassani, F. Hendra and K. Bouchemal, Auto-Associative Amphiphilic Polysaccharides as Drug Delivery Systems, *Drug Discovery Today*, 17:608-614, 2012.
82. S. S. Dhaneshwar, M. Kandpal, N. Gairola and S.S. Kadam, Dextran: A Promising Macromolecular Drug Carrier, *The Indian Journal of Pharmacy*, 68:705-714, 2006.
83. H. Gangliang, C. Yingli, L. Yue, H. Dan, H. Jie and Y. Min, Two Important Polysaccharides as Carriers for Drug Delivery, *Mini-Reviews in Medicinal Chemistry*, 15:1103-1109, 2015.
84. C. Alvarez-Lorenzo, B. Blanco-Fernandez, A. M. Puga and A. Concheiro, Crosslinked Ionic Polysaccharides for Stimuli-Sensitive Drug Delivery, *Advanced Drug Delivery Reviews*, 65:1148–1171, 2013.
85. S. K. Nitta and K. Numata, Biopolymer-Based Nanoparticles for Drug/Gene Delivery and Tissue Engineering, *International Journal of Molecular Sciences*, 14:1629-1654, 2013.
86. V.R. Sinha and R. Kumria, Polysaccharides in Colon-Specific Drug Delivery, *International Journal of Pharmaceutics*, 224:19–38, 2001.
87. X. Y. Wang, L. Zhang, X.-H. Wei and Q. Wang, Molecular Dynamics of Paclitaxel Encapsulated by Salicylic Acid-Grafted Chitosan Oligosaccharide Aggregates, *Biomaterials*, 34:1843-51, 2013.
88. R. Srikanth, G. Siddartha, S. Reddy, B.S. Harish, M. J. Ramaiah and K. B. Uppuluri, Antioxidant and Anti-Inflammatory Levan Produced from *Acetobacter Xylinum* NCIM2526 And Its Statistical Optimization, *Carbohydrate Polymers*, 123:8-16, 2015.
89. J. R. Runyon , L. Nilsson, M. Ulmius, A. Castro, R. Ionescu, C. Andersson and C. Schmidt, Characterizing Changes in Levan Physicochemical Properties in Different pH

Environments Using Asymmetric Flow Field-Flow Fractionation, *Analytical and Bioanalytical Chemistry*, 406:1597-605, 2014.

90. I. Vina, A. Karsakevich, S. Gonta, R. Linde and M. Bekers, Influence of Some Physicochemical Factors on The Viscosity of Aqueous Levan Solutions of *Zymomonas Mobilis*, *Engineering in Life Sciences*, 18:167–174, 1998.

91. O. M. Bondarenko, A. Ivask, A. Kahru, H. Vija, T. Titma, M. Visnapuu, U. Joost, K. Pudovac, S. Adamberg, T. Visnapuu and T. Alamäe, Bacterial Polysaccharide Levan As Stabilizing, Non-Toxic and Functional Coating Material for Microelement-Nanoparticles, *Carbohydrate Polymers*, 136:710-20, 2016.

92. E. Benigar, I. Dogsa, D. Stopar, A. Jamnik, I. K. Cigić, and M. Tomšič, Structure and Dynamics of a Polysaccharide Matrix: Aqueous Solutions of Bacterial Levan, *Langmuir*, 30:4172–4182, 2014.

93. J. Leibovici and Y. Stark, Direct Antitumor Effect of the Polysaccharide Levan in Mice: Effects of Drug Concentration and Time and Temperature of Incubation, *The Journal of the National Cancer Institute*, 72:1417-1420, 1984.

94. J. Leibovici, Y. Stark, T. Eldar, G. Brudner and M. Wolman, Mechanism of the Inhibitory Effect of Levan on Experimental Tumors, *Recent Results in Cancer Research*, 75:173-179, 1980.

95. J. Leibovici, G. S. Brudner and M. Wolman, Direct Antitumor Effect of High-Molecular-Weight Levan on Lewis Lung Carcinoma Cells in Mice, *The Journal of the National Cancer Institute*, 65:391-396, 1980.

96. I. Dahech, B. Harrabi, K. Hamden, A. Feki, H. Mejdoub, H. Belghith and K. S. Belghit, Antioxidant Effect of Nondigestible Levan and Its Impact on Cardiovascular Disease and Atherosclerosis, *International Journal of Biological Macromolecules.*, 58:281-286, 2013.

97. Q. Xu, T. Yajima, W. Li, K. Saito, Y. Ohshima and Y. Yoshikai, Levan (B-2, 6-Fructan), A Major Fraction of Fermented Soybean Mucilage, Displays Immunostimulating Properties via Toll-Like Receptor 4 Signalling: Induction of Interleukin-12 Production and Suppression of T-Helper Type 2 Response and Immunoglobulin E Production, *Clinical and Experimental Allergy*, 36:94-101, 2006.
98. E. J. Roberts, and P. J. Garegg, Levan Derivatives, Their Preparation, Composition and Applications Including Medical and Food Applications, *United States Patents*, WO, 98/03184, 1998.
99. M. Abdel-Fattah, A. M. Gamal-Eldeen, W. A. Helmy and M. A. Esawy, Antitumor and Antioxidant Activities of Levan and Its Derivative from The Isolate *Bacillus Subtilis* NRC1aza, *Carbohydrate Polymers*, 89:314–322, 2012.
100. J. Liu, J. Luo, H. Ye and X. Zeng, Preparation, Antioxidant And Antitumor Activities In Vitro of Different Derivatives of Levan From Endophytic Bacterium *Paenibacillus Polymyxa* EJS-3, *Food and Chemical Toxicology*, 50:767-72, 2012.
101. R. R. Costa, A. I. Neto, I. Calgeris, C. R. Correia, A. C. M. Pinho, J. Fonseca, E. T. Oner and J. F. Mano, Adhesive Nanostructured Multilayer Films Using A Bacterial Exopolysaccharide For Biomedical Applications, *Journal of Materials Chemistry B*, 1:2367-2374, 2013.
102. H. K. Sarilmiser and E. T. Oner, Investigation of Anti-Cancer Activity of Linear And Aldehyde-Activated Levan from *Halomonas Smyrnensis* AAD6T, *Biochemical Engineering Journal*, 92:28–34, 2014.
103. I. Dahech, K. S. Belghith, H. Belghith and H. Mejdou, Partial Purification of A *Bacillus Licheniformis* Levansucrase Producing Levan with Antitumor Activity, *International Journal of Biological Macromolecules*, 51:329–335, 2012.
104. A. Akçay, Sulfated Levan as a Polymer for Biomedical Applications, Msc Thesis, Marmara University, 2014.

105. A.R. Leach, *Molecular Modeling Principles and Applications*, Pearson Education Lmt., 2<sup>nd</sup> Ed., Great Britain, 2001
106. F. Wilfred, D. Xavier and E. M. Alan, *GROMOS Force Field*, Encyclopedia of Computational Chemistry, 2002.
107. R.J. Woods, Computational Carbohydrate Chemistry: What Theoretical Methods Can Tell Us, *Glycoconjugate Journal*, 15:209-216, 1998.
108. A.D. Mackerell and M. Feig, Improved Treatment of the Protein Backbone in Empirical Force Fields, *Journal of the American Chemical Society*, 126:698–699, 2004.
109. O. M. Becker, A. D. MacKerell Jr. and B. R. M. Watanabe, *Computational Biochemistry and Biophysics*, CRC Press, New York, 2001.
110. O. Jardetzky and M. D. Funicane, *Dynamics, Structure, and Function of Biological Macromolecules*, IOS Press, Erice, Italy, 1999.
111. D.A. Puelo and R. Bizio, *Biological Interactions on Materials Surfaces*, Springer, New York, 2009.
112. B.R. Brooks, R. E., Bruccoleri, B.D. Olafson and D.J.S. States, CHARMM: A Program for Macromolecular Energy, Minimization, and Dynamics Calculations, *Journal of Computational Chemistry*, 4:187-217, 1983.
113. J. Wang, M.W. Romain, W.C. James, A.K. Peter and A. David, Development and Testing of a General Amber Force Field, *Journal of Computational Chemistry* 25:1157-1174, 2004.
114. F. Wilfred, D. Xavier and E. M. Alan, *GROMOS Force Field*, Encyclopedia of Computational Chemistry, 2002.



115. H. Sun, S.J. Mumby, J.R. Maple, A.T. Hagler and J. Amer, An Ab-initio CFF93 All-Atom Force-field for Polycarbonates, *Chemical Society Reviews*, 116:2978-2988, 1994.
116. R. J. Woods, Computational Carbohydrate Chemistry: What Theoretical Methods Can Tell Us, *Glycoconjugate Journal*, 15:209-216, 1998.
117. A. D. Mackerell and M. Feig, Improved Treatment of the Protein Backbone in Empirical Force Fields, *Journal of the American Chemical Society*, 126:698–699, 2004.
118. H. Heinz, H. Koerner, K. L. Anderson, R. A. Vaia, and B. L. Farmer, Force Field for Mica-Type Silicates and Dynamics of Octadecylammonium Chains Grafted to Montmorillonite, *Chemistry of Materials*, 17:5658-5669, 2005.
119. D. Hanka and J. Zie, Implicit Runge-Kutta Method for Molecular Dynamics Integration, *Journal of Chemical Information and Modeling*, 33:252-251,1993.
120. N. Gronbech-Jensen and F. Oded, A Simple and Effective Verlet-type Algorithm for Simulating Langevin Dynamics, *Molecular Physics*, 111:983-991, 2013.
121. O. M. Becker, A. D. MacKerell Jr., and B. R.,M. Watanabe, *Computational Biochemistry and Biophysics*, CRC Press, New York, 2001.
122. O. Jardetzky and M. D. Funicane, *Dynamics, Structure, and Function of Biological Macromolecules*, IOS Press, Erice, Italy, 1999.
123. R. Zhou, Free Energy Landscape of Protein Folding in Water: Explicit vs. Implicit Solvent, *PROTEINS: Structure, Function, and Genetics*, 53:148-161, 2003.
124. B. Xia, V. Tsui, D.A. Case, H.J. Dyson and P.E. Wright, Comparison of Protein Solution Structures Refined by Molecular Dynamics Simulation in Vacuum, With a Generalized Born Model, and With Explicit Water, *Journal of Biomolecular NMR*, 22:317-331, 2002.

125. Implicit Solvent Models for Molecular Simulations, ‘ProShape, Understanding the Protein Shape’,  
<http://csb.stanford.edu/~koehl/ProShape/born.php>, [retrieved 07 October 2002].
126. J. Finnerty, Molecular Dynamics Meets The Physical World: Thermostats And Barostats, German Research School for Simulation.
127. P. H. Hünenberger, Thermostat Algorithms for Molecular Dynamics Simulations, *Advanced Polymer Science*, 173:105–149, 2005.
128. E. A. Koopman and C. P. Lowe, Advantages of A Lowe-Andersen Thermostat in Molecular Dynamics Simulations, *The Journal of Chemical Physics*, 124:204103, 2006.
129. H. J. C. Berendsen, J. P. M. Postma, W. F. van Gunsteren, A. Di Nola, and J. R. Haak Molecular Dynamics with Coupling to an External Bath, *The Journal of Chemical Physics*, 81:3684-3690, 1984.
130. U. Gedde, *Polymer Physics*, Springer, Dordrecht, 1999.
131. A. E. Likhtman, S. K. Sukumaran and J. Ramirez, Linear Viscoelasticity from Molecular Dynamics Simulation of Entangled Polymers, *Macromolecules*, 40:6748–6757, 2007.
132. R. Radhakrishnan and P. T. Underhil, Models of Flexible Polymers in Good Solvents: Relaxation and Coil–Stretch, Transition, *Soft Matter*, 8:6991-6700, 2012.
133. J. P. Hansen and I. R. McDonald, *Theory of Simple Liquids*, Academic Press, London, 1986.
134. J. M. Ziman, *Models of Disorder: The Theoretical Physics of Homogeneously Disordered Systems*, Cambridge University Press, Cambridge, UK, 1979.
135. C. Yen and S. W. Mark, Mathematical Modeling of Molecular Diffusion Through Mucus, *Advanced Drug Delivery Reviews*, 61:101–114, 2009.

136. W. Smith, Molecular Dynamics Simulation of Linear Polymers in a Solvent, *Molecular Simulation*, 9:25-39, 1992.
137. M. O. Steinhauser, A Molecular Dynamics Study on Universal Properties of Polymer Chains in Different Solvent Qualities, *The Journal of Chemical Physics*, 122:1-13, 2005.
138. J. E. Mark, *Physical Properties of Polymers Handbook*, Springer, New York, 2007.
139. B. Lu and S. Torquato, Chord-Length and Free-Path Distribution Functions for Many-Body Systems, *The Journal of Chemical Physics*, 98:6472-6482, 1993.
140. R. Ozisik, P. Doruker, W.L. Mattice, E.D. von Meerwall, Translational Diffusion In Monte Carlo Simulations of Polymer Melts: Center of Mass Displacement Vs. Integrated Velocity Autocorrelation Function, *Computational and Theoretical Polymer Science*, 10:411-418, 2000.
141. B.G. Levine, J. E. Stone and A. Kohlmeyer, Fast Analysis of Molecular Dynamics Trajectories with Graphics Processing Units-Radial Distribution Function Histogramming, *Journal of Computational Physics*, 230:3556-3569, 2011.
142. J. D. Perezgonzalez, Fisher, Neyman-Pearson Or NHST? A Tutorial For Teaching Data Testing, *Front Psychology*, 6: 223-227, 2015.
143. J. B. Prel, H. Gerhard, R. Bernd and B. Maria, Confidence Interval or P-Value?, *Medicine*, 106:335-339, 2009.
144. D. B. Kitchen, H. Decornez, J. R. Furr and J. Bajorath, Docking and Scoring in Virtual Screening for Drug Discovery: Methods And Applications, *Nature Reviews Drug Discovery*, 3:935-49, 2004.

145. P. H. Seeberger and C. Rademacher, *Carbohydrates as Drugs*, Springer, New York, 2014.
146. E. Fadda and R.J. Woods, Molecular Simulations of Carbohydrates and Protein-Carbohydrate Interactions: Motivation, Issues, and Prospects, *Drug Discovery Today*, 15:596-609, 2010.
147. S. Shenogin, and R. Ozisik, XenoView: Visualization for Atomistic Simulations, XenoView, <http://xenoview.mat.rpi.edu> [retrieved 1 January 2007].
148. S. Plimpton, Fast Parallel Algorithms for Short-Range Molecular Dynamics, *Journal of Computational Physics*, 117:1-19, 1995.
149. W. Humphrey, D. Andrew and S. Klaus, VMD: Visual Molecular Dynamics, *Journal of Molecular Graphics*, 14:33-38, 1996.
150. A. Grosdidier, V. Zoete and O. Michielin, Swissdock, A Protein-Small Molecule Docking Web Service Based on Eadock DSS, *Nucleic Acids Researchs*, 39:270-277, 2011.
151. E.F. Pettersen, T.D. Goddard, C.C. Huang, G.S. Couch, D.M. Greenblatt, E.C. Meng and T.E. Ferrin, UCSF Chimera--A Visualization System For Exploratory Research And Analysis, *Journal of Computational Chemistry*, 13:1605-1612, 2004.
152. Türk Ulusal e-Bilim e-Altyapısı, 'TRUBA', TUBITAK-ULAKBIM, <http://www.grid.org.tr/> [retrieved 1 January 2007].
153. B. Miller and D.L. Ranum, *Problem Solving with Algorithms and Data Structures using Python*, Franklin, Beedle and Associates Incorporated, Oregon, USA, 2006.
154. M. Dawson, *Python Programming for the Absolute Beginner*, Thomson Course Technology, Boston, USA, 2006.

155. C. Huang, C. Li , P. Y.K. Choi , K. Nandakumar and L. W. Kostiuk, Effect of Cut-Off Distance Used in Molecular Dynamics Simulations on Fluid Properties, *Journal of Molecular Simulation*, 36:856-864, 2010.
156. J. Bois, *Rudiments of Polymer Physics*, California Institute of Technology, 2002.
157. I. Teraoka, *Polymer Solutions: An Introduction to Physical Properties*, John Wiley and Sons, New York, 2002.
158. C. Osuji, Ideal Chain Conformations and Statistics, *Polymer Physics*, 2:1-6, 2013.
159. Massachusetts Institute of Technology, “Polymer Solution Thermodynamics”, [http://web.mit.edu/course/3/3.941j/www/3941\\_S02\\_1.pdf](http://web.mit.edu/course/3/3.941j/www/3941_S02_1.pdf) [retrieved 9 April 2002].
160. R. Young and P. Lovell, *Introduction to Polymers*, CRC Press, New York, 2011.
161. S.W. Cui, *Food Carbohydrates: Chemistry, Physical Properties, and Applications*, CRC Press, New York, 2005.
162. V. S. R. Rao, *Conformation of Carbohydrates*, CRC Press, New York, 1998.
163. M. Yalpani, *Polysaccharides: Syntheses, Modifications and Structure/Property Relations*, Elsevier, New York, 1988.
164. S. M. Hoffmann, Molecular Dynamics Simulations of Poly(3-hexylthiophenes) in Dilute Solutions, Master of Science, University of Washington, 2014.
165. V. D Spoel., P.J. Maaren and C.Caleman, GROMACS Molecule and Liquid Database, *Bioinformatics*, 28(5):752-3, 2012.
166. Q. Wang and S. W. Cui, *Understanding the Conformation of Polysaccharides*, Food Carbohydrates: Chemistry, Physical Properties, and Applications, CRC Press, New York, 2005.

167. J.M.G. Cowie, *Polymers: Chemistry and Physics of Modern Materials*, CRC Press, New York, 2007.
168. A. Guner and G. Kibarer, The Important Role of Thermodynamic Interaction Parameter in The Determination of Theta Temperature, Dextran/Water System, *European Polymer Journal*, 37:619-622, 2000.
169. F. Cilurzo, N. Costa, A. Brun and D. Paolino, Application of Viscotek to Food Chemistry, *Advances in Food Safety and Health*, 6:70-77, 2014.
170. I. Teraoka, *Polymer Solutions: An Introduction to Physical Properties*, John Wiley and Sons, New York, 2002.
171. J. Kestin, H. E. Khalifa and R. J. Correla, Tables of the Dynamic and Kinematic Viscosity of Aqueous NaCl Solutions in the Temperature Range 20-150°C and the Pressure Range 0.1-35 MPa, *Journal of Physical and Chemical Reference Data*, 10:71-87, 1981.
172. Y. Çengel, *Heat and Mass Transfer: a Practical Approach*, McGraw Hill, 2007.
173. C. M. Koka and A. Rudin, Relationship between the Hydrodynamic Radius and the Radius of Gyration of a Polymer in Solution, *Macromolecular Rapid Communications*, 2:655-659, 1981.
174. A. C. F. Ribeiro, O. Ortona, S. M. N. Simoes, C. I. A. V. Santos, P. M. R. A. Prazeres, A. J. M. Valente, V. M. M. Lobo and H. D. Burrows, Binary Mutual Diffusion Coefficients of Aqueous Solutions of Sucrose, Lactose, Glucose, and Fructose in the Temperature Range from (298.15 to 328.15) K, *Journal of Physical and Chemical Reference Data*, 51:1836-1840, 2006.
175. W. R. L. Farias, A. P. Valente, M. S. Pereira and P. A. S. Mourao, Structure and Anticoagulant Activity of Sulfated Galactans. Isolation of a Unique Sulfated Galactan From The Red Algae *Botryocladia Occidentalis* and Comparison of Its Anticoagulant

Action With That of Sulfated Galactans From Invertebrates, *The Journal of Biological Chemistry*, 275:29299–29307, 2000.

176. R. Wang, L. Lai and S. Wang, Further Development and Validation of Empirical Scoring Functions for Structure-Based Binding Affinity Prediction, *Journal of Computer-Aided Molecular Design*, 16:11-26, 2002.

177. S. Raveendran, Y. Yoshida, T. Maekawa and D.S. Kumar, Pharmaceutically Versatile Sulfated Polysaccharide Based Bionano Platforms, *Nanomedicine:Nanotechnology, Biology, and Medicine*, 9:605–626, 2013.

178. K. Zhang, J. Helm, D. Peschel, M. Gruner, T. Groth and S. Fischer, NMR And FT Raman Characterization of Regioselectively Sulfated Chitosan Regarding The Distribution of Sulfate Groups and The Degree of Substitution, *Polymer*, 51:4698–4705, 2010.

179. M. Erginer, A. Akcay, B. Coskuncan, T. Morova, D. Rende, S. Bucak, N. Baysal, R. Ozisik, M.S. Eroglu, M. Agirbasli, E. Toksoy Oner, Sulfated Levan from *Halomonas Smyrnensis* as a Bioactive, Heparin-Mimetic Glycan for Cardiac Tissue Engineering Applications, *Carbohydrate Polymers*, 149:289-296, 2016

180. A.K. Gaigalas, J.B. Hubbard, R. LeSage and D.H. Atha, Physical Characterization of Heparin by Light Scattering, *Journal of Pharmaceutical Sciences*, 84:355-359, 1995.

181. D. Lillicrap, N. Key M. Makris and D. O'Shaughnessy, *Practical Hemostasis and Thrombosis*, Wiley-Blackwell, New York, 2009.

182. P.C.Y. Liaw and J.I. Weitz, *Coagulation Overview. In: Clinical Critical, Care Medicine*, Mosby Elsevier, 2006.

183. N.M. Mestechkina and V.D. Shcherbukhin, Sulfated Polysaccharides And, Their Anticoagulant Activity: A Review, *Applied Biochemistry and Microbiology*, 46: 267–273, 2010.

184. T. Renne, B. Nieswandt and D. Gailani, The Intrinsic Pathway of Coagulation is Essential for Thrombus Stability in Mice Blood Cells, *Molecules and Diseases*, 36:148–151, 2006.
185. J.W. Fenton, T.A. Olson, M.P. Zabinski and G.D. Wilner, Anion-Binding Exosite of Human Alpha-Thrombin and Fibrin(Ogen) Recognition, *Biochemistry*, 67:7106-7112, 1988.
186. W. S. Bode, I. Mayr, U. Baumann, R. Huber, R.S. Stone and J. Hofsteenge, The Refinen 1.9A Crystal Structure of Human A-Thrombine: Interaction With D-Phe-Pro-Arg Chloromethylketone and Significance of The Tyr-Pro-Pro-Trp Insertion Segment, *The Journal of Physical Chemistry B*, 8:3467-3475, 1989.
187. J. Hofsteenge, P.J. Braun and S.R. Stone, Enzymatic Properties Of Proteolytic Derivatives Of Human O-Thrombin, *Biochemistry*, 27:2144–2151, 1988.
188. F.C. Church, C.W. Pratt, C.M. Neyes, T. Kalayanamit, G.B. Sherrill, R. Tabin and J.B. Meade, Structural and Functional Properties of Humanathrombin and Thrombin, *Journal of Biological Chemistry*, 264:18419-18425, 1989.
189. J. Ye, A.R. Rezaie and C.T. Esmen, Glycosaminoglycan Contributions To Both Protein C Activation And Thrombin Inhibition Involve A Common Arginine-Rich Site In Thrombin That Includes Residues Arginine93, Arginine97 And Arginine101, *Journal of Biological Chemistry*, 269:17965- 17970, 1994.
190. P. Gandhi, *Structural and Functional Studies in Thrombin Allostery*, PhD Thesis, Washington University, 2011.
191. S. Alban and G. Franz, Partial Synthetic Glucan Sulfates as Potential New Antithrombotics: A Review, *Biomacromolecules*, 2:354–361, 2001.
192. A. Günther and C. Ruppert, Anticoagulants, *Encyclopedia of Respiratory Medicine* 1:115-128, 2006.



193. A. Quinn and M. Bellamy, Hemostasis and Coagulation. In: Foundations of Anesthesia, Basic Science and Clinical Practise, 2nd ed., Elsevier., 2006.
194. N. Volpi, F. Maccari, J. Suwan and R. J. Linhardt, Electrophoresis for The Analysis of Heparin Purity and Quality, *Electrophoresis*, 33:1531–1537, 2012.
195. O. Yan, J.F. Xue, C.Y. Tan , B. Gui, X. Sun and Jian-Ming, Inhibition of Urinary Macromolecule Heparin on Aggregation of Nano-COM and Nano-COD Crystals, *Molecules*, 20:1626-1642, 2015.
196. T. E. Warkentin, M.D. Mark, N. Levine, M.D. J. Hirsh, M.D. P. Horsewood, R. S. Roberts, M.Tech, M. Gent and J. G. Kelton, Heparin-Induced Thrombocytopenia in Patients Treated with Low-Molecular-Weight Heparin or Unfractionated Heparin, *The New England Journal of Medicine*, 332:1330-1336, 1995.
197. N. C. Maas, A.H.P. Gracher, G.L. Sasaki, P.A.J. Gorin, M. Iacomini And T.R. Cipriani, Sulfation Pattern of Citrus Pectin and Its Carboxy-reduced Derivatives: Influence on Anticoagulant and Antithrombotic Effects, *Carbohydrate Polymers*, 89:1081–1087, 2012.
198. A. Grosdidier, V. Zoete and O. Michielin, Fast Docking Using The CHARMM Force Field With Eadock DSS, *Nucleic Acids Research*, 39:270–277, 2011.
199. N. Sapay, A. Nurisso and Anne Imberty, Simulation of Carbohydrates, from Molecular Docking to Dynamics in Water, *Methods in Molecular Biology*, 924:469-483, 2012.
200. J. Shen, H. Wang and Y. Xia, Molecular Simulation of Model Sulfated Polysaccharides of Low Molecular Weight From Ganoderma Lucidum and Their Interaction With Human Serum Albumin, *Structural Chemistry*, 25:1423–1435, 2012.
201. D. Preamnath, R.V. Angela Asir, J. Adaline Jebamalar, J. Jannet Vennila and M. Patrick Gomez, Insilico Docking and Interaction Analysis of Bioactive Marine Compound

(Sulfated Fucose) Against The Human Mutant P53 Protein Involved in Carcinogenesis, *International Journal of Scientific and Engineering Research*, 3:560-567, 2012.

202. N. E. Ustyuzhanina, M.I. Bilan, A.G. Gerbst, N.A. Ushakova, E.A. Tsvetkova, A.S. Dmitrenok, A.I. Usov and N.E. Nifantiev, Anticoagulant And Antithrombic Activities Of Modified Xylofucan Sulfate From The Brown Alga *Punctaria Plantaginea*, *Carbohydrate Polymers*, 136:826-33, 2016.

203. S. A. Samsonov , J. Teyra and M. T. Pisabarro, Docking Glycosaminoglycans To Proteins: Analysis Of Solvent Inclusion, *Journal of Computer-Aided Molecular Design*, 25:477-489, 2011.

204. S.E. Mottarella, D. Beglov, N. Beglova, M.A. Nugent, D. Kozakov and S. Vajda, Docking Server for The Identification of Heparin Binding Sites on Proteins, *Journal of Chemical Information and Modeling*, 54:2068–2078, 2014.

205. W. Bitomsky and R. C. Wade, Docking of Glycosaminoglycans to Heparin-Binding Proteins: Validation for aFGF, bFGF, and Antithrombin and Application to IL-8, *Journal of the American Chemical Society*, 121:3004–3013, 1999.

206. P.V. Fernández, I. Quintana, A.S. Cerezo, J.J. Caramelo, L. Pol-Fachin, H. Verli, J. M. Estevez and M. Ciancia, Anticoagulant Activity of A Unique Sulfated Pyranosic (1→3)-L-Arabinan Through Direct Interaction with Thrombin, *The Journal of Biological Chemistry*, 288:223–233, 2013.

207. A. Van de Locht, D. Lamba, M. Bauer, R. Huber, T. Friedrich, B. Kröger, W. Höffken and W. Bode, Two Heads Are Better Than One. Crystal Structure of The Insect-Derived Double Domain Kazal Inhibitor Rhodniin in Complex With Thrombin, *The EMBO Journal*, 14:5149–5157, 1995.

208. S. E. Mottarella, D. Beglov, N. Beglova, M.A. Nugent, D. Kozakov and S. Vajda, Docking Server for The Identification of Heparin Binding Sites on Proteins, *Journal of Chemical Information and Modeling*, 54:2068-78, 2014.

209. T. J. Rydel, K.G. Ravichandran, A. Tulinsky, W. Bode, R. Huber and C. Roitsch, The Structure of a Complex of Recombinant Hirudin and Human Alphathrombin, *Science*, 249: 277–80, 1990.
210. C. G. Malmberg and A. A. Maryott, Dielectric Constant of Water from 0° to 100° C, *Journal of Research of the National Bureau of Standards*, 56:1-8, 1956.
211. A. Levy and D. Andelman, Dielectric Constant of Ionic Solutions: A Field-Theory Approach, *Physical Review Letters*, 108:1-5, 2012.



## APPENDIX A: SIMULATIONS AS IMPLICIT SYSTEMS WITH ORIGINAL LEVAN STRUCTURE IN DIFFERENT MEDIA AT 310 K

Implicit systems are method of representing media due to the dielectric constant calculated from electrostatic interactions instead of individual molecules. Total number of the system decreases in implicit systems so that it saves time and computer power. However, implicit systems ignore specific short range effect. It is less accurate than explicit systems.

Table A.1. Simulations with implicit systems

# of levan	# of fructose units	NaCl conc.(M)	Media	Pressure (atm)	Temp (K)	Dt	duration
9	12	0	Water	1	298	1 ps	5 ns
9	12	0.5	Saline	1	298	1 ps	5 ns
9	12	1	Saline	1	298	1 ps	5 ns
9	12	2	Saline	1	298	1 ps	5 ns

The dielectric constant is the ability of an molecule to insulate charges from other molecules. At the same time, it is the measure of polarity of the substances. The vacuum media is presented with the dielectric constant equal to 1 which shows there is no effect of media on other molecules. The dielectric constant of water is calculated from the equation below for between 0.1° C and 99° C,

$$\epsilon = 87.740 - 0.4008T + 9.398(10^{-4})T^2 - 1.410(10^{-6})T^3 \quad (\text{A.1.})$$

where temperature is shown in Celcius. In this study, the dielectric constant of water is found as 78.304 for 298 K. This value shows the coulomb forces of water ions is lower 78.304 times than in vacuum media [210]. There is a linear relationship between concentration and the dielectric constant for lower concentrations of salt solutions. It can be calculated from the equation below [211]:

$$\epsilon(C_s) = \epsilon_w - \gamma C_s \quad (\text{A.2.})$$

The dielectric constant of saline solutions of 0.5 M, 1 M and 2 M is found as 72.9, 67.4 and 56.4 respectively.

Explicit and implicit systems for one levan chain in water were simulated and compared due to its end-to-end distance and radius of gyration. Nine levan chains in water and saline solutions were also simulated as implicit system. As seen in Figure A.1. and A.2. the results are very dissimilar compared to the explicit systems. The systems came to the equilibrium part too fast so the systems could not be analyzed with respect to time. The electrostatic forces are limited in implicit systems.

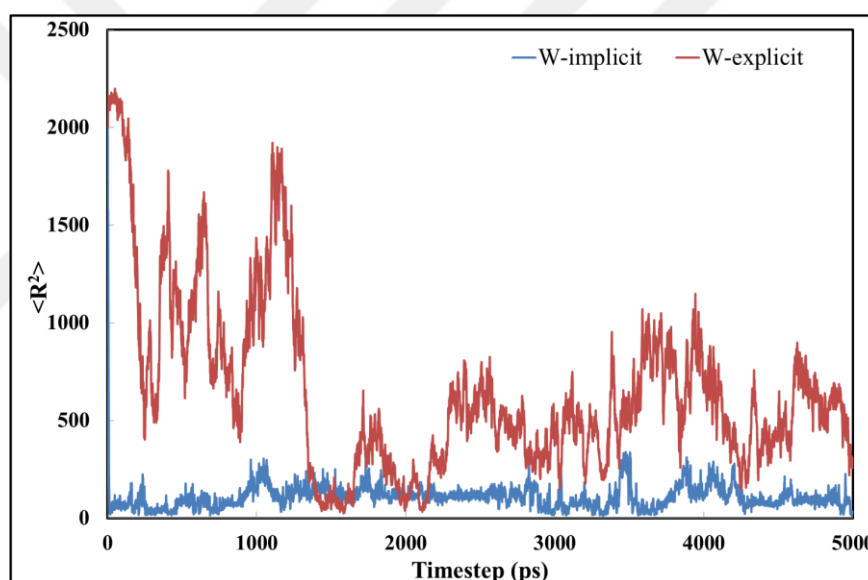


Figure A.1. End-to-end comparison of explicit and implicit systems of one levan chain in water at 298 K

Figure A.1 shows the end-to-end distance for single chain simulated in both implicit and explicit systems. As seen in the figure the end-to-end distance of implicit system shows more sudden decrease than explicit system. In implicit system, the fluctuation of levan chain and the end-to-end distance are less than explicit system. Because the electrostatic forces between atoms are limited in implicit systems.

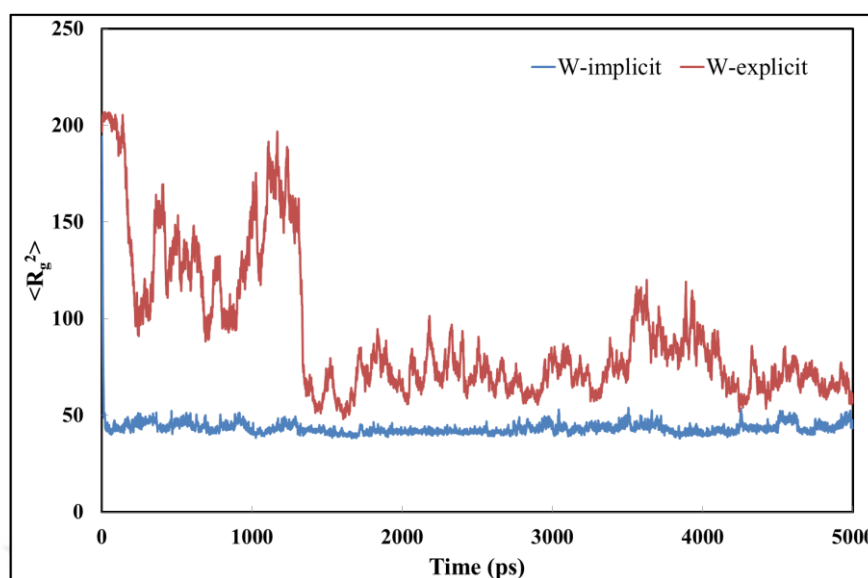


Figure A.2.  $R_g$  comparison of explicit and implicit systems of one levan chain in water

Radius of gyration of these systems are compared as well. As seen in figure A.2., the radius of gyration is affected as same as end-to-end distance by implicit system. To understand the effect of dielectric constant to the final values of end-to-end distance and radius of gyration for different media, Figure A.3. and Figure A.4. is plotted.

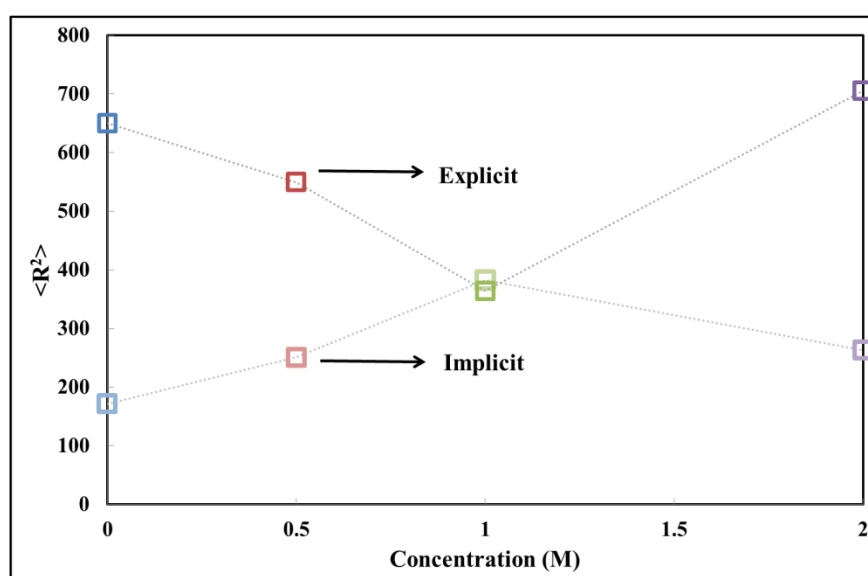


Figure A.3. End-to-end comparison of explicit and implicit systems of nine levan chains in water and saline solutions

As seen these two figures, the final values of levan chain simulated as implicit and explicit systems are different from each other. In explicit system there is a decrease trend until 1 M and then increase for 2 M systems. However in implicit system, the trend is the exact opposite of explicit system. Radius of gyration figure also shows the same trend for both systems (Figure A.4).

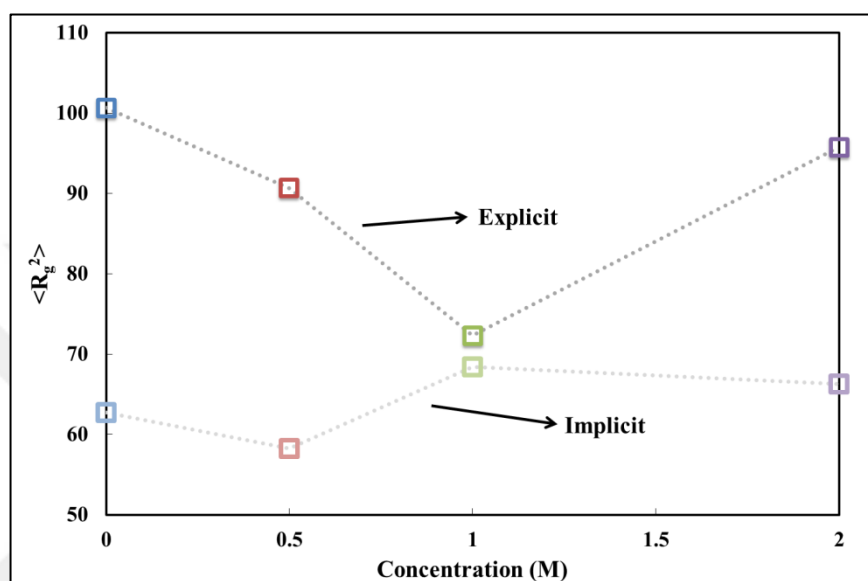


Figure A.4.  $R_g$  comparison of explicit and implicit systems of nine levan chains in water and saline solutions

The molecules, the interactions between atoms and molecules were well defined in explicit systems so the results are accepted as more realistic. Therefore the simulations are continued to be performed in explicit solvent.